Study on ultraprecision finishing method for freeform optical elements

He Wang

Division of Mechanical Science and Technology

Graduate School of Science and Technology

Gunma University

March, 2019

Contents

Chapter 1 Introduction 1
1.1 Research background 2
1.2 The concept of aspherical and its equation 5
1.3 Aspherical ultra-precision machining detection and error compensation technology 7
1.4 Ultra-precision machining of aspheric surfaces 10
1.4.1 Hot briquetting 10
1.4.2 Ion beam polishing 11
1.4.3 Jet polishing 12
1.4.4 Magnetorheological Finishing (MRF) 13
1.4.5 Plasma polishing technology 16
1.4.6 Air bag precession polishing 16
1.4.7 Computer controlled polishing 18
1.5 Development of aspherical ultra-precision machining machines 19
1.6 Purposes and scope of this study 22

Chapter 2 Principle of rotation and revolution polishing method and development of experimental equipment 33
2.1 Polishing of mold in injection molding method 34
2.2 Principle of rotation and revolution polishing method 35
2.3 Overview of polishing equipment 36
2.3.1 Rotation and Revolution polishing unit 37
2.3.2 Polishing load and Polishing tool 37
2.3.3 Workpiece, polishing fluid and truing 39
2.4 Experimental procedure 41
2.5 Measuring device and workpiece measurement 41
2.6 The basic principle of Computer Control Optical Surfacing (CCOS) 42
2.6.1 The theoretical basis of CCOS 42
2.6.2 Principles of CCOS 44
2.6.3 Mathematical model of CCOS 44
2.6.4 Characteristics of ideal removal function 46
2.7 Design of rotating and revolution units and 3D modeling 48
2.7.1 3D Modeling based on SolidWorks 49
2.7.2 Machine tool main body introduction 49
2.7.3 Design and modeling of tool unit 50
2.7.4 Design and modeling of rotation unit 52
2.7.5 Design and modeling of revolution unit 54
2.7.6 Defects in structural design 56
2.8 Summary 57

Chapter 3 Experiment and simulation of rotation and revolution type polishing method 61
3.1 Motivation of deterministic polishing 62
3.2 Principles of the Preston equation 63
3.3 Definition of the contact area 66
3.4 Distribution function of polishing force 69
3.5 Fixed point polishing 71
3.5.1 Pressure distribution function 71
3.5.2 Establish a coordinate system for fixed point polishing 72
3.5.3 Mathematical model of fixed-point polishing 74
3.5.4 Experimental system and conditions 76
3.5.5 Determination of Preston coefficient 77
3.5.6 Results and discussion 80
3.6 Moving polishing 82
3.6.1 Coordinate system of polishing area 82
3.6.2 Description of the posture of the polishing tool 86
3.6.3 Distribution function of relative velocity 89
3.6.4 Mathematical modeling of linear path polishing 90
3.6.5 Verification of the mathematical model of linear path polishing 91
3.7 Mathematical modeling of curve path polishing 95
3.8 Material removal of complex trajectories in rotation and revolution polishing method 98
3.9 Material removal with gentle angle change 99
3.10 Material removal with large angle changes 102
3.10.1 Mathematical modeling of linear path 103
3.10.2 Mathematical modeling of curve trajectories 106
3.10.3 Establishment of a mathematical model for overall material removal 107
3.11 Material removal with sharp changes in angle 108
3.11.1 Mathematical model material removal only for curved traces 109
3.11.2 Mathematical model material removal for straight and curved paths 109
3.12 Summary 110

Chapter 4 Polishing of electroless plated Ni-P as neutron mirror 116
4.1 Introduction of neutron beam 117
4.2 Mathematical modeling of single path polishing of small diameter tools 117
4.3 Experimental verification of the model 122
4.3.1 Experimental system and conditions 122
4.3.2 Determination of Preston coefficient 124
4.4 Results and discussion 126
4.4.1 Experimental verification of single path material removal model 126
4.4.2 Discussion of surface quality 127
4.5 Summary 134

Chapter 5 Conclusions 139
5.1 Summary of this thesis 139
5.2 Further prospect 141

Related articles 142

Acknowledgements 144

List of major symbols in this doctoral thesis

Symbol	Significance
$a_1,\ a_2,\ a_3, \ldots,\ a_n$	Coefficients of the first type of aspheric meridian cut-off equation
$A_1,\ A_2,\ A_3, \ldots,\ A_n$	Coefficients of the second type of aspheric meridian cut-off equation
c	The paraxial curvature
r	The radius of curvature of the vertex
k	A conic constant
B_i	Coefficient of high order term of the third type of cut-off equation
e	The eccentricity rate
$\frac{dz}{dt}$	Material removal
Kp	The polishing coefficient
$V\ (x, y, t)$	The instantaneous velocity
$P\ (x, y, t)$	The instantaneous pressure
$\Delta z\ (x, y)$	The amount of material removed during time t.
l	The length of the polishing path
T	The total polishing time
$D\ (x, y)$	The dwell time function
$E\ (x, y)$	The processing residual error
$\overline{R(\xi, \eta)}$	The Fourier spectrum function
$H\ (x, y)$	Overall removal function
$R\ (x, y)$	The polished removal per unit time
$p\ (x, y)$	The pressure distribution function
$v\ (x, y)$	The relative linear velocity distribution function
c	The contact radius.
F	The contact force.
ρ_1	ρ_1 The radius of the tool
ρ_2	The radius of the workpiece

E_1	The elastic moduli of the tool
E_2	The elastic moduli the workpiece
μ_1	The Poisson's ratio of the tool
μ_2	The Poisson's ratio of the workpiece
p_o	The maximum contact stress
Ω	The revolution angular velocity
ω	The rotational angular velocity
λ	The angle between the two axes
R_1	The inner of the tool
R_2	The outer radius of the tool
ρ_d	The density of the workpiece
v_f	Teed speed
l	The length of the polishing tool along the path
E	The removal depth per unit
Ω	The revolution angular speed
ω	The rotation angular speed
$\boldsymbol{\omega}$	The rotation angular velocities of the tool
$\boldsymbol{\Omega}$	The revolution angular velocities of the tool
$\boldsymbol{z}$	The unit normal vector
$\boldsymbol{Z}$	The polishing axis unit vector
M_{rot}	Rotation matrix
R_p	The tool head radius
a	The polished area radius
θ_1 and θ_2	The polar angles
F_n	The polishing force of the tool
Δm	The weight difference before and after polishing

Chapter 1 Introduction

With the development of many fields such as aerospace, optics, electronics, bioengineering and military equipment, the demand for high-precision curved surfaces complex-shaped parts, and optical parts has increased. Ultra-precision machining technology, as a new technology emerging from the development of modern high-tech, its precision, surface roughness, processing size range and geometry have become an important level of manufacturing technology. As a key technology in ultra-precision machining, aspherical processing technology is attracting more and more attention. In this chapter, the definition of aspheric surfaces, aspherical curve equations are introduced. Next, the measurement method of the aspherical surface will be described. The current ultra-precision manufacturing method is also introduced. Finally, in this chapter, the ultra-precision machine tools with excellent performance are described in detail.

1.1 Research background

Compared to traditional spherical optics, aspherical optics can correct a variety of aberrations and improve system identification for better image quality. Aspherical optics can focus more accurately on complex images than traditional spherical optics (Fig. 1.1). And it can reduce the number of optical components, simplify the system structure, reduce the size and weight of the instrument, and improve the performance of the photoelectric instrument [1].

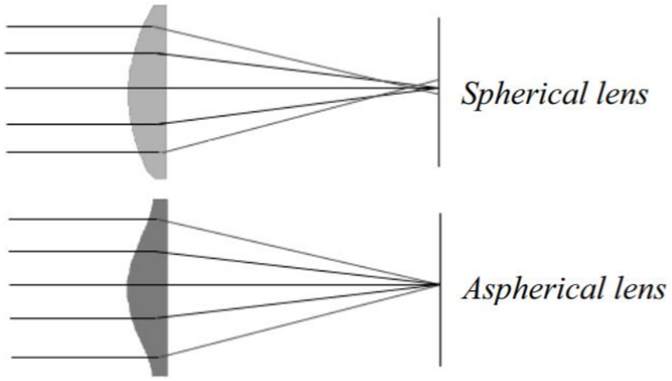

Fig. 1.1 Focusing of optical components [1]

Aspherical optical parts made of quartz glass, silicon carbide, tungsten carbide, single crystal silicon, single crystal germanium, etc. are used in a large number of engineering applications. Whether they are in the field of modern national defense technology or in the industrial field, they have broad application prospects.

However, while optical curved elements are widely used, their processing accuracy and surface quality are becoming more and more demanding. The surface accuracy of optical curved components is required to be developed to a few one-tenth of wavelengths, and the surface roughness requirements are developed from tens of nanometers to less than 5 nanometers.

In military applications, optical materials aspherical mirrors are widely used in laser guidance systems, radar ranging systems, aerospace, space telescopic camera systems,

infrared thermal imaging systems, and optical systems of optical instruments and devices, including military laser devices, thermal imaging devices, low-light night vision helmets, infrared scanning devices, and missile guides.

The aspherical optics in the new generation of weapon systems, the sights of fighters and helicopters, and the missile's aiming window can improve aerodynamic performance, expand the field of view, and reduce the volume and weight of parts. In terms of reconnaissance, aspherical optics are widely used in a new generation of spatial inspection cameras to improve the system's resolution. Expand the field of view and reduce system complexity, thereby directly reducing system weight to reduce launch costs [2-4].

Aspherical lenses also have advantages in civilian application. Instead of three spherical lenses used in the disc reader, an aspherical lens can be applied. It not only reduces the weight of the original optical lens, but also controls and corrects the axial aberration of the large numerical aperture. The aspherical lens is also used in the viewfinder of the digital camera and the lens of the projector to improve the performance of the product.

A large number of aspherical optical components are required in the production of camera zoom lens, camera lens, xenon lens in infrared wide-angle horizon, infrared remote monitors, video camera lens, video disc read heads, laser disc devices, fiber optic communication connectors, X-ray lens for medical diagnosis, indirect ophthalmoscopes, endoscopes, progressive lenses, digital cameras and CCD camera lenses.

In addition, aspherical optical components are also widely used in aerospace, nuclear, and important economic industries to increase the effective resolution. The required effective aperture of aspheric lens also has been enlarged, for example, the Hubble Space Telescope developed by NASA in 1990 (Fig. 1.2). It has a main diameter of 2.4 m [5].

Fig. 1.2 Hubble Space Telescope [5]

The market for aspheric optical parts is growing. High-performance optical lenses have become the difficulty of optical system design and manufacturing. Past grinding and polishing methods have low production efficiency and processing accuracy cannot be guaranteed. For workpieces with complex curved surfaces, they cannot even be machined. Conventional roughing, fine grinding, polishing, and aspherical optical components have been unable to meet the growing demands of high-quality aspherical element. Various aspherical processing technologies have emerged and developed continuously, and various ultra-precision aspherical processing technologies have appeared so far. For example, ultra-precision turning, grinding technology, polishing technology, copy molding technology and extension of some special processing technologies are currently widely used in production [6-8]. The polishing process is the last process in the optical surface ultra-precision manufacturing. However, the optical surface has a long polishing time and low productivity, and the entire polishing time accounts for more than 60% of the total manufacturing time. How to improve the polishing efficiency and enhance the certainty of the polishing process is a research bottleneck and hotspot in the field of ultra-precision optical manufacturing.

The processing of optical surfaces requires a series of processes, including styling,

grinding and polishing. The traditional polishing method only focuses on the improvement of the surface quality during the processing, and the deterministic removal of the surface material of the curved surface cannot be achieved. The uncertainty of the traditional polishing process makes it impossible to perform accurate process control and prediction of the results throughout the polishing process. These lead to not only the low polishing efficiency but also the poor quality.

Various polishing methods have been employed to study the influence of process parameters on surface quality to enhance certainty and controllability of the polishing process. Currently, the core issue with deterministic polishing is the relationship between material removal function per unit polishing time, residence time, moving path, and polishing removal. Overall material removal could be obtained through convolving the polishing removal function per unit time with the dwell time. When the total material removal has been obtained by actual measurement, the dwell time could be worked out through the inverse coiling operation. The polishing process is a linear shift-invariant system, and the polishing removal per unit polishing time does not change with position. For low-steep aspheric surfaces, this theory can be used to control the polishing process. However, for curved surfaces with more complex shapes, the time-dependent curvature of the polishing process and the complexity of the polishing posture make the applicability of the theory lower [9, 10]. This paper constructs a polished surface removal model considering the influence of polishing tool attitude, polishing path, surface geometry, physical properties and other factors. The influence of process parameters and condition changes on polishing removal is revealed, and the process control of deterministic material removal is realized.

1.2 The concept of aspherical and its equation

Aspherical surface is a curved surface without a certain radius of curvature. The aspheric optical surface includes the rotating aspheric surface with rotating symmetry axis, such as paraboloid, ellipsoid, asymptotic surface, hyperboloid, and the non-

rotating aspheric surface without symmetry axis, such as off-axis aspheric surface and free optical surface [11-13].

The aspheric surface is defined relative to the standard sphere. In the X-Z two-axis coordinate system, the radius of curvature of the shape from the center to the edge in the X-axis direction is continuously changed as compared with the standard spherical surface. There are two types of aspheric surfaces: secondary surfaces and high-order surfaces. There are also two types of secondary aspheric surfaces. The first type of surface has superior optical properties, with a pair of aberration-free points, the geometric focus of the quadratic curve. Such as rotating ellipsoids, paraboloids and hyperboloids. The second type of surface includes a cylindrical surface, a conical surface, and an oblate ellipsoid. High-order aspheric surfaces include monotonic meridian curves (monotonic surfaces) and non-monotonic surfaces (Schmidt and other types). For high-order aspheric surfaces, the corresponding secondary aspheric surface with the smallest deviation from it can be found. According to the type of structure, the aspherical surface includes two categories: a rotationally symmetric aspherical surface and a non-rotational symmetric aspheric surface. The rotational symmetrical aspheric surface is formed by rotating the workpiece busbar about its own axis of rotation. There are mainly secondary rotating surfaces such as ellipsoids, parabolas, and hyperboloids. Non-swirl symmetrical aspheric surfaces mainly refer to free optical surfaces. The axisymmetric aspheric surface can be represented by its meridian line equation. In practical applications, it is often represented by three forms of equations. The optical axis is the X axis (symmetry), and the origin is taken at the vertex.

The first type of aspheric meridian cut-off equation is shown,

$$y^2 = a_1 x + a_2 x^2 + a_3 x^3 + \cdots + a_n x^n \qquad (1.1)$$

$a_1,\ a_2,\ a_3, \ldots,\ a_n$ are equation coefficients.

The second type of aspheric meridian cut-off equation is shown,

$$x = A_1 y^2 + A_2 y^4 + A_3 y^6 + \cdots + A_4 y^{2n} \quad (1.2)$$

$A_1,\ A_2,\ A_3, \ldots,\ A_n$ are equation coefficients.

The third type of aspheric meridian cut-off equation is shown,

$$x = \frac{cy^2}{1+\sqrt{1-(k+1)c^2y^2}} + \sum_{i=2}^{n} B_i y^{2i} \quad (1.3)$$

c is the paraxial curvature, and *c = 1 / r*, where *r* is the radius of curvature of the vertex. *k* is a conic constant, also known as an eccentricity of quadratic surface, $k = -e^2$. *e* is the eccentricity rate. B_i is equation coefficient of high order term.

In Eq. (1.1) $a_1 = 2r,\ a_2 = e^2 - 1$, when the other items are *0*, then

$$y^2 = 2rx + (e^2 - 1)x^2 \quad (1.4)$$

It is the quadratic curve equation of the commonly used quadratic aspheric surface, and *e* is the eccentricity rate.

When $e^2 < 0$, the curve is a flat ellipse (the long axis is the y-axis).

When $e^2 = 0$, the curve is a circle.

When $0 < e^2 < 1$, the curve is elliptical (the long axis is the y-axis).

When $e^2 = 1$, the curve is parabolic.

When $e^2 > 1$, the curve is hyperbolic.

1.3 Aspherical ultra-precision machining detection and error compensation technology

Aspherical detection technology has always been a problem that limits the accuracy of aspheric manufacturing. Since the shape accuracy of optical aspherical parts cannot be accurately measured, the compensation processing cannot be performed [14-16]. At this stage, there are two main types of relatively mature aspheric surface detection technologies, one is contact detection and the other is non-contact detection.

The common contact detection is CMM (Coordinate Measuring Machine) triggered measurement method. It is applied to the surface of the workpiece by the measuring

probe of diamond with high hardness. The 3-d coordinate values of each point are measured, and the shape error of the aspheric surface is obtained (Fig. 1.3).

Fig. 1.3 Triggered measurement method by coordinate measuring machine [1]

The contact probe measurement method dominates the aspherical inspection market with its advantages of high precision, high resolution and convenient measurement. However, this method has high precision but low efficiency and is not suitable for detecting soft aspherical lens. In addition, this method can also be applied to in-position contact measurement of ultra-precision machining machines. According to the measurement principle, the following are included:

1. The contour projection method is amplified by the projected image of the workpiece and then transmitted to the CCD, and then converted into a digital signal input to the computer. After proper image pre-processing, the measurement results can be obtained by comparing the corresponding software with the theoretical aspheric curve equation. The measurement method can directly obtain the measurement result with low environmental requirements and can be used in each process of aspherical processing. The accuracy of the measurement system is mainly determined by

measuring the magnification of the objective lens and the pixels of the CCD.

2. The aberration-free detection method utilizes the aberration-free characteristic of a quadric surface. The reference light is interfered with the reflected light with the surface information of the lens under test, and the optical path is cut by the edge cutter at the aberration-free point. Observing the shadow map due to the interference, the face shape of the aspherical surface is determined by the interpretation of the shadow map.

3. The compensation interference method is also called null compensation. It is based on the aspheric surface being measured, and a compensating lens is designed to be attached to the interferometer together with the tested part. The plane wave or the spherical wave incident on the compensation lens is converted into a waveform having the same theoretical shape as the aspherical surface to be measured. And interference with the actual wave front of the measured aspheric surface to form interference fringes to achieve measurement. The design of the compensator is very important for compensating for interferometric measurements. In actual measurement, different compensators and corresponding measuring optical systems are often designed according to actual conditions.

4. Computer generated hologram (CGH) is essentially a compensating interferometry, except that the compensator hologram of the aspherical lens replaces the compensator. Computational holograms reproduce the wave front of an ideal aspheric surface and interfere with the actual wave front of the aspheric surface being measured. In this way, the zero-interferogram of the measured aspherical surface shape error is obtained, and the measurement is realized. When the aspherical surface is measured by the computer generated hologram, the main factor affecting the measurement accuracy is the calculation accuracy and positioning accuracy of the hologram. Due to the advancement of the process level, the precision and positioning accuracy of advanced computational holograms can reach a high level.

5. The shearing interferometry does not require the use of a reference mirror or other compensator to directly obtain the interference fringes of the aspherical lens under test. According to the specific shearing method, the shearing interference method can be further divided into transverse shearing interference method and radial shearing

interference method, and the former is more widely used.

The aspherical non-contact measuring machine is mainly based on the SSI-A series splicing interferometer of QED Company of USA and the white light interferometer of Zygo Company of the United States. It is mainly used for the surface quality detection and surface microscopic observation of aspherical workpieces.

1.4 Ultra-precision machining of aspheric surfaces

The idea of computer numerical control (CNC) was first proposed by W.J. Rupp of Itek in the United States in the early 1970s [16]. Since then, some developed countries led by the United States have conducted in-depth research on this. Representatives are REOSC of France, Optical Science Center of University of Arizona, Kodak Company, Optical Manufacturing Center of Roehester University, Itek, Perkin-Elmer, Tinsley, LLNL Laboratory of USA, Vovfov National Institute of Optics, and Russia.

The development of CNC technology continues to improve itself with the development of integrated technologies such as computers, precision measurement, new processes, and new materials. Every few years a new polishing technique moves from the laboratory to commercial applications. Such as ion beam polishing technology, magnetorheological polishing technology, plasma polishing technology and airbag precession polishing method.

1.4.1 Hot briquetting

Conventional polishing methods are not easy to make aspherical lenses, so it is necessary to use a mold to transfer the surface shape to the glass to form. First, put the pre-formed glass ball into the mold. At this time, the glass ball is still solid, and then the temperature is raised to above the *Tg*, so that glass could be sufficiently heated, and the glass is easily deformed [17]. After that, it turns into the shape of the aspherical surface of the mold, and then passes through steps such as cooling and demolding, and finally takes out the finished product (Fig. 1.4).

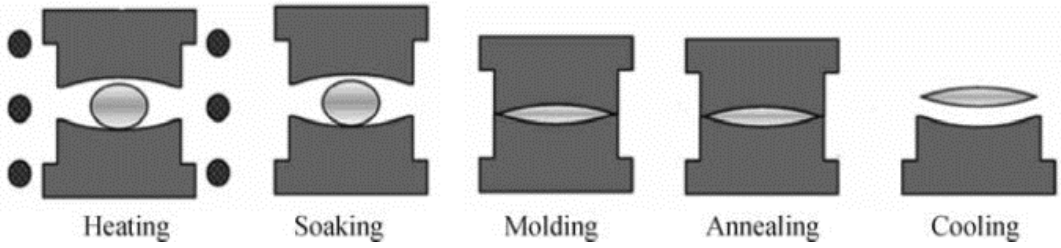

Fig. 1.4 Schematic diagram of hot briquetting process [17]

1.4.2 Ion beam polishing

Ion beam polishing uses charged high-energy ions, which are directed by the ion gun to the workpiece under vacuum, and the material is removed by the ion beam energy transfer under the bombardment of the ion beam. Since ion beam polishing can be removed to an atomic level, ion beam polishing can achieve very high precision. Ion beam polishing is recognized as a shaping process rather than a polishing process. Ion beam polishing method has achieved great success in correcting the shape of a 1.8 m hexagonal symmetrical mirror (Fig. 1.5). This Zerodur mirror was developed for the Keck telescope. During processing, a 25 mm diameter neutral Ar ion beam was processed in a 2.5 m^3 vacuum chamber for 55 hours to reduce the surface profile error from 350 nm to 60 nm and the surface roughness to less than 1 nm. With a small removal rate, the amount of material removed can be reduced [18-21].

Fig. 1.5 The vacuum chamber of the ion beam facility [21]

Compared to conventional optical processing methods that rely on mechanical removal, ion beam polishing includes the following advantage:

1. Deterministic removal of materials at atomic scale.
2. A complete correction of the surface error can be achieved in one polishing cycle, which can reduce the manufacturing cycle of processing, inspection and processing.
3. The process is not sensitive to vibration and temperature.
4. Could process spherical, aspherical and free-form surfaces. Edge effects in conventional polishing methods do not occur during ion beam polishing.

Disadvantages of ion beam polishing are the polishing equipment system is very complicated and the polishing cost is high. Due to the limited energy of the ion beam, the removal speed is low, and processing is difficult to control.

1.4.3 Jet polishing

Compared with traditional polishing technology, jet polishing has the advantages of no tool wear, no heat influence, and high processing flexibility (Fig. 1.6). Jet polishing

is commonly used to polish hard and brittle materials such as optical glass, quartz and ceramics. The jet direction, nozzle shape, target distance and liquid pressure during jet polishing have an effect on material removal [22-24]. At present, the theory of water jet polishing is not very mature, and many problems have not been solved, such as abrasive agglomeration and nozzle clogging. In addition, most of the literature mainly studies the surface roughness of jet polishing, and the research on improving the surface profile by jet polishing has been rarely reported [25-27].

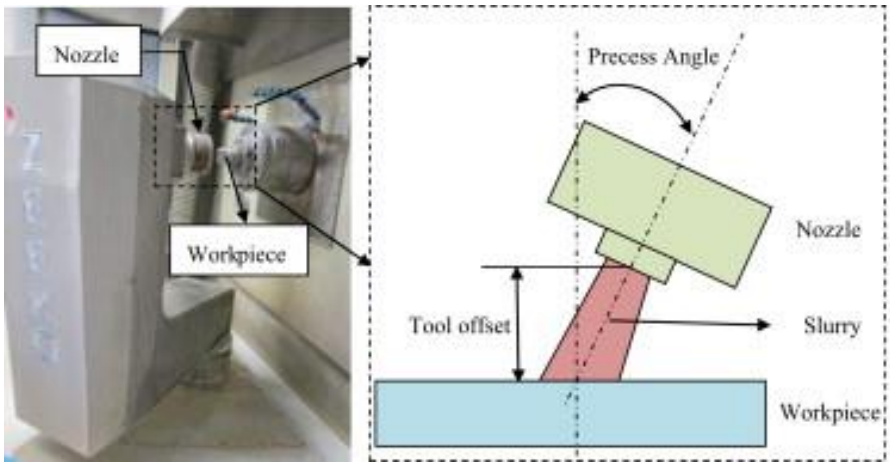

Fig. 1.6 Configuration of jet polishing [27]

1.4.4 Magnetorheological Finishing (MRF)

Magnetorheological finishing techniques emerged in the early 1990s and were invented by W.I. Kordonski, I.V. Prokhorov and their collaborators [28]. It uses a magnetorheological finishing fluid to undergo rheology in a gradient magnetic field to form a Bingham medium with a viscoelastic state to polish the workpiece [29, 30]. The surface accuracy, surface roughness and subsurface damage layer of the workpiece after processing are better than the traditional polishing method, and it is an ideal process for obtaining an ultra-smooth optical surface (Fig. 1.7). In 2004, QED used magnetorheological finishing technology to increase the surface accuracy of a 400 mm single crystal spherical mirror from root mean square (RMS): 120.8 nm to RMS: 5.8

nm in 2 hours. Magnetorheological polishing technology demonstrates efficient and superior polishing capabilities.

Magnetorheological polishing is a major revolution in traditional polishing methods. The main advantages are as follows:

1. There is no polishing disc wear, the polishing removal characteristics are stable, and the processing precision is high.
2. Capable of polishing various complex surfaces such as spherical surfaces, aspheric surfaces, and asymmetric free-form surfaces.
3. Due to the shearing force between the workpiece and the forging projection in the magnetorheological polishing, the subsurface damage layer can be reduced, and it is suitable for processing ultra-thin optical components (the diameter-thickness ratio is greater than 10:1).
4. Processing speed, high efficiency. Debris and heat during processing can be removed in time to avoid affecting polishing accuracy.

The disadvantage of magnetorheological polishing is that the stability of the magnetic field is difficult to control. Only small diameter optical workpieces can be processed and concave surfaces with high steepness cannot be processed [31-33].

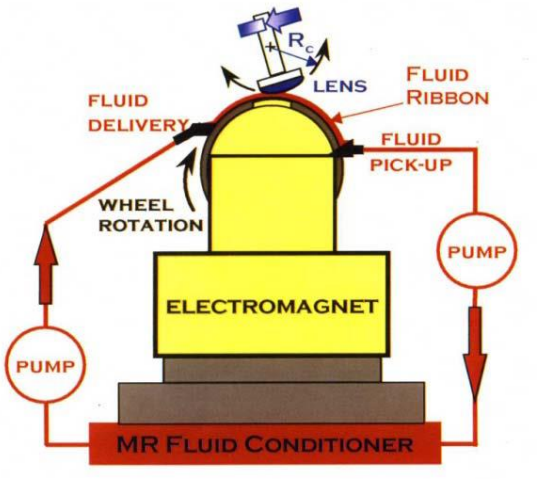

(a) Schematic diagram of magnetorheological polishing

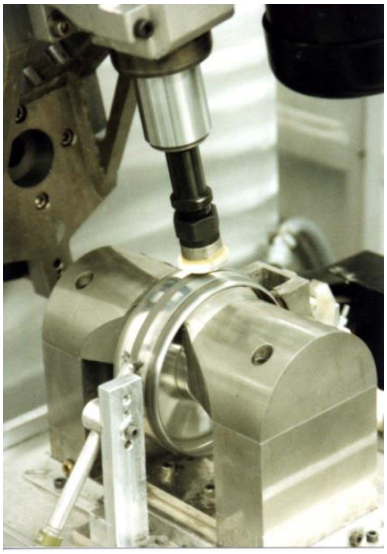

(b) Workbench of magnetorheological polishing

(c) Magnetorheological polishing machine by QED

Fig. 1.7 Magnetorheological polishing technology [33]

1.4.5 Plasma polishing technology

In plasma polishing, a hot reaction gas is sprayed through a hollow cathode nozzle toward the surface of the workpiece to chemically react the material into a gas for removal. The reaction gases SF_6, NF_3, CF_4 can be used to process SiO_2 and SiC, and the reaction gas Cl_2 can be used to process Be. The experiment was carried out in a sealed cylindrical stainless-steel container. The material removal rate is a non-linear function. Because heating requires 30 s, compensation could be achieved through controlling the nozzle. The removal rate at the peak of the chemical pairing between the gas and the surface of the workpiece is 1 μm/min, keeping the distance between the nozzle and the workpiece not more than 500 μm, and removal speed is stable at 0.3%. The workpiece is moved to vaporize the surface of the workpiece to 0.1 μm for polishing. When the nozzle is scanned to a surface that does not need to be removed, the plasma removal speed is reduced. Diameter of 160 mm, the surface error is peak value (PV): 0.5 μm dissolved silicon aspheric surface, after 3 polishing cycles, a total of 3.8 hours of polishing time, the surface error is reduced to PV: 130 nm, RMS: 17 nm [34-36].

The advantage of plasma polishing technology is that polishing does not cause stress damage to the surface of the workpiece. The polishing process is highly efficient and non-polluting. Spherical, aspherical and free surfaces can be processed without edge effects.

The disadvantages of plasma polishing technology are the application range is small, and only the material that chemically reacts with the reaction gas can be processed, the chemical reaction process in the process is difficult to control [37-39].

1.4.6 Air bag precession polishing

The IRP series airbag pre-polishing machine is a 7-axis CNC polishing device developed by ZEEKO and the University of London, as shown in Fig. 1.8. The polishing shaft is one of the key components of the airbag precession polishing machine.

It mainly includes precision bearings, drive motors, polishing airbags, spindles, load monitoring systems and other components. The loading unit of the spindle is also equipped with an overload protection device. The spindle speed is from 0 to 3000 rpm.

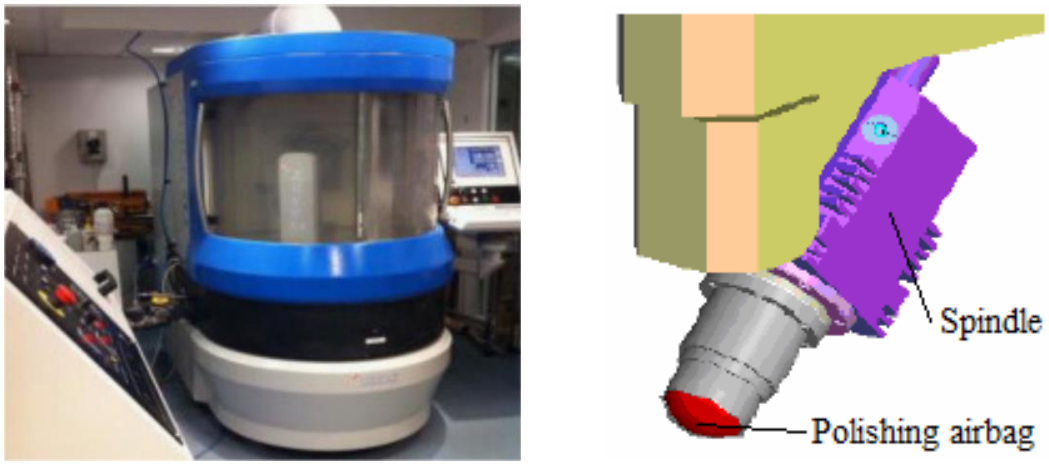

(a) Air bag precession polishing (b) Polishing unit of airbag pre-polishing machine

Fig. 1.8 Air bag precession polishing machine and polishing spindle [27]

The polishing head is fixed to the lower end of the main shaft and consists of three parts. The base is a spherical cap-shaped rubber bladder filled with a gas or a liquid. The middle layer is a reinforcing layer, and a fiber cloth having a high tensile strength and a thin thickness is attached to the spherical crown surface of the rubber bag. The outermost layer in contact with the workpiece is a polyurethane polishing film having a thickness of about 4 mm and is firmly adhered to the reinforcing layer with a glue. The flexible airbag is mounted on the polishing main shaft, and a closed cavity is formed in the airbag, and a low-pressure gas is filled in the cavity, and the pressure of the gas can be adjusted in real time. The airbag itself as a polishing tool not only has good flexibility, but also has a certain strength and has a good resistance to deformation. The polishing head is applied to the surface of the workpiece at a certain approaching distance, so that the airbag spherical surface will undergo some deformation. It is in close contact with the surface of the workpiece to form a polished contact area. At the same time, a polishing liquid is added between the airbag and the surface of the workpiece. The tiny abrasive particles in the polishing solution will mechanically and chemically interact with the surface of the workpiece to remove the material. In the

process, the polishing head speed, the screwing angle, the polished contact area and the pressure can be optimized as process parameters for the polishing process [40, 41].

Airbag polishing has the advantages of high processing efficiency, good surface quality, low cost, high automation and easy operation. It is a deterministic optical processing method. Compared with other polishing methods, airbag polishing has the following characteristics:

1. The polishing tool is a flexible air bag that can conform well to the surface of the workpiece due to the elastic deformation of the air bag. All partial polishing zones are removed in the same amount, which is very important for improving surface roughness and controlling surface accuracy.
2. The special pre-polishing process ensures uniform polishing in all directions, and a Gaussian removal function and smooth polishing scratches are also obtained, which facilitates numerical optimization of the removal of the airbag polishing material and ensures the quality of the entire process.
3. The contact pressure is controllable. The control of the polishing process is achieved by adjusting the position of the balloon to the workpiece and the pressure inside the bladder. Position adjustment and pressure adjustment can be done independently, which enhances the flexibility of polishing parameter selection.
4. High-precision workpieces can be machined with low-precision machines. In the airbag polishing method, the surface profile accuracy of the workpiece is mainly ensured. Under the condition that the precision of the polishing machine is roughly equivalent to that of the ordinary machine tool, the surface with high surface precision can also be processed [42].

1.4.7 Computer controlled polishing

The core idea of computer controlled polishing was proposed by Rupp in the early 1970s [43]. With the small diameter polishing tool head moving along the path along the surface of the workpiece, the wear can be controlled by adjusting the tool head speed

and polishing pressure [44-46].

In the actual calculation of the control machine polishing, the relative linear speed and the contact pressure are kept constant, and the polishing surface residence time is changed to correct the curved surface shape. The computer controlled polishing technology utilizes computer control to achieve high speed, high precision and high efficiency, and is especially suitable for processing large-diameter aspheric optical components [47-49].

1.5 Development of aspherical ultra-precision machining machines

Ultra-precision aspherical turning and grinding technology uses numerical control technology, and aspherical ultra-precision machining is inseparable from computer numerical control ultra-precision machine tools, which determine the quality and performance of industrial products [50-55].

At present, the main manufacturers of ultra-precision machine tools are Moore Precision Machine Tool Company and Precitech Precision Company of the United States, Rank Pneumo Precision Company of the United Kingdom, Toshiba Machine Company of Japan, Toyota Machine JTEKT and NAGASE-i. Companies, as well as companies and research institutions in Germany and the Netherlands [56-60].

The main products produced and sold by Moore Precision Machine Tool Co., Ltd. are Moore M-18, M-40 aspherical processing machine and Moore-T bed machine. Precitech Precision's Freeform 204, Nanoform 2000, Optimum 2400 series aspherical machining machines with fully enclosed feedback for CNC. The feed resolution is up to 1 nm.

The products produced by Punnamemo Precision of the United Kingdom mainly include MSG-325, ASG-2500, Nanform 600 and Ultra 2000. After October 1997, Precitech of the United States merged with the company of Rank Pneumo of the United Kingdom. The company continues to operate under the name Precitech. These machines are not only capable of cutting but also grinding with diamond wheels. It can

process aspherical metal mirrors with a diameter of 300 mm. The shape accuracy of the machined workpiece is 0.3-0.16 μm and the surface roughness (Ra) is 0.01μm. Nanoform250 ultra-precision machining system is a two-axis ultra-precision CNC machine. Ultra-precision turning, and ultra-precision grinding are possible on this machine, as well as ultra-precision polishing (Fig. 1.9). The most outstanding feature is the ability to directly grind optical components of hard and brittle materials that meet the requirements of optical systems [61].

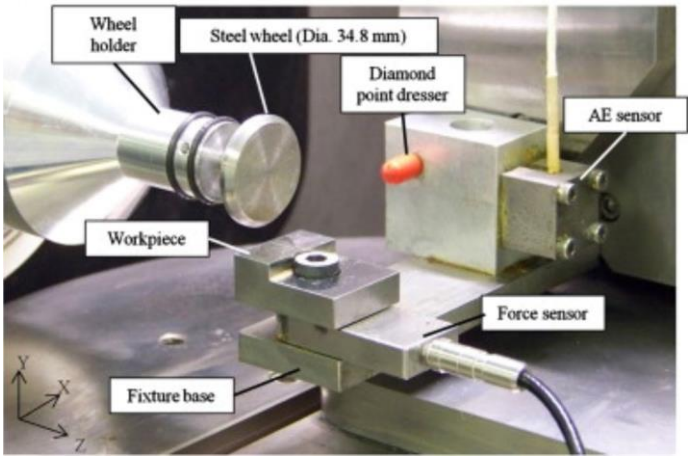

Fig. 1.9 Setup of Nanoform250 Ultra machining center [61]

The CUPE Precision Machining Institute at Cranfield University in the UK is one of the most renowned precision engineering institutes in the world. The OAGM-2500 large ultra-precision machine tool developed by the institute is used for large-scale curved mirrors for precision grinding and coordinate measuring X-ray astronomical telescopes.

TOSHIBA MACHINE's ULC-100, ULG-100 series of ultra-precision aspheric machines are mainly used for diamond turning and grinding. There are 2, 3 and 4 axes to control a variety of models. The main shaft adopts high rigidity and ultra-precision air static bearing, and the numerical control adopts fully enclosed feedback. Feed resolution is up to 10 nm. It can process a variety of optical parts and aspheric lens molds. The metal mold uses a diamond cutter and a grinding wheel for turning and

grinding to achieve mirror quality.

The ultra-precision aspherical machining machine ULG series developed by Toshiba Machinery has its own aerostatic main shaft, VV type rolling bearing, automatic correction function with optical mode resolution of 1 nm, inclined axis table, A-axis turntable, B-axis turntable, additional ultra-precision electronic instruments (Fig. 1.10). For the grinding of large-diameter lenses, cutting and grinding of small-diameter lens molds, micro-groove processing of free-form surfaces, in-position measurement and correction. ULG-100A (H) ultra-precision multi-tasking machine tool, which uses the method of controlling two axes separately to realize the cutting and grinding of the aspherical lens mold. The X-axis and Z-axis strokes are 150 mm and 100 mm respectively. The feedback element is a grating with a resolution of 0.01 μm [62].

Fig. 1.10 Japan TOSHIBA ULG Series [62]

The ultra-precision machine tools of AHN05, AHN15 and AHN15-3D series developed by JTEKT TOYOTA can be extended to 5-axis machining with a minimum resolution of 1 nm and a maximum machining diameter of 150 mm.

The RG series of ultra-precision machining machines developed by NAGASE-i in Japan can also achieve high-performance machining. In addition, the Japan Institute of Physical Chemistry has developed a UPL six-axis machine tool for online electrolytic

dressing compound grinding technology. High hard and high brittle electronic and optical materials such as spherical, aspheric and planar lenses, as well as plastic metal parts. The size and shape are accurate to sub-micron and the surface roughness is up to nanometer.

Japan FINETECH Company developed the SGT-n small lens grinding machine with a feed resolution of up to 1 nm and a super high-speed spindle (80000 rpm) for processing small diameter optical molds. Japan's Nachi has also developed the corresponding ASP series of aspherical machining machines.

In the field of ultra-precision polishing machines, QED Corporation of the United States has developed and produced magnetorheological series polishing equipment such as Q22-XE, Q22-400X, Q22-X/Y and Q22-750P. At the same time, magnetic jet processing equipment is being developed for ultra-precision polishing of tiny optical components and optical molds.

The computerized numerical control polishing equipment developed by the Optical Center of the University of Arizona and the Optical Manufacturing Center of the University of Rochester in the United States has automated the production of aspheric lens polishing. ALG100 computer numerical control aspherical grinding machine and ALP100 computer numerical control aspherical polishing machine manufactured by SCHEIDER Optical Machinery Co., Germany. The production of aspherical optical parts can be performed efficiently [63-71].

1.6 Purposes and scope of this study

In the conventional polishing method, the deviation of the polishing direction may result in polishing stripes. Therefore, in order to improve the surface roughness, it is necessary to polish with the same position of the tool. In addition, when polishing is performed using the end face of the circular tool, a circumferential speed difference is generated in the radial direction, and material removal becomes unstable. In this study, in order to solve these problems, a rotation and revolution polishing (RRP) method was

designed to polish aspheric lens molds.

The traditional polishing removal model can only predict the depth of removal during fixed point polishing. In view of the above deficiencies, this thesis establishes a material removal profile model for moving and polishing. The removal is related to the contact pressure at that point, relative linear velocity and feed rate. The pressure and relative linear speed are modeled according to the contact and tool attitude. The polished removal depth for the unit path length is integrated. The flow chart of the paper is shown in Fig. 1.11.

In chapter one, the definition of aspheric surfaces, aspherical curve equations are introduced. Next, the measurement method of the aspherical surface will be described. The current ultra-precision manufacturing method is also introduced. Finally, in this chapter, the ultra-precision machine tools with excellent performance are described in detail. The purpose of the research and the composition of the doctoral thesis are also described.

In chapter two, the rotation and revolution polishing method was used as a polishing method for an aspherical lens mold. It improves the uniformity and density of path and can process a variety of molds. The structure will be detailed in the next chapter. The experimental and measurement equipment of this paper has also been introduced. The selection of the polishing solution and the truing of the tool are also described in detail. This rotation and revolution polishing device needs to be simple in structure, low in cost and stable in processing. The basic parameters of 3D modeling are calculated and then 3D modeling is built using SolidWorks software.

In chapter three, discusses and describes material removal of the fixed point and plain optical glasses by rotation and revolution type polishing. The mathematical model of the single path scanning type polishing method is studied. The workpiece entire surface was polished, and the characteristics were discussed. In the end of this chapter, we expand on the previous content and builds a material removal model at the vertical bisector of the corner.

In chapter four, the small-diameter polishing tool is used to mount the three-axis CNC machine tool for the entire plane polishing. The plane previously polished by the

rotation and revolution polishing (RRP) method is not ideal. This chapter continues the previous mathematical theory and perfected the rotation and revolution polishing (RRP) method for point, line, and surface studies. In this chapter, a model based on the Preston equation is built and the model is validated. The polishing characteristics of the Ni-P surface were discussed, and an ultra-smooth surface was finally obtained by scanning polishing.

In chapter five, the conclusions of the paper are summarized, and the prospects for future research are also presented.

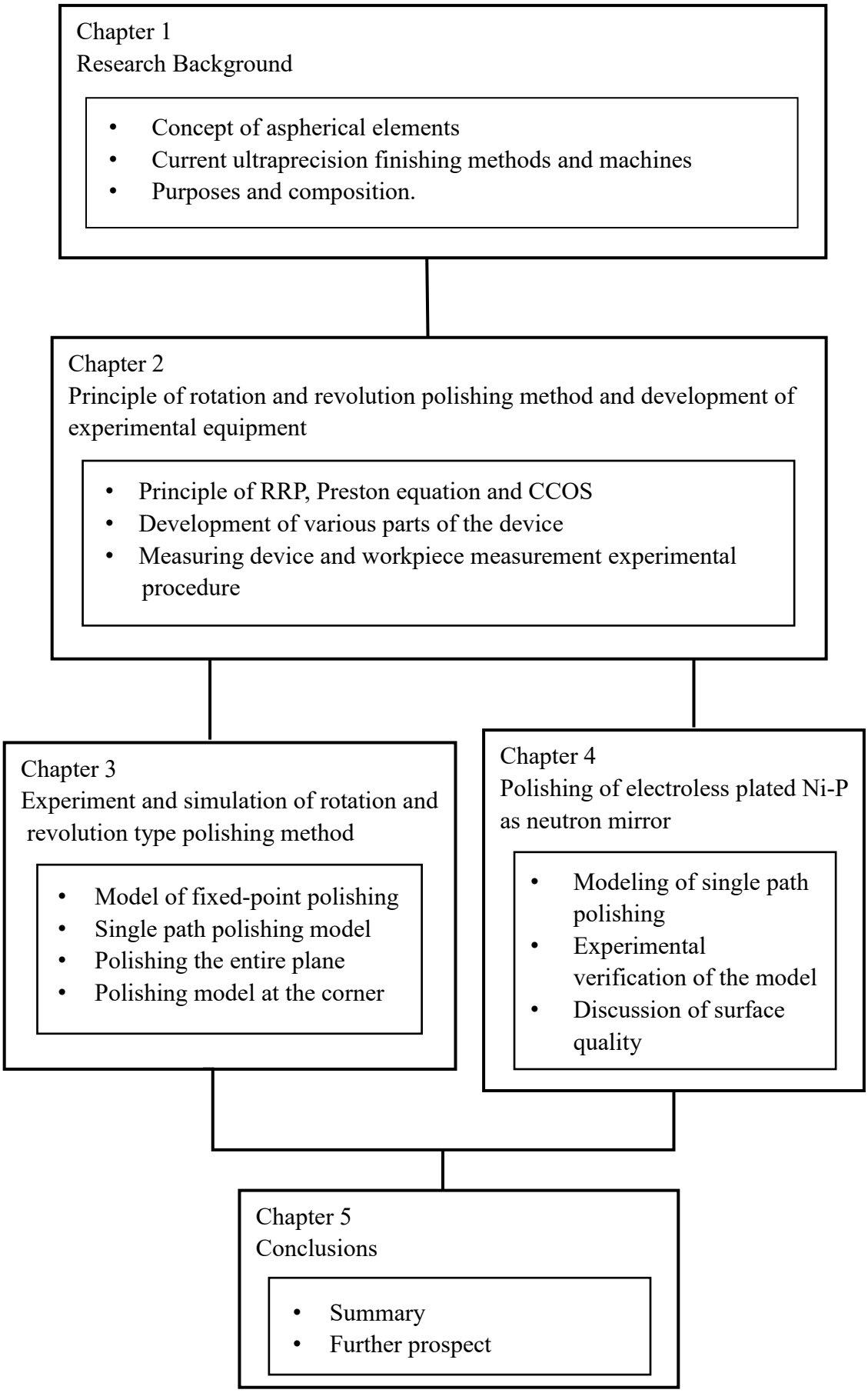

Fig. 1.11 Flow chart of this study

References

[1] R. Henselmans, Non-contact measurement machine for freeform optics, PhD thesis, Technical University of Eindhoven (2009).

[2] L. Zhang, D.P. Huang, W.S. Zhou, C. Fan, S.J. Ji and J. Zhao: Corrective polishing of freeform optical surfaces in an off-axis three-mirror imaging system, The International Journal of Advanced Manufacturing Technology, **88** (2017) 2861-2869.

[3] Y. Xie and B. Bhushan: Effects of particle size, polishing pad and contact pressure in free abrasive polishing, Wear, **200** (1996) 281-295.

[4] H. Park: A solution for NURBS modelling in aspheric lens manufacture, The International Journal of Advanced Manufacturing Technology, **23** (2004) 1-10.

[5] M. Hassanalian, D. Rice and A.Abdelkefi: Evolution of space drones for planetary exploration: A review, Progress in Aerospace Sciences, **97** (2018) 61-105.

[6] M. Vadali, C. Ma, N.A. Duffie, X. Li and F.E. Pfeferkorn: Pulsed laser micro polishing: surface prediction model, Journal of Manufacturing processes, **14** (2012) 307-315.

[7] T.R. Lin: An analytical model of the material removal rate between elastic and elastic-plastic deformation for a polishing process, The International Journal of Advanced Manufacturing Technology, **32** (2007) 675-681.

[8] A. Roswell, F.J. Xi and G. Liu: Modelling and analysis of contact stress for automated polishing, International Journal of Machine Tools and Manufacture, **46** (2006) 424-435.

[9] F. Klocke and R. Zunke: Removal mechanisms in polishing of silicon based advanced ceramics, CIRP Annals-Manufacturing Technology, **58** (2009) 491-494.

[10] Y. Zhao and L. Chang: A micro-contact and wear model for chemical mechanical polishing of silicon wafers, Wear, **252** (2002) 220-226.

[11] A. Yi, C. Huang, F. Klocke, C. Brecher, G. Pongs and M. Winterschladen: Development of a compression molding process for three-dimensional tailored free-form glass optics, Applied Optics, **45** (2006) 6511-6518.

[12] W. Sun, J.W. McBride and M. Hill: A new approach to characterizing aspheric surfaces, Precision Engineering, **34** (2010) 171-179.

[13] F. Fang, X. Zhang, A. Weckenmann, G. Zhang and C. Evans: Manufacturing and measurement of freeform optics, CIRP Annals, **62** (2013) 823-846.

[14] H. Aceves-Campos: Profile identification of aspheric lenses, Applied Optics, **37** (1998) 8149-8150.

[15] H. Wang and W.M. Lin: Removal model of rotation & revolution type polishing method, Precision Engineering, **50** (2017) 515-521.

[16] M. Schinhaerl, G. Smith and R. Stamp: Mathematical modelling of influence functions in computer-controlled polishing: Part II. Applied Mathematical Modelling, **32** (2008) 2907-2924.

[17] S.H. Yin, H.P. Jia, G.H. Zhang, F.J. Chen and K.J. Zhu: Review of small aspheric glass lens molding technologies, Frontiers of Mechanical Engineering, **12** (2017) 66-76.

[18] L. Zhou, Y. Dai and X. Xie: Optimum removal in ion-beam figuring, Precision Engineering, **34** (2010) 474-479.

[19] G. Carter, M. Nobes and I. Katardjiev: The theory of ion beam polishing and machining, Vacuum, **44** (1993) 30330-30339.

[20] K. Soyama, W. Ishiyama and K. Murakami: Enhancement of reflectivity of multilayer neutron mirrors by ion polishing: optimization of the ion beam parameters, Journal of Physics and Chemistry of Solids, **60** (1999) 1587-1590.

[21] P. Gailly, J.P. Collette, K.F. Frenette and C. Jamar: Ion beam figuring of CVD silicon carbide mirrors, Proceedings of 5th International Conference on Space Optics, **554** (2004) 691-697.

[22] S.M. Booij, B.H. Van and O.W. Fähnle: A mathematical model for machining spot in Fluid Jet Polishing, Optical Fabrication and Testing, **42** (2000) 70-72.

[23] F. Tsai, B. Yan and C. Kuan: A Taguchi and experimental investigation into the optimal processing conditions for the abrasive jet polishing of SKD61 mold steel, International Journal of Machine Tools and Manufacture, **48** (2008) 932-945.

[24] S.M. Booij, B.H. Van, J.J Braat: Nanometer deep shaping with fluid jet polishing, Optical engineering, **41** (2002) 1926-1931.

[25] O.W. Fähnle, H. Brug, H.J. Frankena: Fluid jet polishing of optical surfaces,

Applied Optics, **37** (1998) 6771-6773.

[26] H. Fang, P. Guo and J. Yu: Surface roughness and material removal in fluid jet polishing, Applied optics, **45** (2006) 4012-4019.

[27] Z.C. Cao and C.F. Cheung: Theoretical modelling and analysis of the material removal characteristics in fluid jet polishing, International Journal of Mechanical Sciences, **89** (2014) 158-166.

[28] C. Fan, J. Zhao, L. Zhang, W.S. Zhou and L.N. Sun: Local material removal model considering the tool posture in deterministic polishing, Proceedings of the Institution of Mechanical Engineers, Part C: Journal of Mechanical Engineering Science, **230** (2016) 2660-2675.

[29] W.M. Lin, H. Wang and F.M. Ji: Research on effect of parameters in Rotation & Revolution Type Polishing Method, Procedia CIRP, **71** (2018) 358-363.

[30] S.N. Shafrir, J.C. Lambropoulos and S.D. Jacobs: A magnetorheological polishing based approach for studying precision microground surfaces of tungsten carbides, Precision engineering, **31** (2007) 83-93.

[31] T. Wang, H.B. Cheng and Z.C. Dong: Removal character of vertical jet polishing with eccentric rotation motion using magnetorheological fluid, Journal of Materials Processing Technology, **213** (2013) 1532-1537.

[32] D. Golini, M. DeMarco, W. Kordonski and J. Bruning: MRF polishes calcium fluoride to high quality, Optoelectronics World, **37** (2001) S5.

[33] D.C. Harris: History of Magnetorheological Finishing, Proceedings of SPIE - The International Society for Optical Engineering, **8016** (2011) 561-566.

[34] E.E. Yunata, T. Aizawa: Micro-grooving into thick CVD diamond films via hollow-cathode oxygen plasma etching, Manufacturing letter, **8** (2016) 16-20.

[35] E.E. Yunata, T. Aizawa, K. Tamaoki and M. Kasugi: Plasma Polishing and Finishing of CVD-Diamond Coated WC (Co) Dies for Dry Stamping, Procedia Engineering, **207** (2017) 2197-2202.

[36] E.E. Yunata, T. Aizawa: Plasma oxidation polishing and printing into CVD-diamond coatings, International conference for technology of plasticity, (2016) 251-252.

[37] H.B. Hermanns, C. Long and H. Weiss: ECR plasma polishing of CVD diamond films, Diamond and Related Materials, **5** (1996) 845-849.

[38] H. Zeidler and F. Boettger-Hiller: Surface finish machining of medical parts using plasma electrolytic polishing, Procedia CIRP, **49** (2016) 83-87.

[39] E.E. Yunata, T. Aizawa: Micro-texturing into DLC/diamond coated mold and dies via high density oxygen plasma etching, Manufacturing review, **2** (2015) 1-7.

[40] N. Suzuki, Y. Hashimotoa, H. Yasuda, S. Yamaki and Y. Mochizuki: Prediction of polishing pressure distribution in CMP process with airbag type wafer carrier, CIRP Annals, **66** (2017) 329-332.

[41] J. Zhan: An improved polishing method by force controlling and its application in aspheric surfaces ballonet polishing, The International Journal of Advanced Manufacturing Technology, **68** (2013) 2253-2260.

[42] S. Jianfeng, Y. Yingxue and X. Dagang: Effects of polishing parameters on material removal for curved optical glasses in bonnet polishing, Chinese Journal of Mechanical Engineering, **21** (2008) 29-32.

[43] J. Guo, H. Suzuki, S.Y. Morita, Y. Yamagata and T. Higuchi: A real-time polishing force control system for ultraprecision finishing of micro-optics, Precision Engineering, **37** (2013) 787-792.

[44] L. Kong and C. Cheung: Prediction of surface generation in ultra-precision raster milling of optical freeform surfaces using an Integrated Kinematics Error Model, Advances in Engineering Software, **45** (2012) 124-136.

[45] R.A. Jones and W.J. Rupp: Rapid optical fabrication with computer-controlled optical surfacing, Optical Engineering, **30** (1991) 1962-1968.

[46] L. Ho, C. Cheung and S. To: An experimental investigation of surface generation using an integrated ultra-precision polishing process and different polishing trajectories, Proceedings of the Institution of Mechanical Engineers, Part B: Journal of Engineering Manufacture, **226** (2012) 203-220.

[47] R.A. Jones: Computer simulation of smoothing during computer-controlled optical polishing, Applied optics, **34** (1995) 1162-1169.

[48] M. Schinhaerl, G. Smith and R. Stamp: Mathematical modelling of influence

functions in computer-controlled polishing: Part I. Applied Mathematical Modelling, **32** (2008) 2888-2906.

[49] F. Chen, S. Yin and H. Huang: Profile error compensation in ultra-precision grinding of aspheric surfaces with on-machine measurement, International Journal of Machine Tools and Manufacture, **50** (2010) 480-486.

[50] K. Lee, P. Wong and J. Zhang: Study on the grinding of advanced ceramics with slotted diamond wheels, Journal of Materials Processing Technology, **100** (2000) 230-235.

[51] H.B. Cheng, Z.J. Feng, K. Cheng and Y.W. Wang: Design of a six-axis high precision machine tool and its application in machining aspherical optical mirrors, International Journal of Machine Tools and Manufacture, **45** (2005) 1085-1094.

[52] E. Ukar, A. Lamikiz and L. Lacalle: Laser polishing of tool steel with CO2 laser and high-power diode laser, International Journal of Machine Tools and Manufacture, **50** (2010) 115-125.

[53] L. Zhang, X.S. He and H.R. Yang: An integrated tool for five-axis electrorheological fluid-assisted polishing, International Journal of Machine Tools and Manufacture, **50** (2010) 737-740.

[54] J. Lu, Q. Yan and H. Tian: Polishing properties of tiny grinding wheel based on Fe3O4 electrorheological fluid, Journal of Materials Processing Technology, **209** (2009) 4954-4957.

[55] T. Kuriyagawa, M. Saeki and K. Syoji: Electrorheological fluid-assisted ultra-precision polishing for small three-dimensional parts, Precision engineering, **26** (2002) 370-380.

[56] D.D. Walker, D. Brooks, A. King: The Precessions tooling for polishing and figuring flat, spherical and aspheric surfaces, Opt Express, **11** (2003) 958-964.

[57] W. Xu, X. Lu and G. Pan: Ultrasonic flexural vibration assisted chemical mechanical polishing for sapphire substrate, Applied Surface Science, **256** (2010) 3936-3940.

[58] T. Kuriyagawa, M. Saeki and K. Syoji: Electrorheological fluid-assisted ultra-precision polishing for small three-dimensional parts, Precision engineering, **26** (2002)

370-380.

[59] J. Lu, Q. Yan and H. Tian: Polishing properties of tiny grinding wheel based on Fe3O4 electrorheological fluid, Journal of Materials Processing Technology, **209** (2009) 4954-4957.

[60] M. Vadali, C. Ma and N.A. Duffie: Pulsed laser micro polishing: Surface prediction model, Journal of Manufacturing Processes, **14** (2012) 307-315.

[61] T. T. Öpöz and X. Chen: Experimental investigation of material removal mechanism in single grit grinding, International Journal of Machine Tools and Manufacture, **63** (2012) 32-40.

[62] A. Chen, C. M. Chen and J. R. Chen: Toolpath generation for diamond shaping of aspheric lens array, Journal of Materials Processing Technology, **192** (2007) 194-199.

[63] H. Suzuki, S. Hamada and T. Okino: Ultraprecision finishing of micro-aspheric surface by ultrasonic two-axis vibration assisted polishing, CIRP Annals Manufacturing Technology, **59** (2010) 347-350.

[64] F. Fang and G. Zhang: An experimental study of edge radius effect on cutting single crystal silicon, The International Journal of Advanced Manufacturing Technology, **22** (2003) 703-707.

[65] L. Zhang, X.S. He and H.R. Yang: An integrated tool for five-axis electrorheological fluid-assisted polishing, International Journal of Machine Tools and Manufacture, **50** (2010) 737-740.

[66] S. Oh and J. Seok: An integrated material removal model for silicon dioxide layers in chemical mechanical polishing processes, Wear, **266** (2009) 839-849.

[67] D.P. Yu, Y.S. Wong and G.S. Hong: A novel method for determination of the subsurface damage depth in diamond turning of brittle materials, International Journal of Machine Tools and Manufacture, **51** (2011) 918-927.

[68] J. Seok, C.P. Sukam and A.T. Kim: Multiscale material removal modeling of chemical mechanical polishing, Wear, **254** (2003) 307-320.

[69] F. Shi and B. Zhao: Modeling of chemical-mechanical polishing with soft pads, Applied Physics A: Materials Science & Processing, **67** (1998) 249-252.

[70] T. Leung, W. Lee and X. Lu: Diamond turning of silicon substrates in ductile-regime, Journal of Materials Processing Technology, **73** (1998) 42-48.

[71] J. Yan, K. Syoji and T. Kuriyagawa: Ductile regime turning at large tool feed, Journal of Materials Processing Technology, **121** (2002) 363-372.

Chapter 2 Principle of rotation and revolution polishing method and development of experimental equipment

In this chapter, the rotation and revolution polishing method was suggested as a polishing method for an aspherical lens mold. It improves the uniformity and density of path and can process a variety of molds. The structure will be detailed in the following section. The experimental and measurement equipment of this paper has also been introduced. The selection of the polishing solution and the truing of the tool are also described in detail. This rotation and revolution polishing device needs to be simple in structure, low in cost and stable in processing. The basic parameters of 3D modeling are calculated and then 3D modeling is built using SolidWorks software.

2.1 Polishing of mold in injection molding method

Injection molding is realized by injecting a material that is heated and melted into a mold, cooling and solidifying. This method is suitable for mass production of complex shape products. The injection molding process consists of six steps: mold clamping, injection molding, holding, cooling, mold opening and product ejection. In order to achieve high replication quality of products and long service life of the mold, the requirements for the shape accuracy and roughness of the mold are strict. In the conventional polishing method, the deviation of the polishing direction may result in polishing stripes [1-3]. Therefore, in order to improve the surface roughness, it is necessary to polish with the same position of the tool. In addition, when polishing is performed using the end face of the circular tool, a circumferential speed difference is generated in the radial direction, and material removal becomes unstable [4-9].

When polishing an aspherical lens mold, a method of polishing using a mold and a polishing tool in reverse rotation is always performed. The purpose of this method is to make the directionality of the polishing unidirectional by the rotation of the mold. Since the mold must be rotated, there may be a difficulty depending on the characteristics of the mold (Fig. 2.1). In this study, in order to solve these problems, rotation and revolution polishing (RRP) method was designed to polish aspheric lens molds.

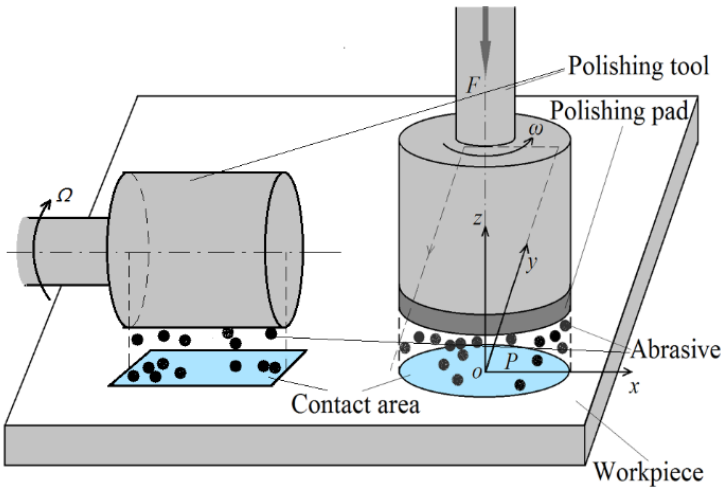

Fig. 2.1 Single axis polishing methods

2.2 Principle of rotation and revolution polishing method

In this chapter, rotation and revolution polishing method is used as a polishing method for an aspherical lens mold. It improves the uniformity and density of path and can process a variety of molds. The working principle of the RRP method will be described. The structure will be also detailed.

Fig. 2.2 shows the principle of the RRP method. The polishing tool rotates around the rotation axis and revolves with the revolution axis. The revolution axis is perpendicular to the polished area and just passes through the contact center. Both axes are in the same plane and maintain a fixed angle [10-12]. In this study, the angle between the axis of rotation and the axis of revolution is 5 degrees. The angle between the two axes can be designed to any angle. However, if the angle between the two axes is too large, the actual size of the rotating unit will be larger. Considering the size of the actual machine tool, an angle of 5 degrees is used. As the end face of the tool progresses, it becomes a spherical surface due to wear. Free abrasive grains were used in this study and the tool itself did not contain abrasive grains. In the future research, the polishing stone can also be selected as a tool by processing the polishing stone into a tubular polishing tool [13-17].

With such a tool structure, the direction of the movement path of the tool in the contact surface continuously changes during polishing, and the directionality and uniformity of the path can be improved. Further, even if the polishing tool wears over time, the polishing area could be kept constant and polishing conditions could be stabilized by applying a constant pressure in the rotation axis direction. The diameter of the tubular tool is inherently small, and the wall thickness is smaller. The polished contact area is basically the thickness of the tube wall. In actual polishing, the tool is slightly worn, and the contact area can still be considered unchanged. This is also an advantage of the small diameter tubular tool.

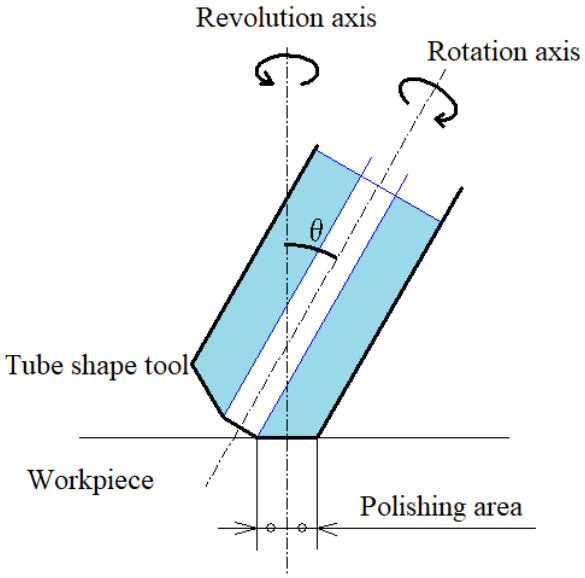

Fig. 2.2 Schematic of rotation and revolution polishing method

2.3 Overview of polishing equipment

The polishing equipment consists of a three-axis control system and a rotation and revolution unit. The movement of the three axes along the coordinates is controlled by the computer. The speed of rotation and revolution are controlled by the speed controller [18-20].

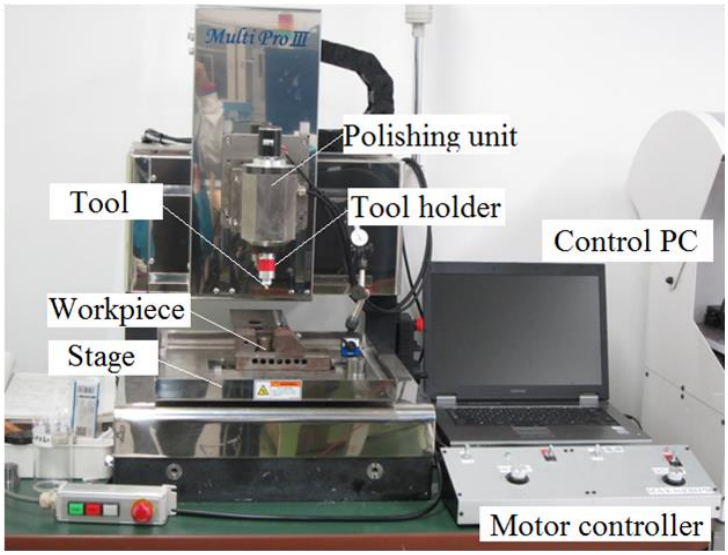

Fig. 2.3 The photo of rotation and revolution polishing equipment

2.3.1 Rotation and revolution polishing unit

Regarding the power supply, the revolution motor drives the revolution shaft through a belt. Inside the hollow revolving shaft, the rotation motor is powered by a slip ring, and the rotation motor directly drives the rotation shaft to rotate (Fig. 2.4). The revolution speed is from 160 to 300 min^{-1}, due to the limitation of the slip ring. Rotation speed is from 0 to 600 min^{-1}.

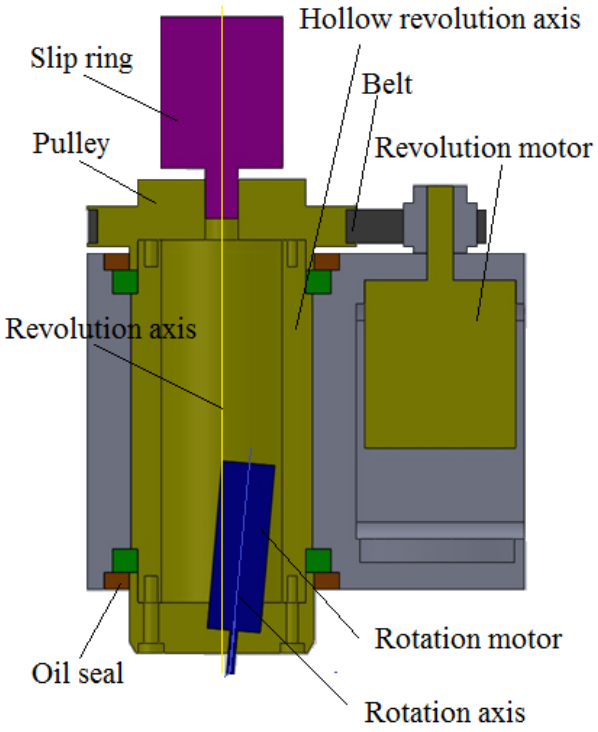

Fig. 2.4 Cutaway view of rotation and revolution polishing unit

2.3.2 Polishing load and polishing tool

As shown in Fig. 2.5, the tool holder is fixed on the shaft of the rotation motor, and the polishing load is applied by the force of a spring in the polishing tool. The polishing tool needs to be slidable on the inner rotating shaft of the tool holder. Therefore, a keyway is formed on the circumferential surface of the polishing tool, and the tool is prevented from rotating by set screws. The set screws only prevent the tool from falling off and do not limit the sliding.

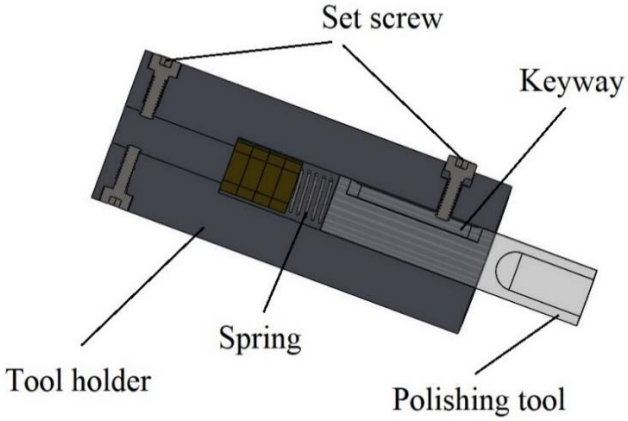

Fig. 2.5 Sectional view of tool holder

The polishing tools in this study are shown in Fig. 2.6. Acrylic resin is used as the material. The inner radius is R_1 1.5 mm and the outer radius is R_2 3 mm. The polishing surface of the polishing tool is worn to a radius of 25.81 mm curvature.

Fig. 2.6 Acrylic polishing tool

2.3.3 Workpiece, polishing fluid and truing

In this research, we used slide glass as a workpiece. The Vickers hardness of the slide glass was HV 598.8.

Cerium oxide was used as a polishing abrasive. Cerium oxide is considered to be the most suitable polishing abrasive for glass polishing. It is known that cerium oxide chemically reacts with glass during polishing, which is called chemical/mechanical polishing. In ultra-precision polishing, chemical effects dominate. SiO_2 is a covalent bond between Si and O, but the electronic state of Ce is similar to that of Si and enters SiO_2. After entering, the Ce-O bond does not have as many covalent bonds as the Si-O bond, so the network of the Si-O bond cannot be kept stable, and the portion is easily destroyed under a small force (Fig. 2.7).

The following two points serve as advantages of the reaction of solid grains with the object to be polished.

1. Solvent is neutral water. If it is other non-neutral liquid, other items are reactive to the solvent, and things other than the polished object will corrode.

2. Abrasive grains are chemically stable and harder than polished objects. For example, diamond, SiC, Al_2O_3, SiO_2, etc. are examples. However, since the chemical reaction causes the polishing object to deteriorate, the polishing material can be polished even if it is softer than the object to be polished.

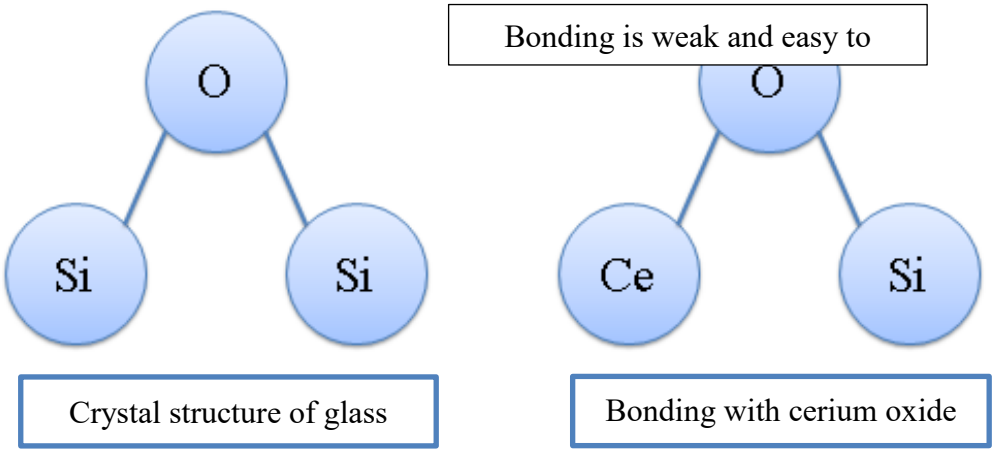

Fig. 2.7 Polishing principle for cerium oxide

Truing refers to removing the abrasive grains attached to the surface of the tool or finishing it into a predetermined shape according to the shape of the workpiece. In this study, we used acrylic without abrasive grains as a tool material. As the polishing progresses, the tool wears out and truing it into an initial state without wear is necessary. Fig. 2.8 shows the condition of polishing tool, measuring cross section of the tip of the polishing tool. The truing method is as follows.

1. Install a strip grindstone for truing on the vise.
2. Adjust the distance between the grindstone and the end face of the tool.
3. Operate according to the conditions in Table 2.1.

Table 2.1 Truing conditions

Dresser	Stick whetstone # 1000
Rotation speed	630 min^{-1}
Revolution speed	160 min^{-1}
Angle of polishing tool	5 °
Truing load	360 g
Truing time	4 min

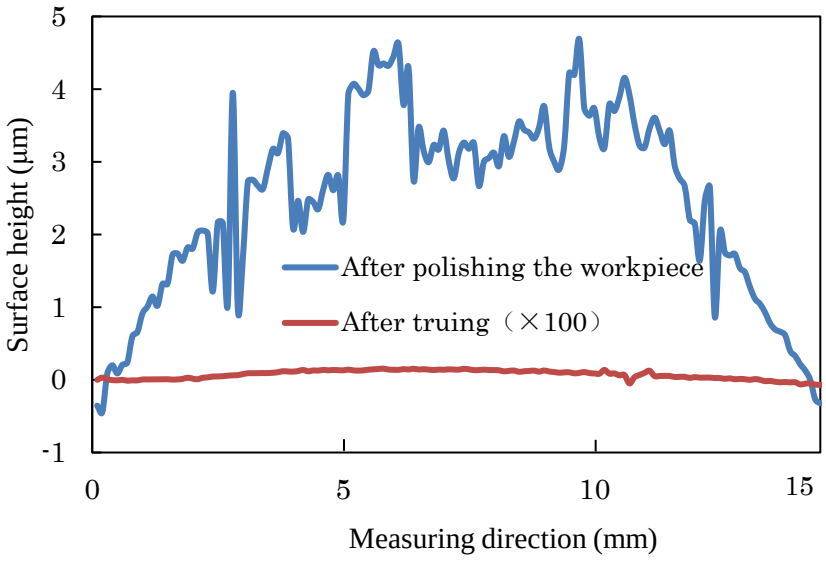

Fig. 2.8 Shape of polishing tool after truing

2.4 Experimental procedure

This section describes the preparation for polishing and the polishing steps.

1. Fix the workpiece to the fixture.
2. Set the polishing load.
3. First truing.
4. Fix the workpiece on the fixture and fix the fixture on the vise.
5. View the value of the control PC and adjust the X / Y / Z axis with the position controller to make the tool contact the workpiece.
6. Set the polishing time and speed.
7. After polishing, remove the fixture from the vise.
8. Remove the polishing tool from the holder, wipe the polishing solution attached to the polishing tool, and apply grease to the tool keyway.
9. Place the polishing tool in the tool holder.

2.5 Measuring device and workpiece measurement

The surface profile of the workpiece was measured after polishing, using the non-contact surface measuring instrument (PF-2SA Mitaka Koho Co., Ltd.). In this device, a laser is passed through an objective lens to the workpiece. An image is formed on the surface of the measuring workpiece, the reflected light passes through the objective lens again, and an image is formed on the AF sensor. The height position of the Z-axis is measured. By moving the workpiece on the XY stage, XYZ coordinates and corresponding shapes can be obtained.

Using the cross-measurement function, the shape of the spherical surface was obtained and the surface profile through the center was evaluated. The elements to be evaluated are the polishing depth, the radius of curvature of the polishing area, and the polishing roughness. The polishing depth and polishing area are defined in Fig. 2.9 and Fig. 2.10.

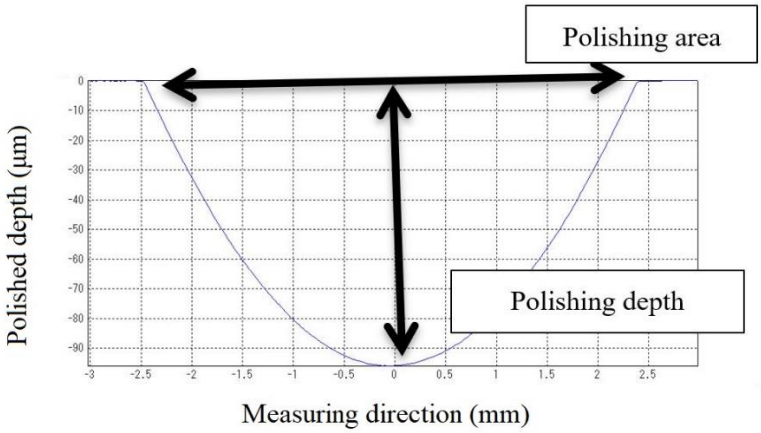

Fig. 2.9 Definition of polishing depth

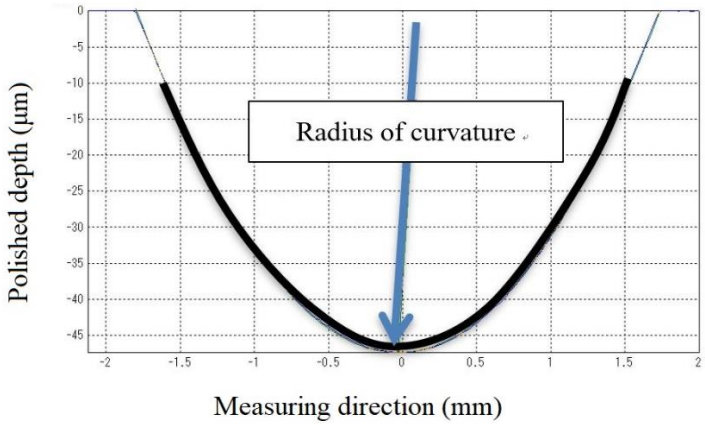

Fig. 2.10 Definition of radius of curvature

2.6 The basic principle of computer control optical surfacing (CCOS)

2.6.1 The theoretical basis of CCOS

The interaction between various factors in the polishing process is complicated. There is also a phenomenon of plastic flow of molecules on the surface of an optical workpiece due to frictional heat. The properties and particle size of the abrasive, the polishing fluid concentration and pH polishing fluid, material of the tool, the pressure distribution and speed of the tool, the mode of motion, and the ambient temperature all have an effect on the polishing effect. For a long time, optical craftsmen have been trying to explore the mathematical relationship between polishing parameters through

established mathematical physics models. But so far, CNC polishing has mainly followed the famous Preston hypothesis proposed by Preston in 1927. He pointed out that in a large range, polishing can describe a linear equation.

$$\frac{dz}{dt} = KP(x, y, t)V(x, y, t) \tag{2.1}$$

In the formula, $\frac{dz}{dt}$ is material removal, K is a coefficient that is determined by all factors except speed and pressure, such as the material of the polishing tool, the material of the workpiece, the polishing liquid, the concentration and the ambient environment.

$V\ (x,\ y,\ t)$ is the instantaneous velocity. $P\ (x,\ y,\ t)$ is the instantaneous pressure. According to Preston's assumption, the relative material speed and pressure can be used to calculate polishing removal. $\Delta z\ (x,\ y)$ is the amount of material removed during time t. And l is the length of the polishing path.

$$\Delta z(x, y) = K \int_0^l P(x, y, t)\, V(x, y, t) dt \tag{2.2}$$

Preston's theory simplifies the optical polishing process and is very beneficial for the control process. CCOS is also based on this as an advanced deterministic polishing technique. Eqs. (2.1) and (2.2) are the basic equations of CCOS technology [21-25].

Since the Preston equation is based on experimental results, the following points should be noted when using:

(1) The Preston equation is only an empirical assumption. A large number of experiments have proved that this equation is basically correct. For the polishing process, chemical removal also plays a considerable role.

(2) During the processing, the material is removed, and the polishing tool itself is also worn due to the superposition of various effects, so the removal characteristics of the polishing tool are also constantly changing.

(3) During the processing, each process parameter is difficult to maintain constant.

2.6.2 Principles of CCOS

The basic idea of CCOS technology is to use a polishing tool (generally less than 1/3 of the diameter of the workpiece). Under the control of the computer, the surface of the optical part moves along a specific path. Parameters such as relative speed, dwell time and process pressure in each zone are precisely controlled. The purpose of correcting errors and improving accuracy is achieved. For an aspheric surface, the smaller the polishing area, the easier the two surfaces are to match and the more uniform the force distribution. The small tool head in this study is to polish the workpiece over a much smaller size than the workpiece. Under the setting of other process parameters, the computer can control the dwell time of the small tool head at different positions to control the amount of polishing removal around the aspheric surface. After several iterations, the surface error is gradually converging [26].

2.6.3 Mathematical model of CCOS

The Preston equation can be used to determine the amount of material removed at each point of the tool as it moves across the surface of the workpiece. The entire surface is then calculated point by point to obtain the total material removal. However, such calculations are too large, and the control system is too complicated. Therefore, it is necessary to make some assumptions. A new mathematical model was built using linear system theory to represent the material removal process.

(1) Assuming removal is due to a polishing tool movement. The material removed by the tool during the residence time of a certain area of the workpiece is necessary to be clarified, the microscopic mechanism of material removal is without consideration.

(2) Material removal is only related to the movement of the tool itself and is independent of the movement of the tool on the workpiece. The linear velocity generated by the tool rotation during machining is much larger than the moving speed.

(3) Assuming that the polishing rate of the tool on the entire surface of the workpiece does not change. The tool must be completely flexible to ensure that the same pressure

is applied to each point. However, in the case where the removal rate is low, and the tool is not exposed, it can be approximated that the rate of the tool on the workpiece is constant, that is, the polishing mold is completely flexible.

(4) It is assumed that other process parameters remain unchanged during the processing. There are many parameters in the processing process that affect the processing results, but some parameters have little effect on the results, such as auxiliary materials, surface roughness, polishing fluid, processing materials, temperature and other process parameters.

From the above assumptions, computer-controlled polishing can be considered as a process in which the motion parameters of the tool are converted into material removal by a mathematical model. And this mathematical model is linear and does not change with the movement of the tool position. Such a system is called a linear and shift invariant system.

In the system, we take the input function as *D (x, y)* of the tool in any given area of the workpiece surface, normalize it.

$$T = \iint D(x, y)dxdy \tag{2.3}$$

Where *T* is the total polishing time. *D* (*x, y*) is the dwell time function. Define the removal function *R* (*x, y*) (Removal Function) as the average amount of polishing removal per unit time of a tool that does not move, as shown in the following equation.

$$R(x, y) = \frac{1}{T}\int_0^T KP(x, y, t)V(x, y, t)dt \tag{2.4}$$

Tool moves on the surface of the workpiece according to a predetermined path and stays at each point for a certain time *D* (*x, y*). By superimposing the material removed from each area of the workpiece surface, the distribution function *H* (*x, y*) of total surface polishing removal amount can be obtained.

$$H(x,y) = \int_{\alpha}^{1} \int_{\beta}^{1} R(x-\alpha, y-\beta)\, D(x,y) d\alpha d\beta \tag{2.5}$$

This is essentially the convolution of the tool removal function $R(x, y)$ with the dwell time $D(x, y)$.

$$H(x,y) = R(x,y) * D(x,y) \tag{2.6}$$

In actual machining, $H(x, y)$ is the surface error distribution. The known amount could be determined by measurement. R is relevant to tool size, material, polishing pressure, relative speed and other factors, and can also be obtained through theoretical simulation and process experiments. When R, H are known, the dwell time $D(x, y)$ can be found using a suitable algorithm. On this basis, the process parameters are selected, and a CNC machining file is generated to guide the CCOS for polishing. Finally, the processing residual error $E(x, y)$ is obtained.

$$E(x,y) = H(x,y) - R(x,y) * D(x,y) \tag{2.7}$$

2.6.4 Characteristics of ideal removal function

The removal function is used to describe the motion characteristics.

$$R(0,0) = \int \int_{-\infty}^{\infty} \overline{R(\xi,\eta)}\, d\xi d\eta \tag{2.8}$$

The Fourier spectrum of the $\overline{R(\xi,\eta)}$ function,

$$R(\xi,\eta) = \int \int_{-\infty}^{\infty} R(x,y)\, exp[-j2\pi(\xi x + \pi y)] dx dy \tag{2.9}$$

Note that if the center of the function is zero, the integral value of its Fourier spectrum must also be zero. This implies that although this type of function can correct a certain

spatial frequency error, it can easily increase the high frequency error of the workpiece surface. Experiments have also shown that a zero-center removal function can also reduce surface errors at the beginning of polishing. However, after a certain degree, the surface shape error will increase. Because the amplitude at the beginning and the low frequency are reduced faster than the high frequency error, only the high frequency error is left. Since the amplitude of many high frequency errors also increases as the number of polishing times increases, in some cases the entire surface error increases with polishing time.

The function used satisfies the following characteristics as much as possible.

(1) The removal characteristics of the material are rotationally symmetric, and the removal function is a strict rotational symmetry function.

(2) The center of the removal function has the largest removal. The function has a single peak and decays to zero as the radius increases.

(3) There is no ability to remove material beyond the maximum radius of the removal function.

(4) Taking the radius of the removal function as an independent variable, the slope of the function is required to be zero at the center peak and edge.

(5) The removal function is a continuous smooth function.

The removal function containing the above characteristics is perfect. Suppose the parent function is a cubic polynomial of radius r.

$$m(r) = a_3 r^3 + a_2 r^2 + a_1 r + a_0 \tag{2.10}$$

Where a_0 to a_3 represent the coefficients of the constant term. Boundary conditions are used.

$$m(0) = a_0 = 1 \tag{2.11}$$

$$m(1) = a_3 + a_2 + a_1 + a_0 = 0 \tag{2.12}$$

$$\dot{m}(0) = a_1 = 0 \tag{2.13}$$

$$\dot{m}(1) = 3a_3 + 2a_2 + a_1 = 0 \tag{2.14}$$

The constant term coefficient can be solved, and the bus equation of the ideal removal function is obtained.

$$m(r) = 2r^3 - 3r^2 + 1 \tag{2.15}$$

The normalized ideal removal function graph is obtained by rotating the busbar around the axis (Fig. 2.11).

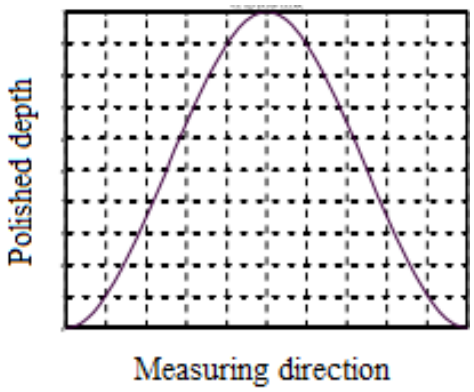

Fig. 2.11 Ideal removal profile

The removal function is the basis for computer-controlled small-diameter tool polishing. The tool moves in different ways, so its removal function is also different. The removal function with the largest central removal can be achieved by different motion mechanisms. At present, the tool mainly adopts two kinds of movement modes: one is planetary motion which the tool rotates around the revolution axis while rotating. The other is that the tool rotates around the axis while translational, called flat rotation. The research shows that the removal of materials in the center of rotation reaches the maximum under these two modes of motion.

2.7 Design of rotating and revolution units and 3D modeling

It is necessary to develop a prototype that could have a double rotating shaft and that

the two-axis intersection should be in the center of the polishing area. At present, the theory of rotation and revolution polishing method is only verified in geometry and simple kinematics. It is necessary to design a prototype that can achieve the special machining posture of the principle of rotation and revolution and can verify the further theoretical feasibility. This prototype needs to be simple in structure, low in cost and stable in processing. The basic parameters of 3D modeling are calculated and then 3D modeling is built using SolidWorks software.

2.7.1 3D Modeling based on SolidWorks

Through the 3D modeling function of SolidWorks software, in this chapter we build the 3D modeling of different parts. In the future, simulation analysis will be carried out in ANSYS to analyze the motion characteristics of the complex structure in space. The stress, strain and deformation of the structure are determined, so that the designed polishing machine can reach the most stable state. Accurate realization of the 3D model of the polishing tool provides a basic guarantee for the analysis of the polishing force in the processing area. At the same time, the optimization design of the finite element simulation analysis of the polishing axis also has important practical value.

2.7.2 Machine tool main body introduction

The machine body of the RRP method uses the MultiPro III TS-102 by Takashima Industrial Co., Ltd. This machine tool can be used as a desktop multi-platform, and can handle various processing (Fig. 2.12). The main body consists of three coordinate axes and the system is controlled by the AC servo motor. By changing the processing unit (option), it can correspond to various processes.

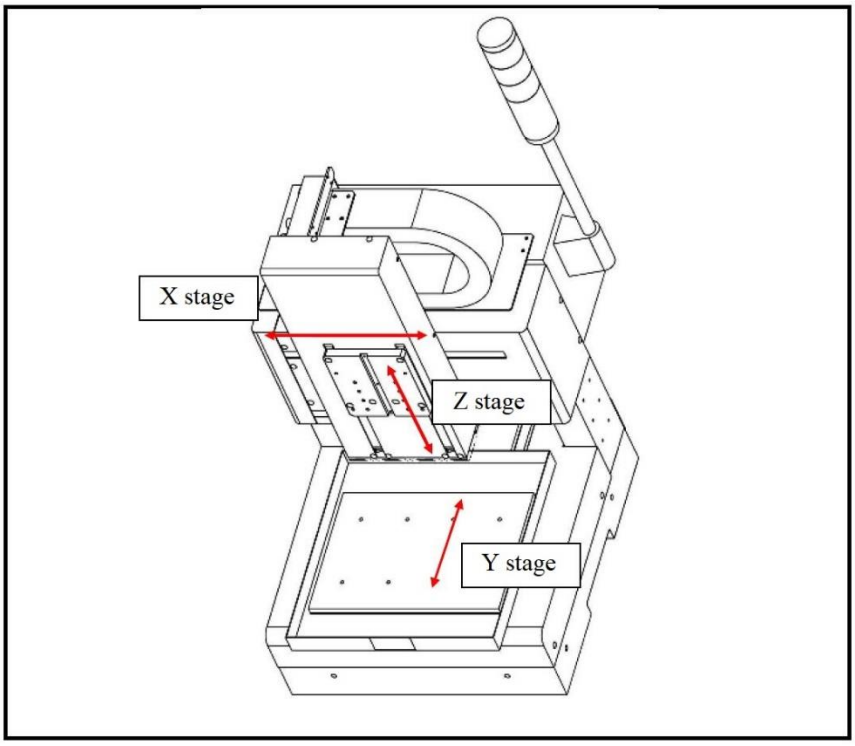

Fig. 2.12 Structure chart of Multi Pro III TS-102

When installing the rotation and revolution polishing unit, prepare two screws and washers according to the specifications. The RRP unit is aligned with the groove of the main shaft of the rail on the Z stage.

Rotation and revolution polishing unit, from bottom to top according to motion mode, consists of three parts, tool unit, rotation unit, and revolution unit. Above the tool unit is connected the rotation motor, which can rotate with the rotation unit. The rotation unit is installed inside the hollow type revolution axis and can rotate with the revolution axis. The hollow type revolution axis is installed in the housing and together forms a revolution unit. The housing is fixed to Z stage of the machine tool. When the rotation and revolution polishing unit is working, it can be regarded as the tool unit is moving around two axes at the same time. The design principle of rotation and revolution polishing method can be achieved (Fig. 2.4).

2.7.3 Design and modeling of tool unit

In the tool unit, the tool is made of a thin cylinder of acrylic resin material with a

diameter of 3 mm. Drill holes in the tool end face and machine the keyway on the other side (Fig. 2.13). The internal structure of tool holder is shown in the Fig. 2.5. The internal structure adopts simple lightweight design. On the tool side, the holder is equipped with a spring that provides polishing force, and the positioning screw on the holder tool side is tightened into the tool keyway. It only prevents the tool from falling off, but does not interfere with the tool freely sliding up and down.

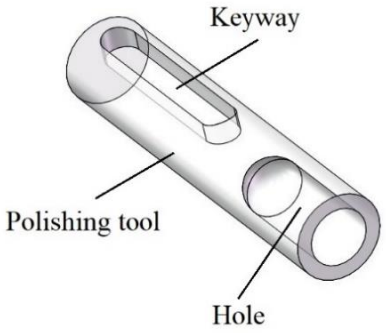

Fig. 2.13 3D illustration of the polishing tool

On the other side of the holder, the positioning screw fastens the shaft of the rotation motor to the holder. The holder and the rotation motor together constitute the rotation unit (Fig. 2.14).

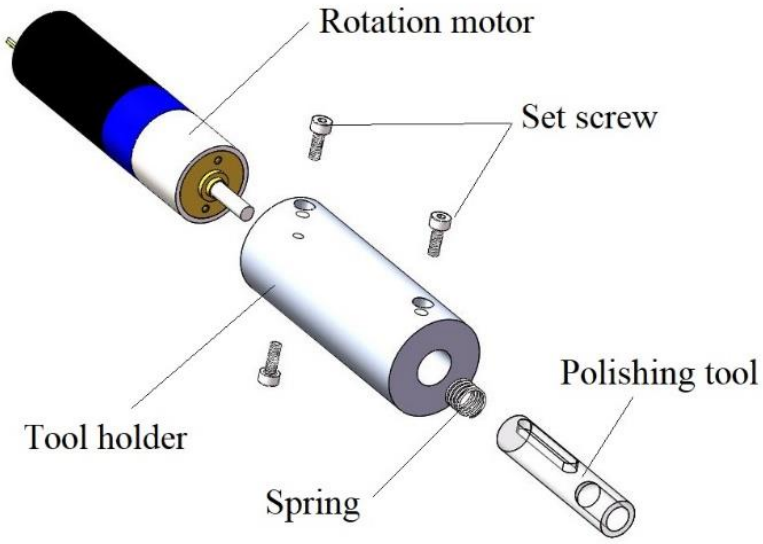

Fig. 2.14 Explosion of the tool unit

2.7.4 Design and modeling of rotation unit

Angle selector of rotation and revolution polishing method, which is a very important part in RRP system. It connects the rotation unit and the revolution unit, realizing the rotation and revolution in the same plane, two axes always maintain a fixed angle. After discussing many schemes, as shown in the Fig. 2.15, an angle selector with easy material, simple structure and low cost was designed. Materials are common plastics. The outer wall of the selector is matched with the inner surface of the hollow type revolution axis. In practice, the rotation unit can be ensured to rotate smoothly in the hollow type revolution axis (Fig. 2.16). Because of the simple processing, the angle selector can easily make different angles, which is convenient for further experiments.

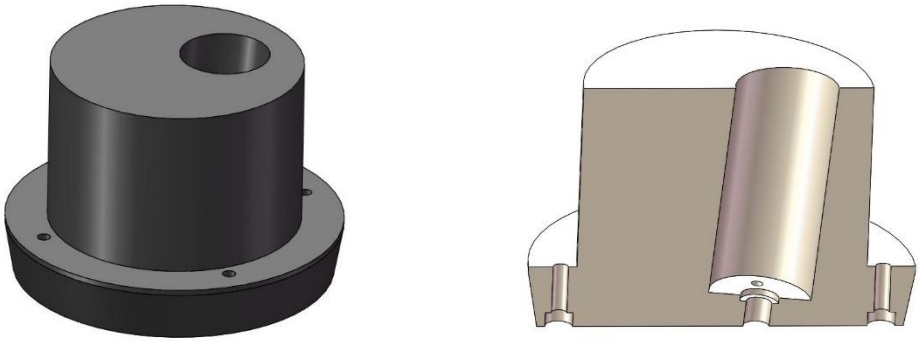

(a) 3D illustration of angle selector (b) Internal structure of

Fig. 2.15 Angle selector of RRP method

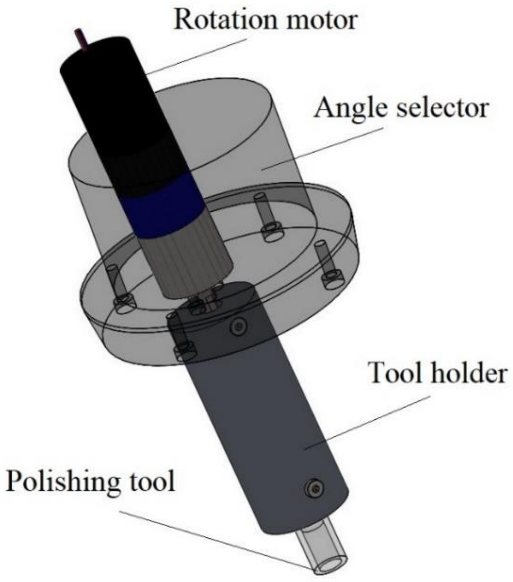

Fig. 2.16 Combination diagram of rotation unit

The rotation motor and the tool unit constitute the rotation unit. The tool unit is installed in the angle selector of RRP system, and the angle selector is connected with the revolution unit to realize the rotation axis rotating around the revolution axis (Fig. 2.17).

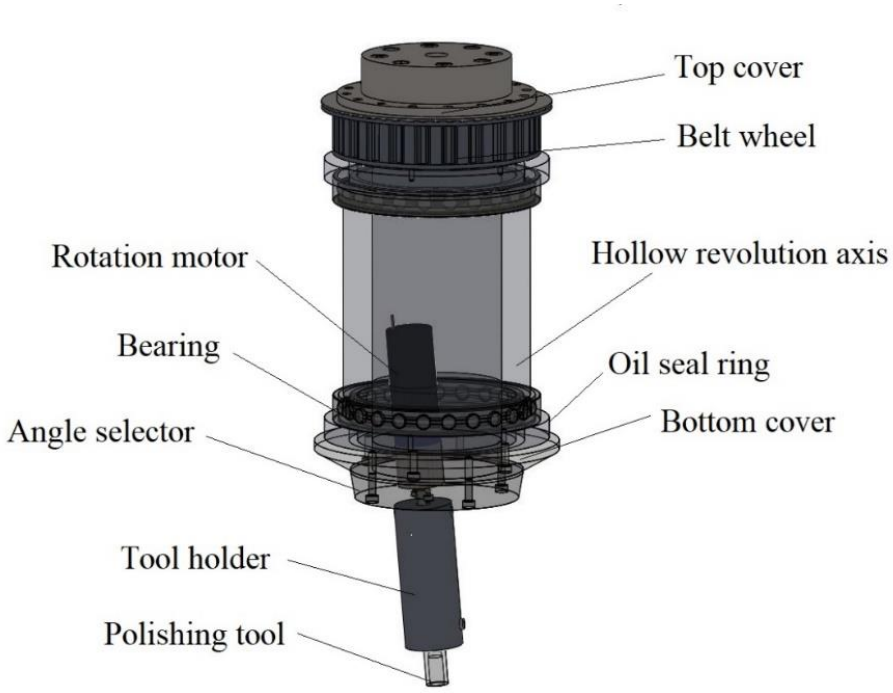

Fig. 2.17 Connection of angle selector and hollow type revolution axis

2.7.5 Design and modeling of revolution unit

In the revolution unit, the rotation unit is installed inside the hollow type revolution axis. Install the hollow type revolution axis in the housing, the bottom of the hollow axis is fixed by the bottom cover, and the top of the hollow axis is connected with the top cover. The revolution motor drives the top cover through the revolution belt, driving the hollow revolution axis. The problem of winding the rotating motor wire when it is in revolution is solved by sliding ring.

The rotation unit and tool unit inside the hollow type revolution axis, top cover, the angle selector and the bottom cover all move in revolution with the drive of the revolution motor. The housing, the slide ring, and the slide ring bracket all remain relatively static with the machine tool (Fig. 2.18). Finally, the installation diagram of all parts is shown in Fig. 2.19.

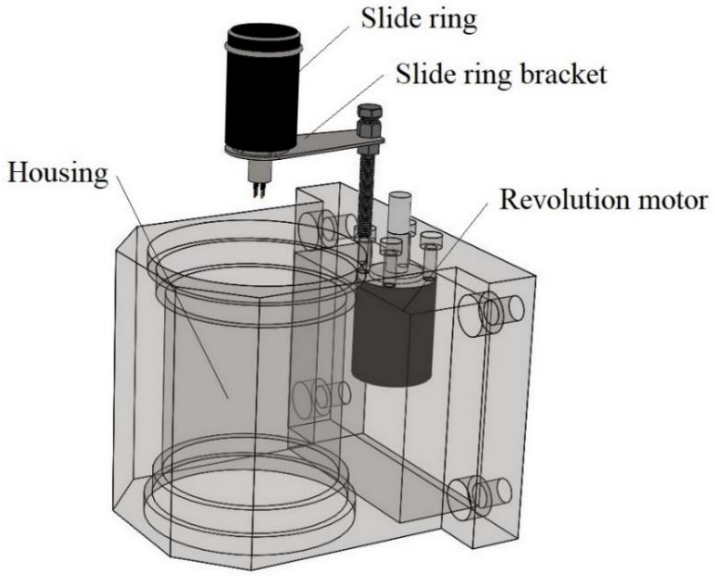

Fig. 2.18 Structure that is relatively stationary with the machine tool

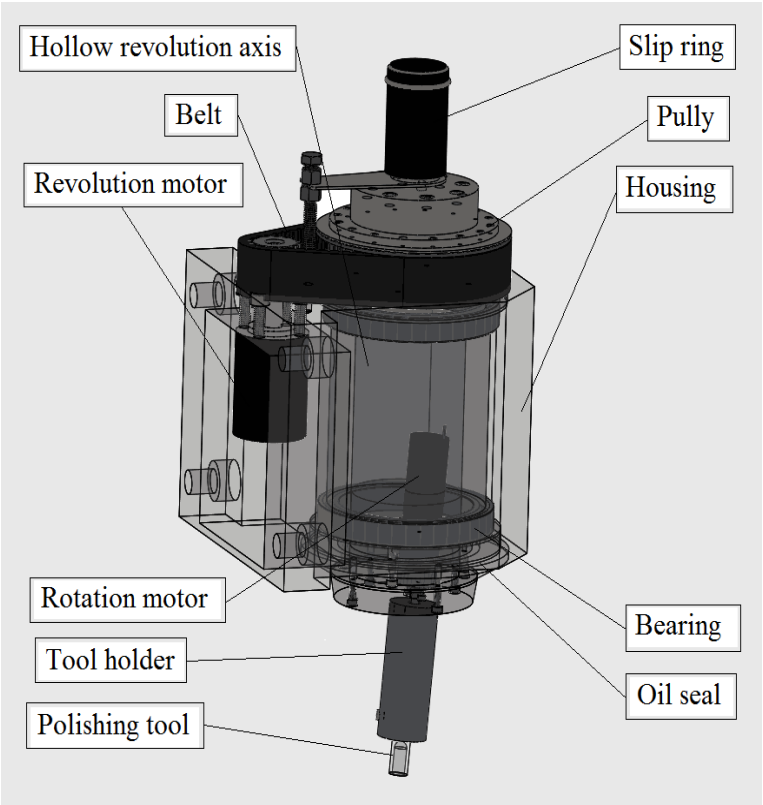

Fig. 2.19 Structure of RRP method

2.7.6 Defects in structural design

From the two aspects of the structural characteristics of the polishing device and the structural optimization design method, the structural design of the polishing device currently has the following problems.

First, for structural optimization design, it is necessary to build a model that is suitable and contains structural parameters and responses. The support structure of the polishing device is complex, and there are many geometric characteristic parameters. The requirements for structural performance are in many aspects. Although 3D CAD modeling software has been widely used in design, and some structural design work is done using finite element software, the relationship between design parameters and structural response is implicit and difficult to express with an explicit expression. In addition, due to the structure of the polishing device, the finite element model has many nodes and units, and the calculation amount model is large. In the structural optimization design, by continuously changing the finite element model for analysis and obtaining the corresponding response results, the calculation cost and calculation time will be greatly increased. Therefore, structural optimization design needs to establish a suitable model of the polishing device component, which can not only express the relationship between structural parameters and response explicitly, but also the cost of calculation is low.

Second, it is necessary to find a global optimization method suitable for solving multi-objective problems for structural design. The problem of structural optimization design of the polishing device is actually a multi-objective optimization problem, and many performance indicators affect each other. For example, in the light weighting of the structure of the polishing device, the reduction in mass and the improvement in dynamic performance are two contradictory aspects. It is necessary to use the advantages of the global optimization algorithm in the parameter domain to find the optimal parameter configuration scheme.

Third, in order to establish a correct analytical model, it is necessary to study the parameters of the polishing device structure that are not easily obtained through

experiments. Due to experimental theory and conditions, key parameters are not directly available through experiments and are usually dependent on empirical values. Especially in the modeling process, the default values of the commercial analysis software, such as the dynamic characteristics of the joint of the polishing device, the damping coefficient, etc., are directly used. In order to provide the correct model and structural response values for the optimal design of the structure, it is necessary to conduct reverse research on these critical and difficult to obtain parameters.

2.8 Summary

In this chapter, rotation and revolution polishing method was suggested as a polishing method for an aspherical lens mold. It improves the uniformity and density of the path and could process a variety of molds. The structure of rotation and revolution polishing device was detailed. The experimental and measurement equipment of this paper has also been introduced. The selection of the polishing solution and the truing of the tool were also described in detail. This rotation and revolution polishing device needs to be simple in structure, low in cost and stable in processing. The basic parameters of 3D modeling were calculated and then 3D modeling was built using SolidWorks software.

References

[1] W.M. Lin, S. K. Chee, H. Suzuki and T. Higuchi: Polishing Characteristics of a Low Frequency Vibration Assisted Polishing Method, Advanced Materials Research, **797** (2013) 450-454.

[2] H. Wang and W.M. Lin: Removal model of rotation & revolution type polishing method, Precision Engineering, **50** (2017) 515-521.

[3] C. Fan, J. Zhao, L. Zhang, W.S. Zhou and L.N. Sun: Local material removal model considering the tool posture in deterministic polishing, Proceedings of the Institution of Mechanical Engineers, Part C: Journal of Mechanical Engineering Science, **230** (2016) 2660-2675.

[4] F. Klocke, C. Brecher and R. Zunke: Corrective polishing of complex ceramics geometries, Precision Engineering, **35** (2011) 258-261.

[5] L. Zhang, H. Tam and C. Yuan: An investigation of material removal in polishing with fixed abrasives, Proceedings of the Institution of Mechanical Engineers, Part B: Journal of Engineering Manufacture, **216** (2002) 103-112.

[6] H.Y. Tam, M. Hua and L. Zhang: Aspheric surface finishing by fixed abrasives, The International Journal of Advanced Manufacturing Technology, **34** (2007) 483-490.

[7] G.L. Wang, X.Q. Zhou, X. Yang, H.B. Zhou and G.J. Chen: Material removal profile for large mould polishing with coated abrasives, The International Journal of Advanced Manufacturing Technology, **80** (2015) 625–635.

[8] H.C. Wang: Research on Geometric Model for Axial Symmetry Aspheric Optical Parts Machining by Normal Equidistance Method, Advanced Materials Research, 154-**155** (2010) 913-916.

[9] C. Fan, J. Zhao, L. Zhang, Y. S. Wong, G. S. Hong and W.S. Zhou: Modeling and analysis of the material removal profile for free abrasive polishing with subaperture pad, Journal of Materials Processing Technology, **214** (2014) 285-294.

[10] W.M. Lin, H. Wang and F.M. Ji: Research on effect of parameters in Rotation & Revolution Type Polishing Method, Procedia CIRP, **71** (2018) 358-363.

[11] W.M. Lin, Y. Watanabe, H. Ohmori and T. Kasai: Nano Precision Mirror Surface Finishing Method of Optical Elements with Combined Fabrication Process, Journal of

the Japan Society of Polymer Processing, **18** (2006) 842-847.

[12] W.M. Lin, S. Yin, H. Ohmori, Y. Uehara and T. Suzuki, Fabrication of silicon mirror with ultraprecision synergistic finishing process of ELID-grinding and MRF, Journal of the Japan Society for Abrasive Technology, **49** (2005) 701-702(in Japanese).

[13] L. Zhang, H. Tam and C. Yuan: On the removal of material along a polishing path by fixed abrasives, Proceedings of the Institution of Mechanical Engineers, Part B: Journal of Engineering Manufacture, **216** (2002) 1217-1225.

[14] F.W. Preston: The theory and design of glass plate polishing machines, Journal of the Society of Glass Technology, **11** (1927) 247–256.

[15] J.F. Song, X.Y. Yao and D.G. Xie: Effects of polishing parameters on material removal for curved optical glasses in bonnet polishing, The Chinese Journal of Mechanical Engineering, (2008) 29–33.

[16] T.I. Suratwala, M.D. Feit and W.A. Steele: Toward deterministic material removal and surface figure during fused silica pad polishing, Journal of the American Ceramic Society, (2010) 1326-1340.

[17] C. Cheung, L. Kong and L. Ho: Modelling and simulation of structure surface generation using computer controlled ultra-precision polishing, Precision Engineering, **35** (2011) 574-590.

[18] W.M. Lin, T. Kasai, K. Horio and T. Doi: Surface Characteristics of the Polyurethane Polisher in Mirror-Polishing Process, Japan Society of Precision Engineering, **65** (1999) 1147-1152.

[19] W.M. Lin, H, Ohmori, Y. Yamagata, S. Moriyasu, A. Makinouchi and C. Liu, 503 Ultraprecision Polishing Method of Large X-Ray Mirrors, The Japan Society of Mechanical Engineers, (2000) 121-122 (in Japanese).

[20] W.M. Lin, M. Ohmura, M. Fujimoto, Y. Wu and Y. Yamagata: Proposal of a rotation & revolution type polishing (RRP) method and fundamental study on the precision profile polishing, Journal of the Japan Society for Abrasive Technology, (2012) 256-261.

[21] C. Fan, J. Zhao, L. Zhang, W.S. Zhou and J.C. Wu: Modelling of the polished profile in computer-controlled polishing by a sub-aperture pad, Machining Science and

Technology, **19** (2015) 536-558.

[22] W.B. Zhang, M.W. Shu, B. Lin and X.F. Zhang: Study on the removal function of annular polishing pad based on the computer controlled polishing technology, Applied Mechanics and Materials, **457-458** (2013) 552-555.

[23] C. Fan: Predictive models of the local and the global polished profiles in deterministic polishing of free-from surfaces, Journal of Engineering Manufacture, **228** (2014) 868-879.

[24] H. Lee and M. Yang: Dwell time algorithm for computer-controlled polishing of small axis-symmetrical aspherical lens mold, Optical Engineering, **40** (2001) 1936-1943.

[25] F. Klocke, O, Dambon and R. Zunke: Modeling of contact behavior between polishing pad and workpiece surface, Production Engineering, (2008) 9-14.

[26] R.A. Jones: Computer controlled optical surfacing with orbital tool motion, Optical Engineering, **25** (1986) 785–790.

Chapter 3 Experiment and simulation of rotation and revolution type polishing method

This chapter discusses and describes material removal of the fixed point and plain optical glasses by rotation and revolution type polishing. This chapter mainly examines whether the removal profile is a Gaussian curve and the predictability of the profile. Fixed point polishing means that the tool does not move, and the workpiece is polished in only one position. The mathematical model of the single path scanning type polishing method is studied. The workpiece entire surface was polished, and the characteristics were discussed. In the end of this chapter, we expand on the previous content and builds a material removal model at the vertical bisector of the corner.

3.1 Motivation of deterministic polishing

Optical curved parts are the key components of an optical system. To achieve deterministic polishing surface accuracy control, this chapter explores the material removal theory during polishing.

At present, the core issues in deterministic polishing process research include unit time material removal function modeling, dwell time calculation, polishing path planning, and material removal prediction. This chapter studies the polishing process parameters (including polishing pressure, revolution speed, rotation speed, feed rate, polishing attitude angle, etc.), material physical properties (Poisson's ratio and elastic modulus, etc.) and a series of factors on the removal of abrasive materials. The polishing surface removal model considering the influence of the above factors was constructed and the polishing process control of deterministic material removal was realized.

The traditional polishing removal model can only predict the depth of removal during fixed point polishing. In view of the above deficiencies, this chapter establishes a material removal profile model for moving and polishing. The removal is related to the contact pressure at that point, relative linear velocity and feed rate. The pressure and relative linear speed are modeled according to the contact and tool attitude. The polished removal depth for the unit path length is integrated [1].

The tubular tool profile is deduced, and a material removal profile model considering the polishing pressure, the revolution speed, the rotation speed, the polishing attitude, the feed speed, and the workpiece/tool geometry is established. Optical aspherical, free-form surface elements have advantages in optical applications compared to conventional optical spherical elements. The aspherical component can not only correct aberrations, improve image quality, expand the field of view, but also reduce the number of optical components. Aspherical mirrors also reduce instrument weight, simplify assembly and reduce instrument costs.

The processing of optical surfaces requires a series of processes, including styling, polishing. The traditional polishing method only pays attention to the improvement of

the surface quality during the processing, and the deterministic removal of the surface material of the curved surface cannot be realized. The uncertainty of the traditional polishing process makes it impossible to predict the results of the entire polishing process, with low polishing efficiency and poor quality. In this chapter, a material removal profile model for polishing is established. There is a growing demand for high quality optical aspheric surfaces on the market. A more precise polishing technique can be achieved by a tubular tool shape and a unique processing posture RRP machining method. By adjusting the polishing speed of the two axes, the shape of the end face of the polishing tool is maintained, and finally a smooth surface is uniformly formed. The author believes that the RRP method will be a promising precision polishing method. Under different conditions, it was determined that the mathematical model was effective in predicting the polished contour.

It is difficult to realize accuracy and high-quality surfaces using traditional soft tools. Various new polishing methods can be processed into high quality surfaces, but they are difficult to operate and high cost that limit the practical application of these methods. The proposed method improves the shortcomings of traditional tools by a stable polishing volume, a tubular tool, and a unique processing position. Stable processing into a smooth polished surface requires a stable polishing rate. The market demand for high quality aspheric optics is growing, and this chapter introduces polishing techniques that are more precise, simpler, and more economical. This chapter is based on the removal mathematical model of the Preston equation. It is proved below that we can control the polishing shape [2].

3.2 Principles of the Preston equation

Based on the Preston equation, the polished removal per unit time can be represented by $R(x, y)$.

$$R(x,y) = \frac{k_p}{T}\int_0^T p\,(x,y)v(x,y)dt \tag{3.1}$$

Where *Kp* is the polishing coefficient, *T* is the unit time, *p* (*x, y*) is the pressure distribution function, and *v* (*x, y*) is the relative linear velocity distribution function.

The rotation and revolution polishing removal functions can be used to determine the maximum removal depth and also to predict the polishing area profile [3]. This chapter combines two traditional polishing methods, axial face polishing and radial face rotation polishing. The conventional polishing method includes the following two types, a radial circular surface (left) or an axial curved surface (right) as shown in Fig. 2.1. Both of these methods have disadvantages. First, in the radial circular surface polishing, a radial speed difference is generated on the surface of the workpiece to be polished, resulting in uneven removal. When the workpiece is machined by an axial surface, the polishing tool does not adapt well. This chapter combines the above two polishing methods, thereby ensuring a stable removal rate and achieving a smooth surface.

Fig. 3.1 shows a tubular tool. The two-axis polishing combined with the conventional method is as shown. After the combination, the two rotating shafts are kept at a fixed angle in one plane.

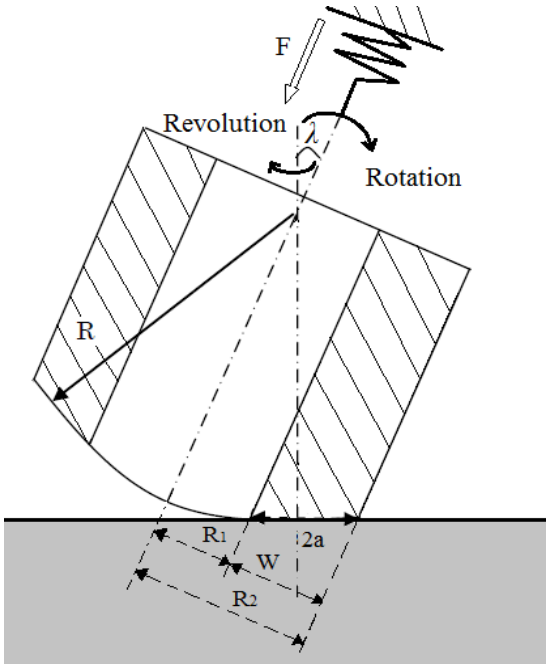

Fig. 3.1 Geometry relationship of tubular tool

The spring inside the tool holder provides polishing pressure (Fig. 3.2). The photo of the tool holder is shown in Fig. 3.3. The rotation axes intersect the center of the contact area at a defined angle. RRP unique process improves the relative speed instability compared to the simple single axis rotary axis drive in conventional polishing. Various surfaces can be polished using different parameters under the CNC.

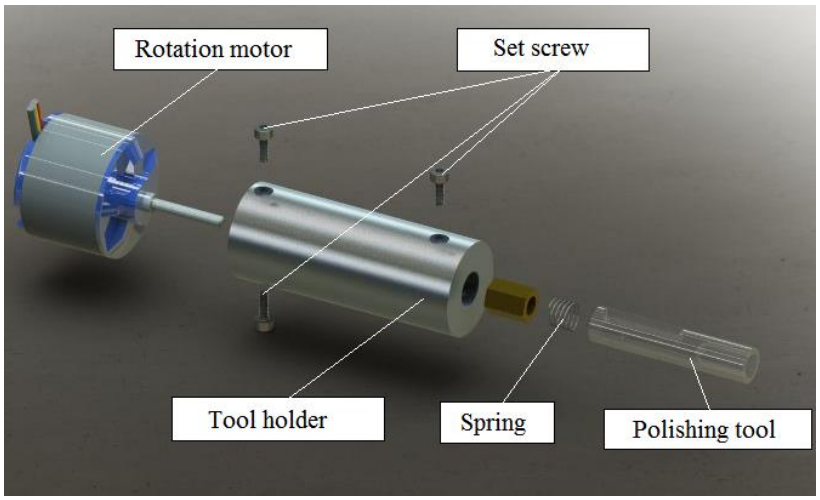

Fig. 3.2 3D-explosion of tool holder

Fig. 3.3 Photograph of tool holder

In the progresses, the shape of the end face of the polishing tool changes from a plane to a spherical shape. In Eq. (3.2), R represents the radius of contact area, and λ represents the angle between the two axes. R_1 and R_2 are the inner and outer radius of

the tool as shown in Fig. 3.1.

$$R = \frac{R_1 + R_2}{2 \sin \lambda} \tag{3.2}$$

The final convergence of the computerized polished surface profile requires that the unit material removal function is a Gaussian-like distribution. The tubular polishing head in the device has the advantages of small contact area, no deformation, and uniform speed in the polishing area. The figure below shows the deterministic polishing ideal unit material removal function and the 3D measurement of rotation and revolution polishing removal areas (Fig. 3.4).

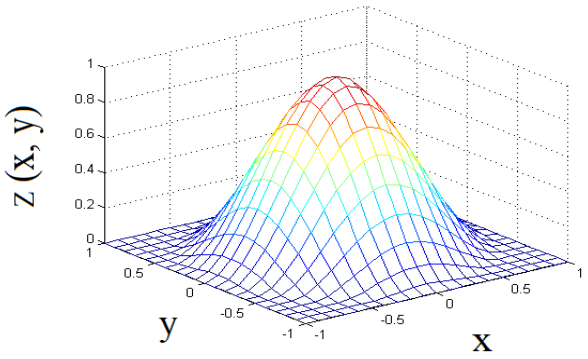

Fig. 3.4 Schematic diagram of Gaussian distribution

3.3 Definition of the contact area

Tool head is in contact with the surface of the workpiece. A shaped contact area is formed under the normal polishing pressure, and material removal occurs. Tool is usually an elastomer. Hertz contact theory describes the local stress and stress distribution law when two objects are pressed into contact with each other without considering friction between them [4]. The elastic polishing head undergoes elastic deformation when it is in contact with the optical aspherical surface, and the following figure is a schematic view of the contact area (Fig. 3.5 and Fig. 3.6).

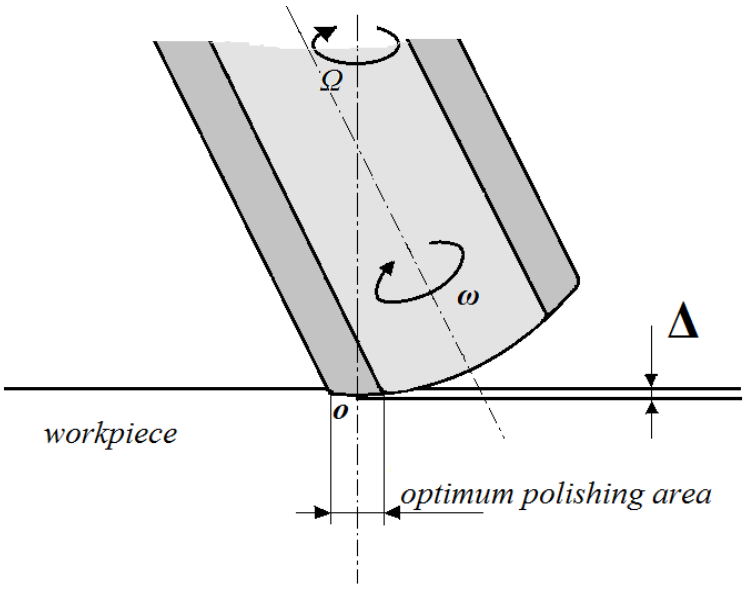

Fig. 3.5 Instantaneous contact

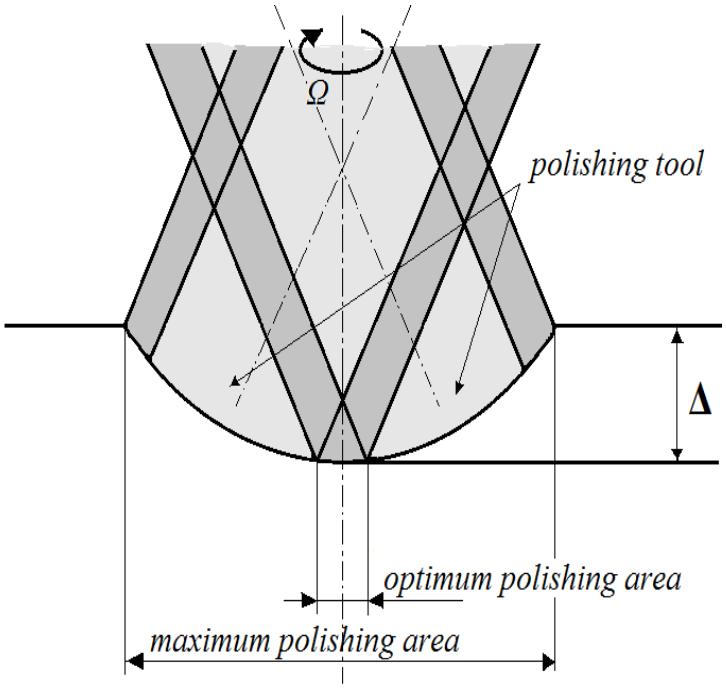

Fig. 3.6 Contacting after the rotation

Schematic of the optimum polished area is shown in Fig. 3.7. The polishing speed is the most uniform in this area, and the shape and size of the tubular tool head are the easiest to maintain. Due to the revolution, the moving tool head presents an axisymmetric figure with the revolution axis. The maximum polishing diameter is shown in the figure. When machining in the largest polishing area, the instantaneous contact shape of the tool head and the polishing area is the end surface of the tubular

tool.

The top view of the contact area is shown in Fig. 3.8. The circular ring with a section line is the polished area where the instant tool head contacts the workpiece. During the polishing process, the annular region rotates at a revolution angular velocity. D_1 area is the best polished area and is always in the polished state when the tool head rotates, so it is the most stable. In the D_2 region, each time the tool head is rotated about the revolution axis, two polishing occur, each time the width of the region is approximately equal to the wall thickness of the tubular tool, and the removal efficiency is lowered. In the D_3 area, the tool head is polished only once per revolution, and the efficiency is the lowest, and the closer to the limit polishing position, the lower the polishing efficiency and the polishing amount.

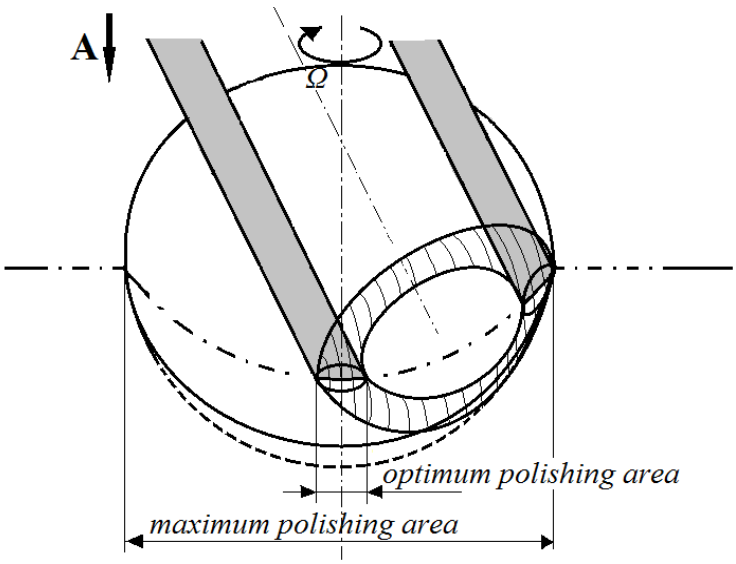

Fig. 3.7 Diagram of the contact area

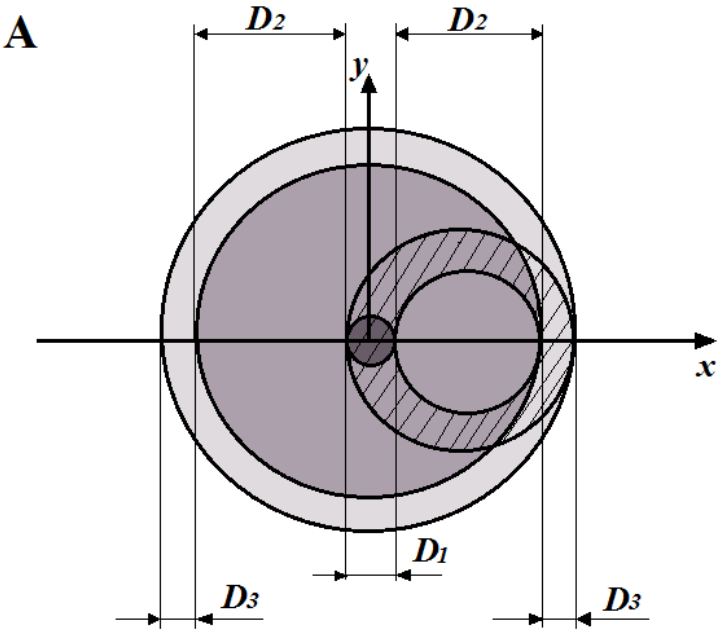

Fig. 3.8 Top view of the contact area

The tube type tool head is selected, so it can be divided into three parts according to the efficiency in the maximum polishing area. The tool head size used in the rotation and revolution polishing device is designed to have a small diameter. Moreover, the biggest advantage of the tubular tool head is that it maintains the stability of the shape and ensures the controllability and stability of the polishing during high-speed polishing. Laboratory seniors have pointed out that high surface quality is often achieved when it is larger than the optimum polishing area. Therefore, when the removal model is established, it can be considered that the tubular tool head can be approximated as a spherical tool head in the maximum polishing area. After polishing for a while, the tool head does change into a spherical shape. It can be estimated using the Hertz theorem.

3.4 Distribution function of polishing force

In the Hertzian contact theory, the size and pressure are related to the curvature properties of polishing points on the optical aspheric surface, the size of the polishing head, physical properties. For the tubular tool head polishing process, in order to avoid

local interference during processing (Fig. 3.9), the radius of curvature of the spherical tool head should be smaller than the minimum radius [5, 6].

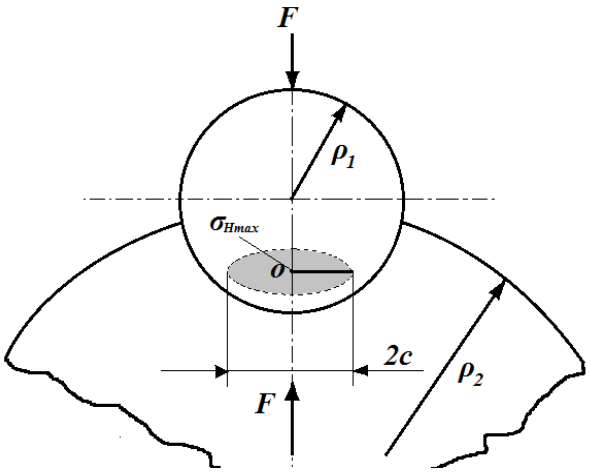

Fig. 3.9 Schematic of Hertz contact on two spheres

When the radius on a curved surface is much larger than the radius of a spherical tool head, the contact area is approximately a circle (Fig. 3.9), wherein the radius of the circle and the pressure of the maximum pressure point are given by the following formula [7, 8]. c is the contact radius. F is the contact force. ρ_1 and ρ_2 are the radius of the tool and the workpiece, respectively. E_1 and E_2 are the elastic moduli of the tool and the workpiece, respectively. μ_1 and μ_2 are the Poisson's ratio of the tool and the workpiece, respectively. p_o is the maximum contact stress.

$$c = \sqrt[3]{\frac{3F}{4}\frac{\frac{1-\mu_1^2}{E_1}+\frac{1-\mu_2^2}{E_2}}{\frac{1}{\rho_1}+\frac{1}{\rho_2}}} \tag{3.3}$$

$$p_o = \frac{1}{\pi}\sqrt[3]{6F\left(\frac{\frac{1}{\rho_1}+\frac{1}{\rho_2}}{\frac{1-\mu_1^2}{E_1}+\frac{1-\mu_2^2}{E_2}}\right)^2} \tag{3.4}$$

The Hertz contact theory is combined with the rotation and revolution polishing device to establish a coordinate system, as shown below (Fig. 3.10).

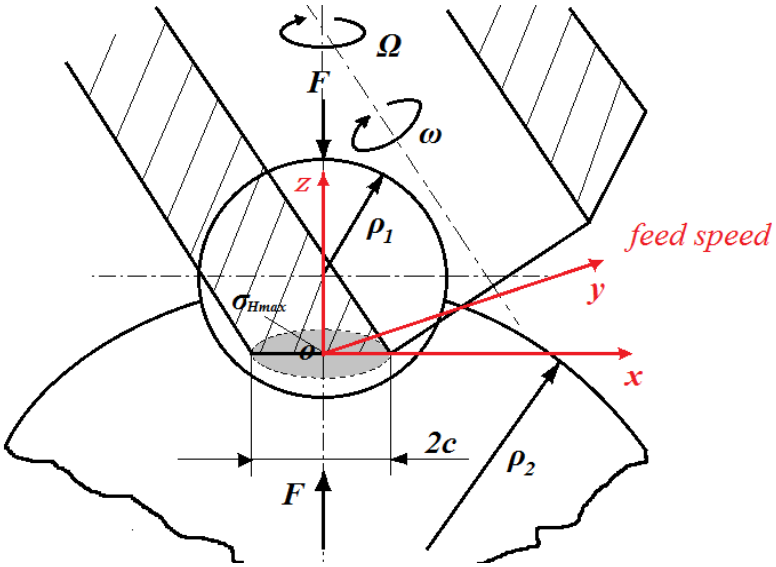

Fig. 3.10 Hertz contact principle applied to rotation and revolution polishing

3.5 Fixed point polishing

3.5.1 Pressure distribution function

Based on the Preston equation, the function of material removal is represented by Eq. (3.5), where k is the Preston coefficient.

$$\delta = k \cdot P \cdot V \cdot t \tag{3.5}$$

P and V represent pressure functions and relative speed functions. t represents polishing time. According to the Hertz theory described above, in the RRP polishing method, the pressure is not uniform. The maximum pressure is at the center [9-13]. Eq. (3.6) represents the pressure distribution function, and Eq. (3.7) represents the maximum pressure P_o at the center of the polished zone, where F represents the polishing force. a is the contact radius.

$$P = -\frac{P_o}{a}\sqrt{a^2 - x^2} \tag{3.6}$$

$$P_o = \frac{3F}{2\pi a^2} \tag{3.7}$$

3.5.2 Establish a coordinate system for fixed point polishing

Establish a Cartesian coordinate system to describe the RRP special machining posture. X-axis is defined as the measurement direction, y-axis is the vertical direction of the measurement direction, and z-axis is defined as the direction opposite to the polishing removal (Fig. 3.11). In the coordinate system, the revolution axis and the rotation axis (*OQ* and *MN*, respectively) maintain a certain angle λ. The origin of the coordinate system *o-xy* is at the center point *O* in the polishing zone. The coordinate system *o-xy* is in the tangent plane of point *P*. *M* is located at the intersection of *MN* and *o-xy* plane, *MN′* is the projection of the rotation axis on the *xy* plane, and the angle between *MN′* and the x-axis direction is θ.

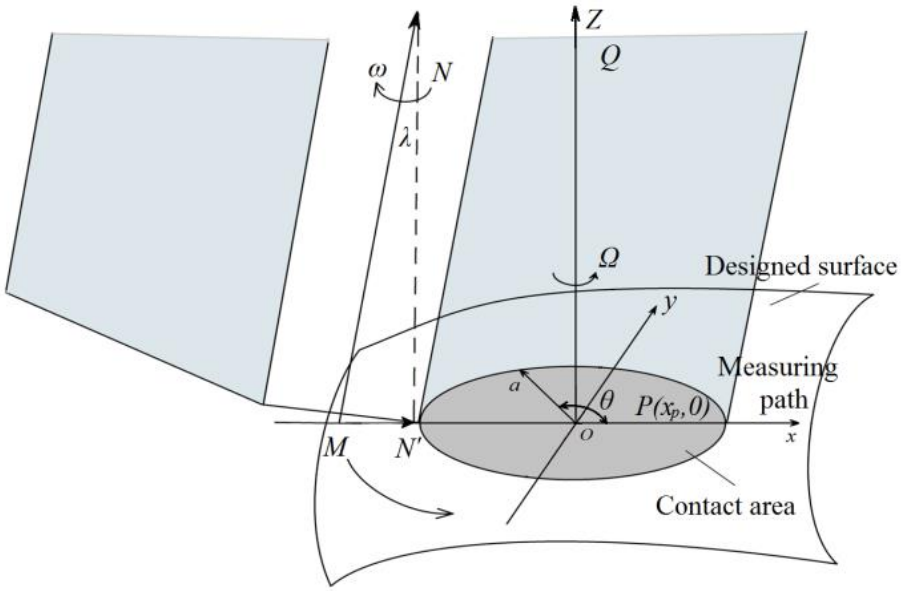

Fig. 3.11 Definition of polishing area coordinate system

Since the two axes are at a fixed angle, the rotation axis rotates around the revolution axis, resulting in a complicated distribution function. Fig. 3.12 shows a velocity composite map of the contact area, V_p is the linear speed of any point P on the x-axis, and θ is the angle between the MN' and the x-axis direction. Where ω and Ω are the tool's revolution angular velocity and rotation angular velocity.

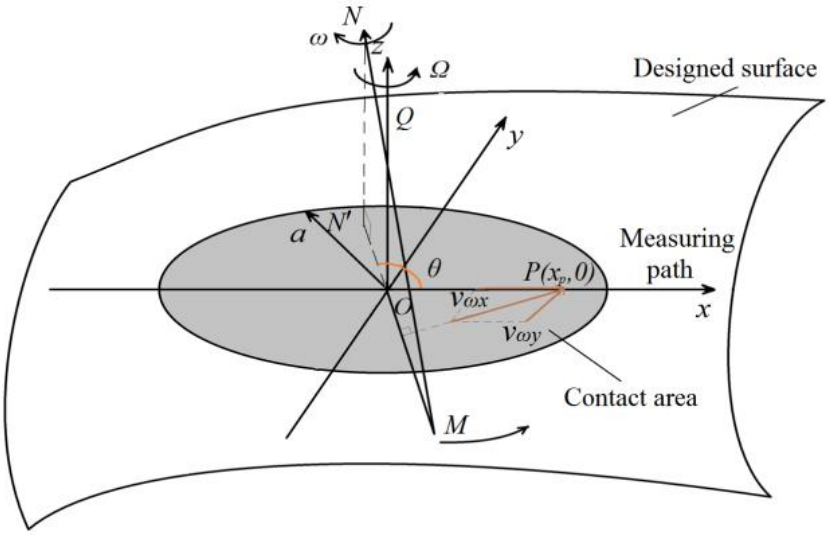

Fig. 3.12 Polishing area velocity distribution

The line speed of point P is based on the motion law and geometric relationship, as shown in Eq. (3.8). P is on the x-axis, and the velocity of P is perpendicular to the projection MN' of the revolution axis [14-18]. The instantaneous linear velocity of point P is decomposed into the x and y directions (Eqs. (3.9) and (3.10)), and θ is the angle between MN' and the x-axis.

$$v_{\Omega} = \Omega x \tag{3.8}$$

$$v_{\omega y} = \omega\left(\frac{R_1+R_2}{2} - \cos\lambda x\right)\cos\theta \tag{3.9}$$

$$v_{\omega x} = \omega\sqrt{\left(\frac{R_1+R_2}{2}\right)^2 + x^2}\sin\theta \tag{3.10}$$

Based on the particle velocity composition law, the relative velocity V between the polishing tool and the surface of the workpiece to be processed can be obtained by Eq. (3.11).

$$V = \sqrt{v_{\omega x}^2 + \left(v_{\omega y} + \Omega x\right)^2} \tag{3.11}$$

Fig. 3.13 shows the various components of speed. The V_x is perpendicular to the V_y, and according to speed composition law, the length of the orange line indicates the relative speed. It can be seen that substantially stable relative speeds are maintained during one revolution of the polishing process.

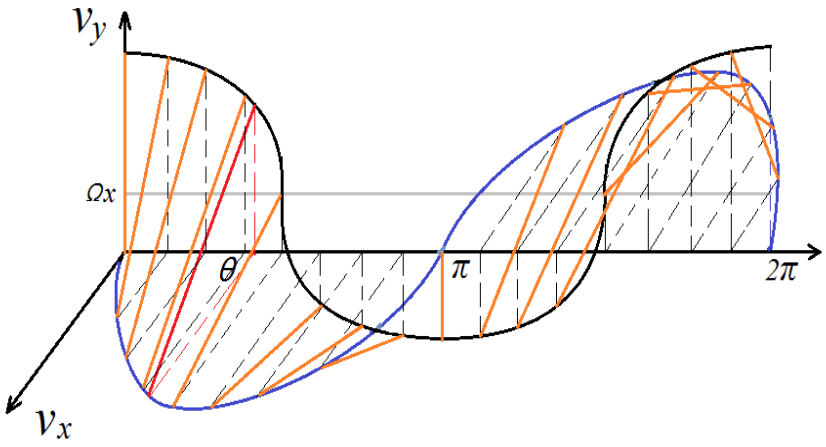

Fig. 3.13 Condition of velocity composition

3.5.3 Mathematical model of fixed-point polishing

In the Preston removal theory, we choose any point P on the x-axis. v_s represents the relative speed, and p_c represents the positive pressure of the point P. Based on the Preston principle, Eq. (3.12) can be used to understand the depth of removal dh during

dwell time *dT*.

$$dh = k_p p_c v_s dT \tag{3.12}$$

The relative angle of rotation during that dwell time,

$$dT = \frac{d\theta}{\Omega} \tag{3.13}$$

Substituting Eq. (3.13) into Eq. (3.12), the material removal at a unit angle (*E*) could be obtained by Eq. (3.14).

$$E = \frac{dh}{d\theta} = k_p \frac{p_c v_s}{\Omega} \tag{3.14}$$

From the integral in mathematics, the depth of removal of point *P*(*h*) is the sum of the angles of each infinitesimal element on a rotation period.

$$h = \int_0^{2\pi} k_p \frac{p_c v_s}{\Omega} d\theta \tag{3.15}$$

The material removal of the integral elements is related to the polishing pressure and relative velocity of each point. The removal of one cycle multiplied by the number of cycles can be used to simulate the polished depth and polishing profile [19-21]. The specific method is as shown in Eq. (3.16), and the Preston wear coefficient k_P is obtained experimentally.

$$h = \int_0^{2\pi} k_p \frac{p_c v_s}{\Omega} d\theta \cdot \frac{T \cdot \Omega}{2\pi} \tag{3.16}$$

3.5.4 Experimental system and conditions

The RRP polishing machine consists of a polishing body and a control section. Fig. 3.14 shows a schematic of the RRP control system. The movements of the XYZ axis are controlled by the PC, and the direction and speed of rotation are controlled by the motor controller.

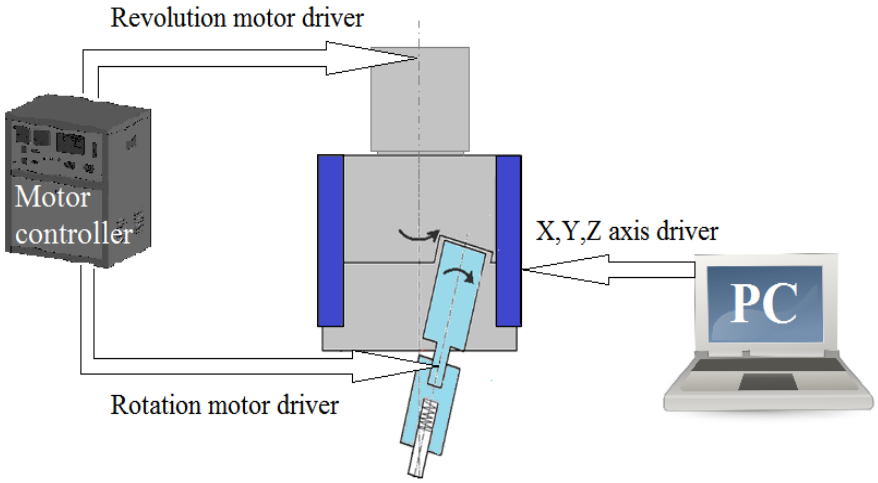

Fig. 3.14 Schematic of RRP system

The spot polishing experiment was performed on an RRP system with a machine resolution of 0.001 mm. Fig. 3.15 shows the experimental setup. The polishing liquid is dropped on the polishing zone through the abrasive nozzle, and the new polishing liquid is continuously applied. Fig. 3.16(a) shows a photograph of a tubular tool made of acrylic resin, and Figs. 3.16(b) and 3.16(c) show photographs of a glass slide workpiece and a workpiece fixing base. Use wax to fix the workpiece to the base during polishing.

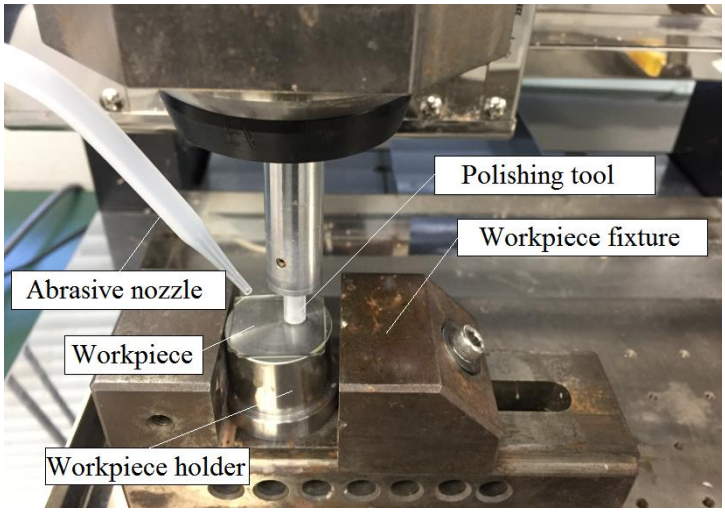

Fig. 3.15 Photograph of experimental setup

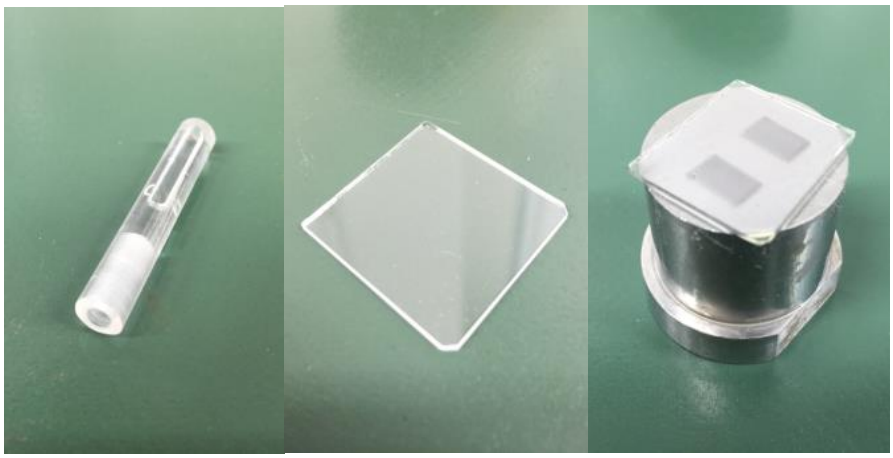

(a)Polishing tool (b)Workpiece (c)Workpiece holder

Fig. 3.16 Photograph of experimental consumables

3.5.5 Determination of Preston coefficient

The Preston wear coefficient k_P needs to be measured in the experiment. Polishing using the point polishing method, the relative speed can be considered to be constant. The simplified relative speed is shown in the equation below.

$$v_s = \omega \frac{R_1+R_2}{2} \tag{3.17}$$

Based on the Preston equation, x and y are selected as the double integral variation. x and y are integrated to obtain Eq. (3.18).

$$\iint_S^S h(x,y)dxdy = k_P T \iint_S^S p_c(x,y)v_s(x,y)dxdy \tag{3.18}$$

The left side of the equation can be considered as the product of the bottom area and the height, and the result of the multiplication is the material removal volume. The right side can be regarded as the product of area and pressure, and the result of multiplication is positive pressure.

$$V = k_P T v_s \iint_S^S p_c(x,y)dxdy = k_P T v_s F_n \tag{3.19}$$

Finally, the Preston coefficient can be determined by Eq. (3.20), where ρ_d is the density of the workpiece. Δm is the weight difference before and after polishing.

$$k_P = \frac{V}{v_s F_n T} = \frac{\Delta m}{v_s F_n T \rho_d} \tag{3.20}$$

In Eq. (3.20), if the Preston coefficient k_p is calculated, the following physical quantities are necessary. The mass change before and after the workpiece is polished, relative velocity, pressure and workpiece density. Experimental data is linearly fitted, we could get the value of k_P. The results of several sets of experiments are shown in Fig. 3.17. k_P is obtained by linear fitting, approximately 6.8×10^{-13}.

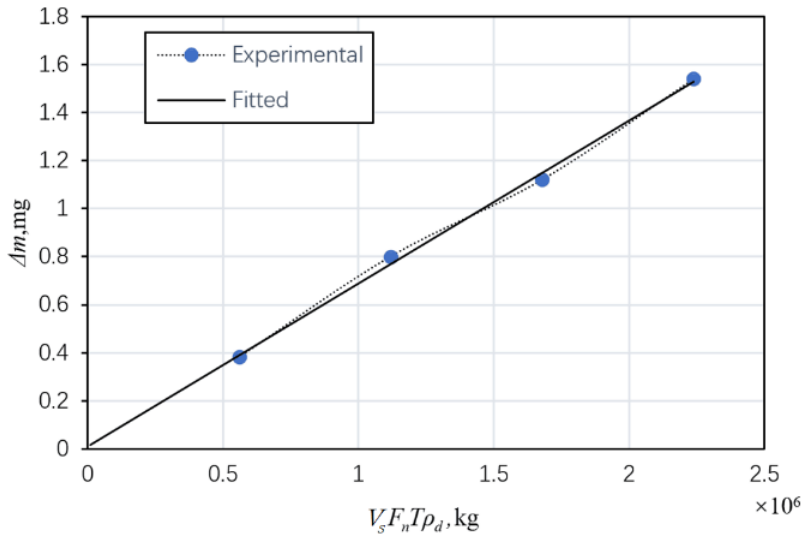

Fig. 3.17 Linear relationship between Δm and $v_s F_n T \rho_d$

After a large number of experiments, we have found efficient and stable data for the revolution speed, the rotation speed, the angle between the two axes and the polishing pressure. The slides were polished using free abrasive particles under these highly efficient and stable conditions (Table 3.1).

Table 3.1 Main experimental conditions.

Experimental conditions	Values
Workpiece material	flat glass
Tool material	acrylic resin (end-face dressing)
Rotational speed	600 *rpm*
Revolution speed	160 *rpm*
Angle of tool axis	5 °
Abrasive material	Cerium oxide 10 *wt* %
Polishing load	165 *g*
Abrasive supply	0.05 *g* / 5 *min*
Polishing time	5, 10, 15, 20 *min*, respectively

3.5.6 Results and discussion

The actual removal region is a hemispherical shape as shown in Fig. 3.18 (a). In the cross-sectional measurement chart, it is examined whether it is a Gaussian curve. Polished cross sections are shown in Fig. 3.18(b). The profile and polishing depth of the polished area corresponding to different polishing times are given.

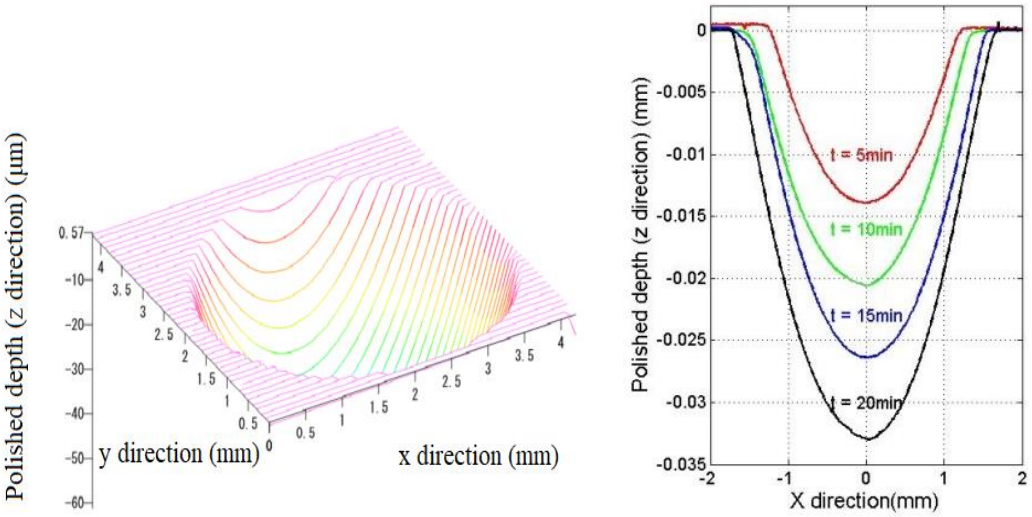

(a) 3-D image (b)Experimental section profile

Fig. 3.18 Image of polishing area

The relationship between the spot polished depth and polished time is shown in Fig. 3.18(b). The results show that the polished depth increases linearly with increasing polishing time from 5 minutes to 20 minutes. The removal rate is very fast in the first 5 minutes of polishing. Due to the complicated factors, it is also a difficult research point in the field of polishing. The red curve in Fig. 3.19 shows the theoretical removal curve simulated using MATLAB software. The blue curve indicates the actual profile.

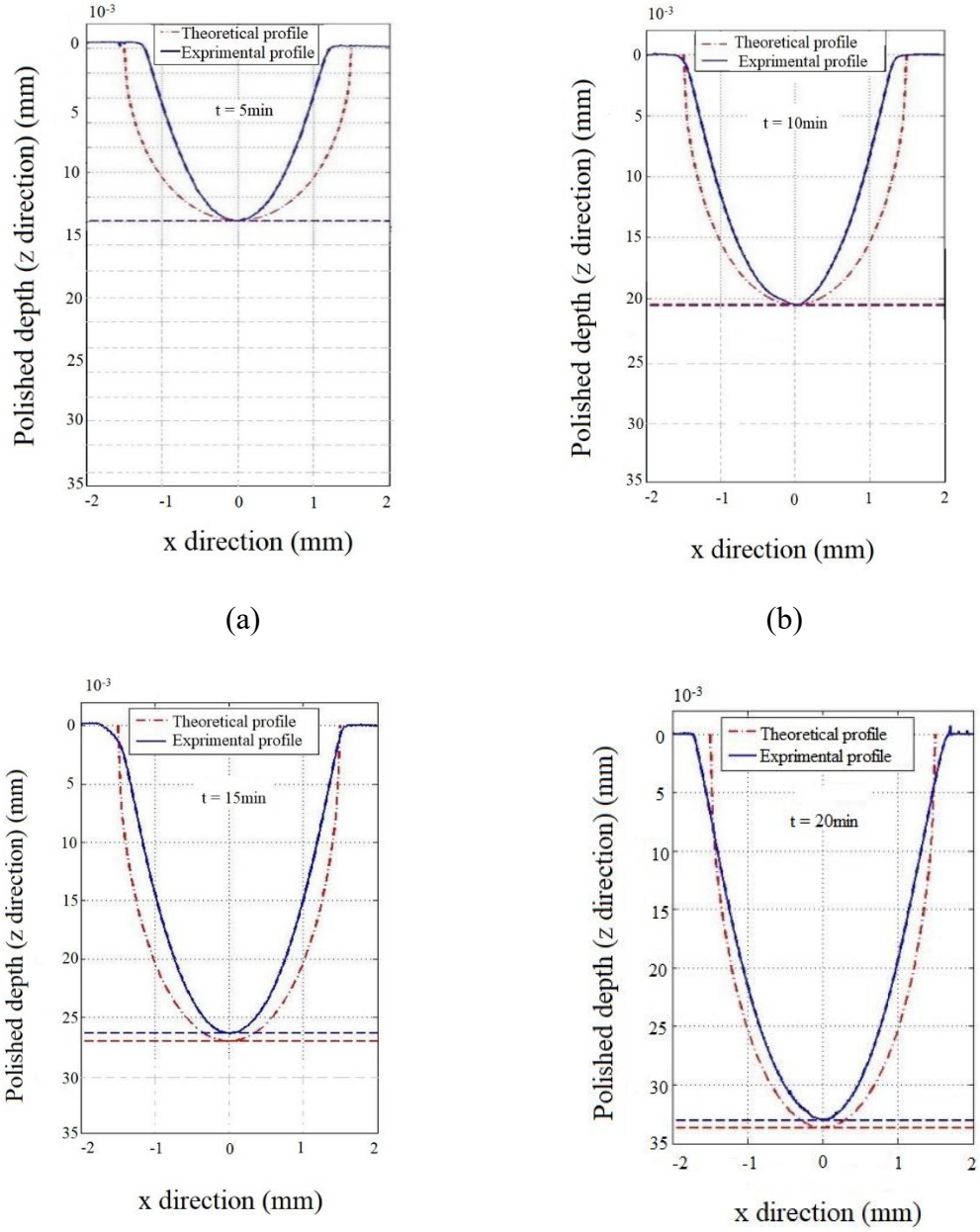

Fig. 3.19 Difference between theoretical and experimental profiles

First, the polishing tool will be described, and the RRP method uses a tubular polishing tool. The wall of the tube is relatively thin, and the wear of the polishing tool can be neglected, and the shape of the contact surface of the workpiece is considered to remain unchanged. Therefore, the polishing tool maintains a stable polishing rate. The blue curve shows practical material removal depth. Increasing the polishing time can

steadily increase the polishing depth. Although the polishing depth increases with polishing time, it can be found that there is a gap between theory and reality. The experimental results are a little difference from the theoretical shape. Fig. 3.19(c) and (d) show that the actual polishing depth at 15 minutes and 20 minutes are reduced compared to the theoretical depth. After polishing for 15 minutes, the error between the theoretical and actual results is 3.85%. After polishing for 20 minutes, the error between the theoretical and actual results is 5.98%. It seems that it is caused by the reduction of polishing pressure. After 10 minutes, the polishing tool was moved down due to the surface of the workpiece being removed. As the spring is slightly elongated, the polishing force becomes smaller.

3.6 Moving polishing

3.6.1 Coordinate system of polishing area

Based on the experience of fixed-point polishing for rotation and revolution polishing, this section focuses on the material removal model for moving polishing. The figure below is a schematic diagram of moving polishing. Feed speed is always defined as y-axis direction, and the material removal depth is defined as the z-axis (Fig. 3.20). Ω represents the revolution angular velocity, and ω represents the rotational angular velocity.

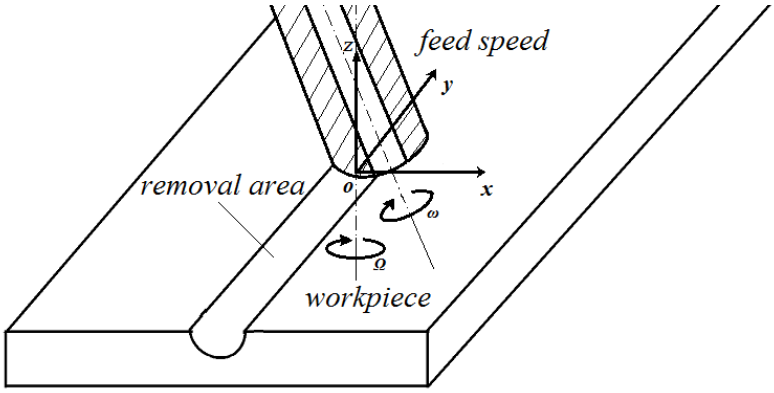

Fig. 3.20 Establishment of polishing area coordinate system

Another important formula is introduced, namely the overall removal function $H(x, y)$, which can be expressed as an unit removal function $R(x, y)$ with t he dwell time $T(x, y)$.

$$H(x,y) = \iint_2^1 T(x,y)R(x,y)\,dxdy \tag{3.21}$$

Moving polishing is compared to fixed point polishing. As shown in the figure below, the polishing tool head moves along the path at a certain feed speed v_f. The coordinate system o-xy is established at point O. y is the tangential direction of the path, and x is the vertical direction of the path. H is a small area in the direction of the contact region x. Assuming that the pressure on H is p_c and the linear velocity is v_s, the depth of material removal in the dT at point H could be calculated (Fig. 3.21).

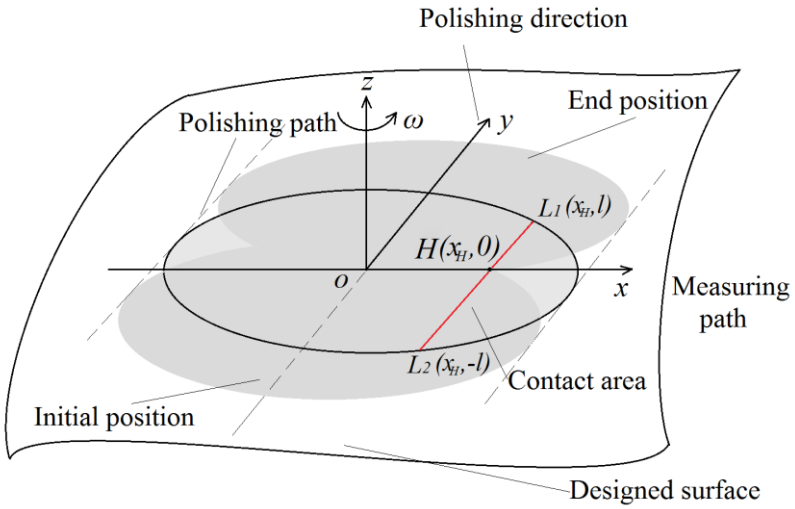

Fig. 3.21 Schematic diagram of moving polishing

Based on the Preston equation

$$dh = k_p p_c v_s dT \tag{3.22}$$

As shown above, during the dT time, the length of the polishing tool along the path is dl.

$$dT = \frac{dl}{v_f} \tag{3.23}$$

Substituting equation

$$dh = k_p p_c v_s \frac{dl}{v_f} \tag{3.24}$$

A new physical quantity E is defined, indicating the removal depth per unit path length.

$$E = \frac{dh}{dl} = k_p \frac{p_c v_s}{v_f} \tag{3.25}$$

Material removal of the H point on the x-axis in the polishing zone is considered. Assuming that the shape and size of the contact area are not abrupt near the point P, L_1 and L_2 can be regarded as the starting point and the ending point of the contact area in contact with H.

L_1L_2 could be a polishing strip at point H, and the amount of material removed by each micro-element on the polishing strip depends on the contact pressure, line speed and feed rate of the micro-element through H. The material removal depth at point H can represent the integral of E along L_1L_2.

$$h = \int_{L_2}^{L_1} E \, dl \tag{3.26}$$

The final effect of building the model is determined by the direction of each axis of the coordinate system. The curve below is the removal function. When the function is found, the profile is removed. The depth of removal corresponding to any x value is known. It has great reference significance for processing complex curved surfaces in the future (Fig. 3.22).

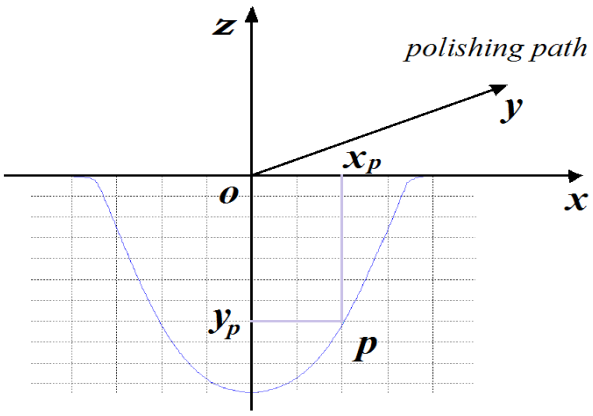

Fig. 3.22 Schematic diagram of mathematical model results

Establish the polishing area coordinate system as shown below. Establish a Cartesian coordinate system to describe the RRP special machining posture. The *x*-axis is defined as measurement direction, the y-axis is vertical direction of measurement direction, and the z-axis is defined as the direction opposite to the material removal depth (Fig. 3.23). In the coordinate system, the revolution axis and the rotation axis (*OQ* and *MN*, respectively) maintain a certain angle λ. The origin of the coordinate system o-xy is at the center point *O* in the polishing zone. The coordinate system o-xy is in the tangent plane of point *H*. *M* is located at the intersection of *MN* and *o-xy* plane, *MN′* is the projection of the rotation axis on the *xy* plane.

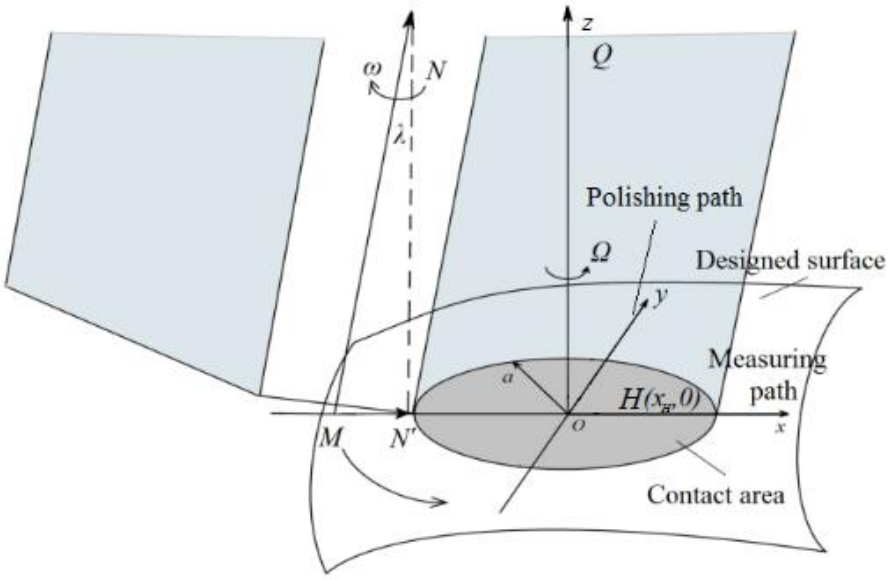

Fig. 3.23 Schematic of polishing area coordinate system

A circle with a radius a is formed, and the polishing area in *o-xy* can be expressed.

$$x^2 + y^2 = a^2 \tag{3.27}$$

Pressure distribution is obtained.

$$P(x,y) = -\frac{p_o}{a}\sqrt{a^2 - x^2 - y^2} \tag{3.28}$$

The center point pressure could also be expressed.

$$P_o = \frac{3F}{2\pi a^2} \tag{3.29}$$

F is the polishing pressure. Applying this formula also requires measuring the Poisson's ratio and modulus of elasticity of tool and the workpiece separately. It can be seen that the size and pressure are related to the geometric parameters, the physical properties, and the positive pressure of the normal phase.

3.6.2 Description of the posture of the polishing tool

Tool attitude planning has always been a key point in the polishing process. A

reasonable polishing posture not only avoids interference during the polishing process, but also improves the polishing efficiency. It can be seen from the Preston equation that the material removal during the polishing process is affected by the relative linear velocity in the polishing zone. The polishing attitude has a large influence on the relative linear velocity in the polishing zone, so the tool attitude is described before deriving the relative linear velocity.

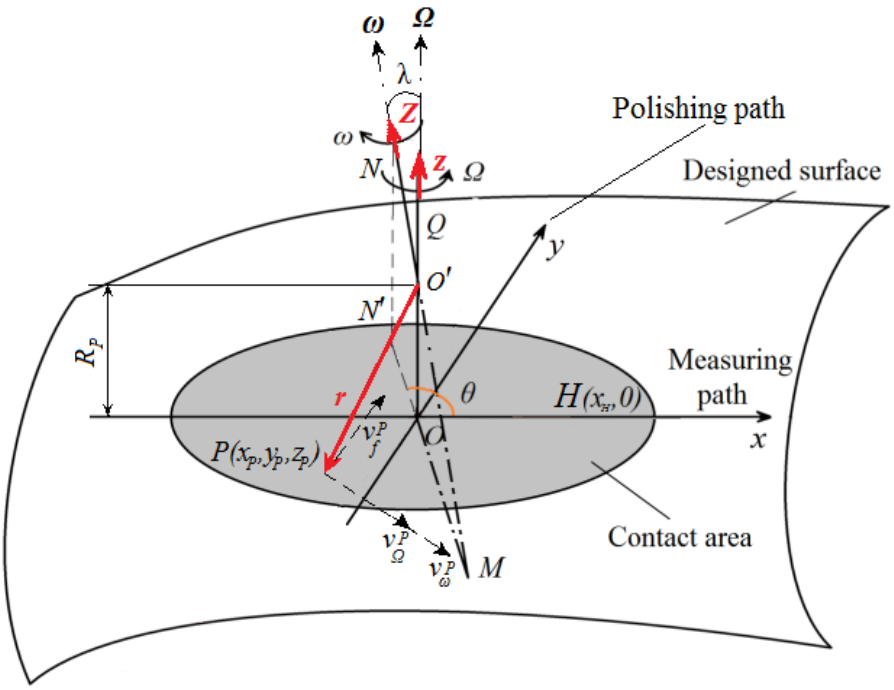

Fig. 3.24 Polishing area with velocity distribution

The figure above shows polishing attitude. The tubular tool head moves along the polishing path and contacts the point *o*. The local coordinate system established at point *o* is *o-xyz*, where *o* is the center, *x* and *y* axes are defined the same as before, and ***z*** is the unit normal vector. ***ω*** and ***Ω*** represented the rotation and revolution angular velocities of the tool. To describe the pose of the tool, the tool coordinate axis *O'-XYZ* (The *X, Y, Z* axis are not drawn in order to make the picture brief) is established at point *O*, where *O* is the center point and ***Z*** is polishing axis unit vector. The angle between the unit vectors ***z*** and ***Z*** is polishing inclination angle *λ*, and the angle between ***Z*** and

the x axes is defined as the polishing angle θ. The local coordinate system first rotates the θ angle around the z-axis and then rotates the λ angle around the y-axis. The resulting coordinate system is parallel to the tool coordinate system. Regardless of the translation transformation between the local coordinate system and the tool coordinate system, the tool coordinate system and the local coordinate system have the following rotation transformation. MN' is the projection of the rotation axis onto the xOy plane while the angle between MN' and the x-axis direction is θ (Fig. 3.24).

$$(X, Y, Z) = (x, y, z)M_{rot} \tag{3.30}$$

Where M_{rot} is a rotation matrix, which can be expressed as

$$M_{rot} = \begin{bmatrix} \cos\theta & -\sin\theta & 0 \\ \sin\theta & \cos\theta & 0 \\ 0 & 0 & 1 \end{bmatrix} \begin{bmatrix} \cos\lambda & 0 & \sin\lambda \\ 0 & 1 & 0 \\ -\sin\lambda & 0 & \cos\lambda \end{bmatrix} \tag{3.31}$$

Rewritten as

$$M_{rot} = \begin{bmatrix} \cos\lambda\cos\theta & \cos\lambda\sin\theta & 0 \\ -\sin\theta & \cos\theta & 0 \\ \sin\lambda\cos\theta & \sin\lambda\sin\theta & \cos\lambda \end{bmatrix} \tag{3.32}$$

Finally, the tool coordinates can all be represented by the polishing area coordinates.

$$\boldsymbol{Z} = \sin\lambda\cos\theta\, x + \sin\lambda\sin\theta\, y + \cos\lambda\, z \tag{3.33}$$

The polishing posture is mainly described by the vector $\boldsymbol{Z}$, and the vector $\boldsymbol{Z}$ can be represented by θ and λ. The attitude angle of the tool head during polishing affects the relative linear velocity in the polishing zone, which in turn affects material removal.

3.6.3 Distribution function of relative velocity

The contact area during polishing is not a point but an area having a certain area. The linear velocity in the polishing zone is not a fixed value, and its distribution function is related to the rotational angular velocity and the polishing posture change. The material removal rate at each point is primarily dependent on the contact pressure and relative linear velocity at that point. The pressure has been given, and relative linear velocity in the polished area is derived below.

As shown in the Fig. 3.24, the tool head rotates around the axis Z during polishing. The revolution angular speed is Ω, and the rotation angular speed is ω. The revolution angular speed vector is $\boldsymbol{\Omega}$, the rotation angular speed vector is $\boldsymbol{\omega}$, and the rotation angular speed vector is the same or opposite to $\boldsymbol{Z}$. It is shown that ω is positive when $\boldsymbol{\omega}$ and $\boldsymbol{Z}$ are in the same direction, and ω is negative when $\boldsymbol{\omega}$ and $\boldsymbol{Z}$ are in the same direction. $\boldsymbol{Z}$ is a unit vector, so ω can be expressed as

$$\boldsymbol{\omega} = \omega \boldsymbol{Z} = \omega(\sin\lambda\cos\theta\,, \sin\theta\sin\lambda\,, \cos\lambda) \tag{3.34}$$

Point P is any point of polished area, and $\boldsymbol{r}$ is a vector from O' to point P.

$$\boldsymbol{r} = \overrightarrow{O'P} = \left(x_p, y_p, -R_p\right) \tag{3.35}$$

$$R_p \approx \sqrt{R^2 - a^2} \tag{3.36}$$

Where R_p is the tool head radius and a is the polished area radius. The tool head rotation produces a line speed in the polishing zone as the revolution speed and the rotation speed. The line velocity is the angular speed vector forked by radius vector. At the same time, the linear velocity vector of the feed rate at P is given.

$$\boldsymbol{v}_{\omega}^{P} = \boldsymbol{\omega} \times \boldsymbol{r} = \omega \begin{bmatrix} -R_P \sin\theta \sin\lambda - \cos\lambda\, y_P \\ \cos\lambda\, x_P + R_P \cos\theta \sin\lambda \\ \cos\theta \sin\lambda\, y_P - \sin\theta \sin\lambda\, x_P \end{bmatrix} \tag{3.37}$$

$$\boldsymbol{v}_{\Omega}^{P} = \boldsymbol{\Omega} \times \boldsymbol{r} = \Omega \begin{bmatrix} 0 \\ 0 \\ 1 \end{bmatrix} \times \begin{bmatrix} x_P \\ y_P \\ -R_P \end{bmatrix} = \Omega \begin{bmatrix} -y_P \\ x_P \\ 0 \end{bmatrix} \tag{3.38}$$

$$\boldsymbol{v}_{f}^{P} = \left(v_{fx}^{P}, v_{fy}^{P}, v_{fz}^{P}\right) \tag{3.39}$$

The removal amount of the material is only related to the linear velocity on *x*, *y* direction. Revolution velocity, rotation velocity, and the feed velocity of the *P* point are synthesized.

$$v = \sqrt{(v_{\omega x}^{P} + v_{\Omega x}^{P} + v_{ax}^{P})^2 + \left(v_{\omega y}^{P} + v_{\Omega y}^{P} + v_{ay}^{P}\right)^2} \tag{3.40}$$

Feed rate is small, so feed line speed in the polishing area can be ignored.

$$\begin{aligned} v &\approx \sqrt{(v_{\omega x}^{P} + v_{\Omega x}^{P})^2 + \left(v_{\omega y}^{P} + v_{\Omega y}^{P}\right)^2} \\ &= \sqrt{[\omega(-R_P \sin\theta \sin\lambda - y\cos\lambda) - \Omega y]^2 + [\omega(x\cos\lambda + R_P \cos\theta \sin\lambda) + \Omega x]^2} \end{aligned} \tag{3.41}$$

3.6.4 Mathematical modeling of linear path polishing

As shown in the Fig. 3.21, when the tool is polished in a straight line, the polished area is a circle with a radius *a*, the *y* axis is the path direction, and the *x* axis is perpendicular to the path direction.

$$dl = dy \tag{3.42}$$

$$h(x) = \int_{-l}^{l} E dy \tag{3.43}$$

Where l is the coordinate component of the intersection of the contact circle and L_1L_2 on the y-axis. L_1L_2 can be regarded as the removal zone on H, and each point on line L_1L_2 is polished to the point H, and the sum of the polishing amounts of all the points is equal to the final removal amount of the point H. The entire polished area can be seen as the sum of numerous polishing strips parallel to the path. Models can be built using integral geometric meaning.

$$l = \sqrt{a^2 - x^2} \tag{3.44}$$

Substituting equation

$$h(x) = \frac{k_P}{v_f} \int_{-l}^{l} p_c v_s dy \tag{3.45}$$

Finally, the contact area, pressure distribution function, relative speed function is substituted and sorted.

$$h(x) = -\frac{3k_p F}{\pi v_f a^3} \int_0^{\sqrt{a^2-x^2}} \sqrt{(a^2 - x^2 - y^2)} \cdot \sqrt{[\omega(-R_P \sin\lambda \sin\sigma - y\cos\sigma) - \Omega y]^2 + [\omega(x\cos\sigma + R_P \cos\lambda \sin\sigma) + \Omega x]^2}\, dy \tag{3.46}$$

After the above formula is used for y integration, it is an expression with x as the variable. When x is taken from -a to a, the material removal profile (function shape) and the removal depth (value of z) can be obtained.

3.6.5 Verification of the mathematical model of linear path polishing

After many experiments, and the experimental data is linearly fitted, a more accurate k_P value 3.18×10^{-15} can be achieved. Experiments are needed to prove the proposed mathematical model. After a large number of experiments, we have found efficient and

stable data for the rotation speed and the polishing pressure. The workpiece was polished using free abrasive particles under these highly efficient and stable conditions. The experimental conditions are shown in Table 3.2.

Table 3.2 The experimental conditions.

Experimental conditions	Values
Workpiece material	flat glass (MATSUNAMI GLASS IND. LTD., S2111)
Tool material	acrylic resin (end-face dressing)
Rotational speed	600 rpm
Revolution speed	160 rpm
Angle of tool axis	5 °
Abrasive material	Cerium oxide 10 wt %
Polishing load	300 g
Abrasive supply	0.05 g / 5 min
Feed speed	10 μm

For the entire plane processing, after several tests, it can be found that stable and effective material removal can be achieved. The final condition was a scan pitch of 0.1 mm and a feed speed of 40 μm per second. Other experimental conditions were unchanged from the single pass polishing experiment. Fig. 3.25 shows the scan path used for planar polishing.

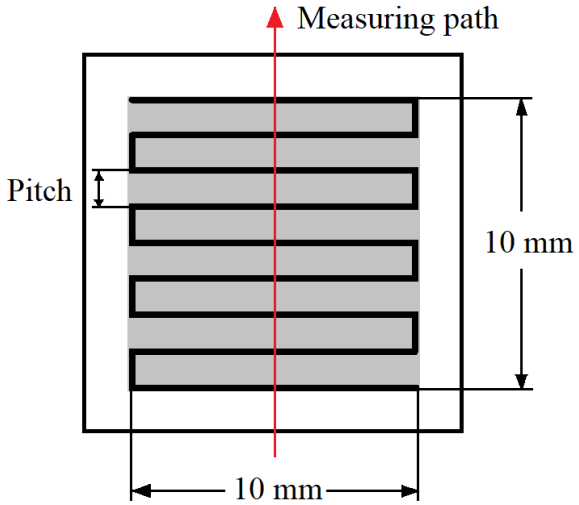

Fig. 3.25 Polishing scan path

The two figures below show the results of single path polishing and overall planar polishing. The blue curve is the actual polishing result and the red curve is theoretically simulated by MATLAB software (Fig. 3.26). The experimental results are basically consistent with the theory, which confirms that the proposed model is effective. The polishing tool is thin-walled, and the shape of the tool remains essentially the same, so the wear of the polishing tool can be ignored.

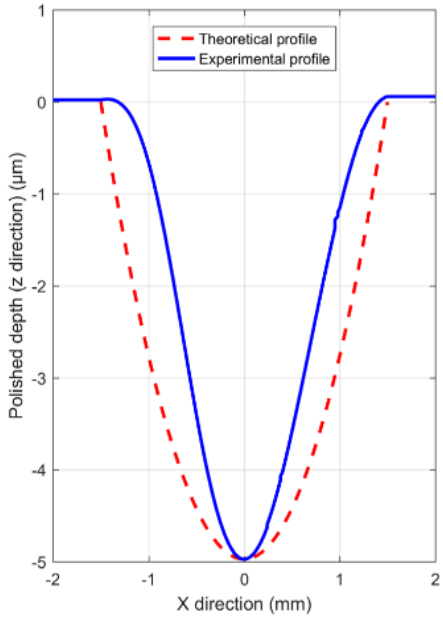

Fig. 3.26 MATLAB results of theoretical and experimental removal profiles

Fig. 3.27 shows the actual removal area after the entire planar polishing. The shape of the bottom is undulating, with an average polishing depth of approximately 16 μm, which does not reach a smooth plane. After analysis, it is currently thought to be caused by the connection between the tool and the bracket.

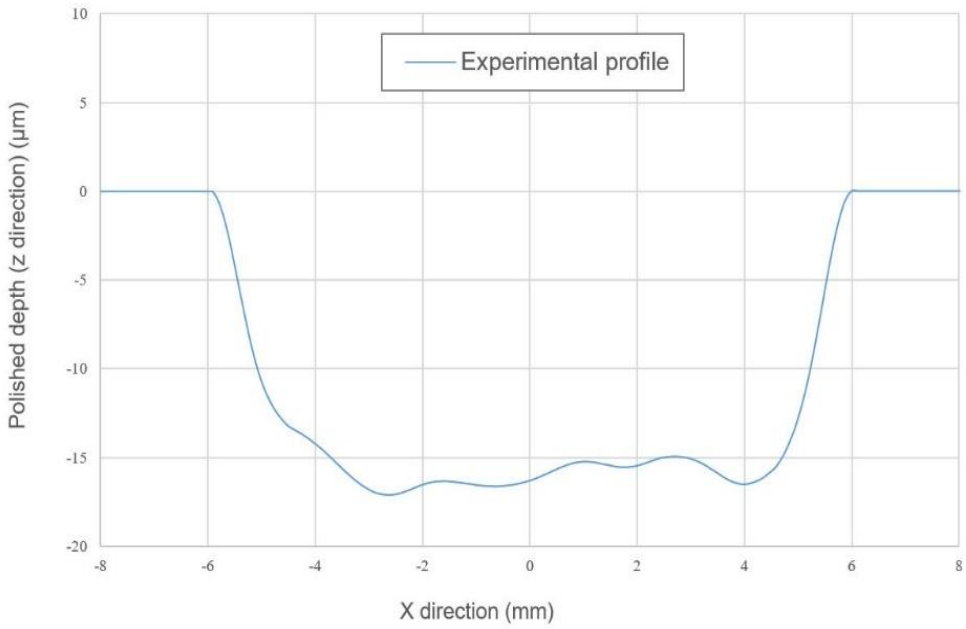

Fig. 3.27 Removal depth of scan-type polishing

In practice, there is a clearance fit between the tool and the holder. In the scan-type polishing, the tool has a slight swing inside the holder due to the frequent change of the polishing direction. Leads to the tool axis, the holder axes do not coincide. The polishing force is not stable as the experiment progresses.

To achieve the principle of rotation and revolution polishing method as mentioned earlier. It is necessary to design a prototype that can achieve the special machining posture of the principle of rotation and revolution and can verify the further theoretical feasibility. This prototype needs to be simple in structure, low in cost and stable in processing.

3.7 Mathematical modeling of curve path polishing

Based on the study of linear path points, the curve path is basically the same. The biggest difference is that the radius is increased, and polar coordinates are used to describe the function [22-24]. As can be seen from the figure below, the polishing path on the curved surface is actually a three-dimensional curve, and the center of curvature of the path through o point is *O′*. Since material removal studies are performed in the tangent plane *xoy*, the projection of *O′* on the plane xoy is denoted as *O*, and now *Oo* is the radius of curvature. The coordinate system *O-XY* is established at point *O*, *X* axis is parallel to the *x* direction. *Y* axis is parallel to the *y* direction (Fig. 3.28).

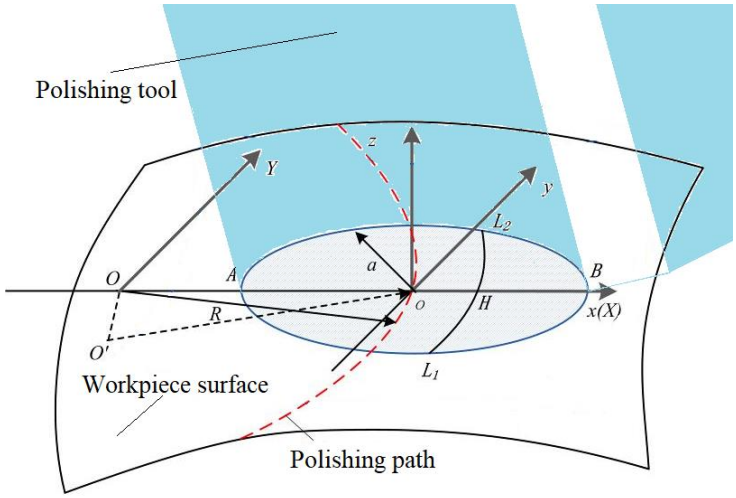

Fig. 3.28 Polishing schematic of the curved path

Coordinate transformation

$$\begin{cases} x = X - R \\ y = Y - R \end{cases} \tag{3.47}$$

In the coordinate system *OXY*, the pressure of polished zone is

$$p(X,Y) = -\frac{p_o}{a}\sqrt{a^2 - (X-R)^2 - Y^2} \tag{3.48}$$

It is more convenient to convert the problem into polar coordinates in the curve path.

$$\begin{cases} X = \rho\cos\theta \\ Y = \rho\sin\theta \end{cases} \tag{3.49}$$

$$p(\rho,\theta) = -\frac{p_o}{a}\sqrt{a^2 - (\rho\cos\theta - R)^2 - \rho^2\sin^2\theta} \tag{3.50}$$

O is the center of curvature, *R* is radius of curvature, and curve L_1L_2 is the intersection of the path and the contact area. The axes are created, and the directions of the axes are the same as before (Fig. 3.29).

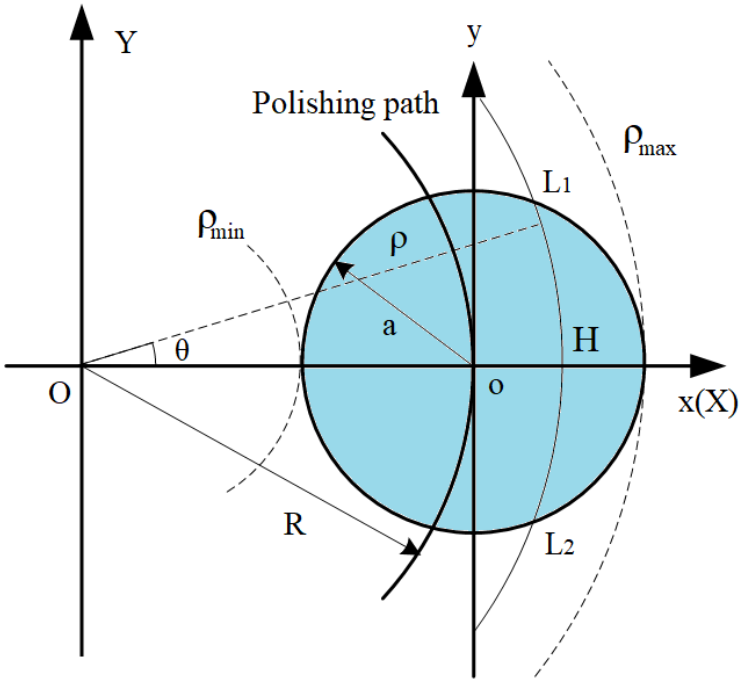

Fig. 3.29 Establish a coordinate system for curved path polishing

L_1L_2 is an arc with a radius of ρ

$$dl = \rho d\theta \tag{3.51}$$

$$h(\rho) = \int_{\theta_2}^{\theta_1} w_P \rho d\theta \tag{3.52}$$

θ_1 and θ_2 are the polar angles of L_1 and L_2 in the *O-XY* coordinate system. Combined with the Preston equation

$$h(\rho) = \int_{\theta_2(\rho)}^{\theta_1(\rho)} k_P p_c \frac{v_s}{v_f} \rho d\theta \tag{3.53}$$

Where v_f is the feed rate of point H. When polishing along the curve, the feed rate increases.

$$v_f = \frac{v_{fo} \cdot \rho}{R} \tag{3.54}$$

In the above formula, v_{fo} is the feed speed of the polishing zone and is substituted.

$$h(\rho) = \frac{k_P R}{v_{fo}} \int_{\theta_2(\rho)}^{\theta_1(\rho)} p_c(\rho, \theta) v_s(\rho, \theta) d\theta \tag{3.55}$$

The pressure distribution function is converted to polar coordinates, and the relative linear velocity distribution is as follows.

$$v_s(\rho, \theta) = \sqrt{\begin{matrix}[\omega(-R_P \sin\lambda \sin\sigma - \rho \sin\theta \cos\sigma) - \Omega\rho \sin\theta]^2 + \\ [\omega(\rho \cos\theta \cos\sigma - R\cos\sigma + R_P \cos\lambda \sin\sigma) + \Omega(\rho\cos\theta - R)]^2\end{matrix}} \tag{3.56}$$

When point O is outside the contact area, ie $R>a$, then $\rho_{min}=R-a$, $\rho_{max}=R+a$. The contact circle in the new coordinate system could be expressed.

$$a^2 - (\rho\cos\theta - R)^2 - \rho^2 \sin^2\theta = 0 \tag{3.57}$$

$\cos\theta$ can be expressed as

$$\cos\theta = \frac{\rho^2 + R^2 - a^2}{2R\rho} \tag{3.58}$$

θ can be expressed as

$$\theta = arc\cos\left(\frac{\rho^2+R^2-a^2}{2R\rho}\right) \tag{3.59}$$

Substituting

$$h(\rho) = -\frac{3k_P FR}{\pi v_a a^3}\int_0^{arc\cos\left(\frac{\rho^2+R^2-a^2}{2R\rho}\right)} f(\rho,\theta)d\theta \tag{3.60}$$

$$f(\rho,\theta) = \sqrt{a^2-(\rho\cos\theta-R)^2-\rho^2\sin^2\theta}\cdot v_s(\rho,\theta) \tag{3.61}$$

F is the polishing pressure. The removal profile model established in this chapter depends on physical properties (contact elastic modulus, Poisson's ratio, tool head radius, surface principal curvature, etc.), polishing process parameters (polishing normal pressure, feed rate), revolution speed, rotation speed, etc.), polishing path geodesic radius and polishing attitude (polishing angle and declination).

3.8 Material removal of complex trajectories in rotation and revolution polishing method

The tool changes the polishing direction frequently as it moves along complex polishing trajectories. The stability is reduced, and processing marks are visible at the corners [25-28]. This section expands on the previous content and builds a material removal model at the vertical bisector of the corner.

The aspherical polishing path needs to cover the entire surface evenly. Various complex trajectories have emerged, including scanning path, lissajoue path and paeno path (Fig. 3.30). However, a uniform polishing path does not represent a uniform material removal. It has been deduced from previous studies that the material removal profile perpendicular to the polishing path can be obtained by integrating along the polishing path. Material removal problems in complex path polishing were investigated. One is the removal of the corner region of the path with large curvature. Typical

polishing path, such as linear reciprocating trajectories, frequently change the polishing direction during polishing [29-31]. The actual polished surface always has obvious traces at the corner of the path transition.

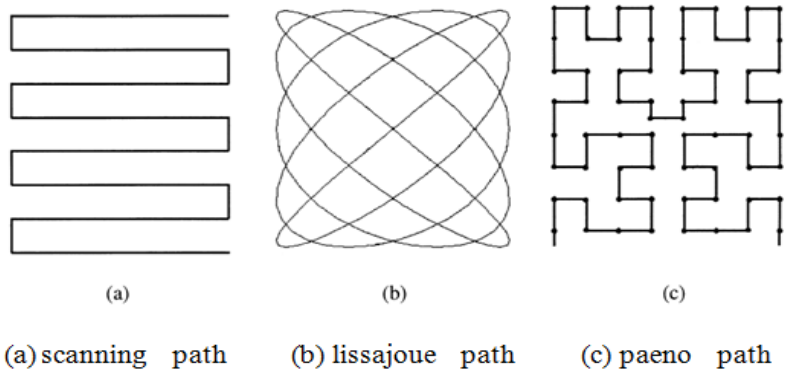

Fig. 3.30 Various polishing paths

In this section, the material removal of linear trajectories and circular trajectories on the vertical bisector of transitional corners is classified and the material removal of the polished path corners is modeled. Other complex polishing paths can be modeled and analyzed using similar methods in this chapter to optimize the polishing process.

3.9 Material removal with gentle angle change

According to the relationship between the tool radius and the contact radius, it is divided into two cases. This section only makes an intuitive rough analysis. The next section gives a detailed calculation step [32, 33].

When $R_P < R\sin\frac{\theta_1}{2}$, the situation is the simplest. The tool goes straight, then goes to the arc, and finally goes straight. The vertical bisector of the corner is studied, and only the circular path produces material removal for the vertical bisector. See the following Fig. 3.31 and the following figure shows the law of the division of the polished area.

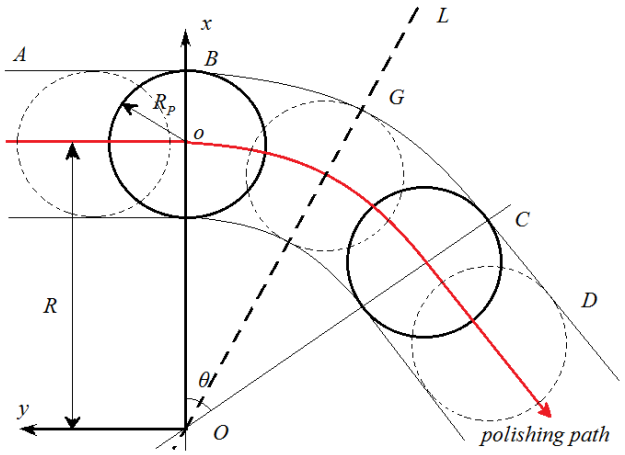

Fig. 3.31 Movement of the tool along the curve ($R_P < R \sin\frac{\theta_1}{2}$)

The polishing tool first grinds along a straight line and transitions through a circular arc to another straight path. The material removal profile on the arc segment is formed by the movement of the polishing tool along the straight-line segment and the arc segment.

The radius of the arc of the arc segment is R, the arc angle is θ_1, and the vertical bisector of the arc angle is L. In order to simplify the problem, the material removal profile in the direction of the vertical bisector L in the arc segment $\theta_1/2$ is discussed (Fig. 3.32).

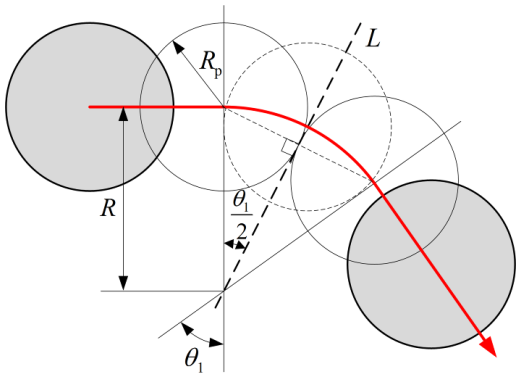

Fig. 3.32 Geometric relationship of the polishing process ($R_P < R\, sin\frac{\theta_1}{2}$)

It is discussed whether the straight-line polishing path has influence on the material removal profile on the vertical bisector L. It needs to be discussed in the following three cases.

When the tool moves to the end of the straight-line path, the contact circle has no intersection on the vertical bisector L of the arc angle θ_l. The tool moves along a straight path without material removal on the L line. The material removal profile at the arc segment $\theta_l/2$ is only affected by the polishing path of the arc segment. Therefore, polished removal profile is the same as the tool polishing, and polished removal profile on L can be abbreviated into the following form by the formula studied before.

$$h(\rho) = -\frac{3k_P F_n R}{\pi v_a a^3} \int_0^{\phi_1(\rho)} f(\rho, \phi)\, d\phi \tag{3.62}$$

$$R - R_P \le \rho \le R + R_\rho$$

In the equation

$$\phi_1(\rho) = arc\cos\left(\frac{\rho^2 + R^2 - a^2}{2R\rho}\right) \tag{3.63}$$

$$f(\rho, \theta) = \sqrt{a^2 - (\rho\cos\theta - R)^2 - \rho^2\sin^2\theta} \cdot v_s(\rho, \theta) \tag{3.64}$$

$$v_s(\rho, \theta) = \sqrt{\begin{matrix}[\omega(-R_P\sin\lambda\sin\sigma - \rho\sin\theta\cos\sigma) - \Omega\rho\, sin\,\theta]^2 + \\ [\omega(\rho\cos\theta\cos\sigma - R\cos\sigma + R_P\cos\lambda\sin\sigma) + \Omega(\rho\cos\theta - R)]^2\end{matrix}} \tag{3.65}$$

Substituting the equation

$$h(\rho) = -\frac{3k_P F_n R}{\pi v_a a^3} \int_0^{arc\cos\left(\frac{\rho^2 + R^2 - a^2}{2R\rho}\right)} \sqrt{a^2 - (\rho\cos\theta - R)^2 - \rho^2\sin^2\theta} \cdot$$

$$\sqrt{\begin{matrix}[\omega(-R_P\sin\lambda\sin\sigma - \rho\sin\theta\cos\sigma) - \Omega\rho\, sin\,\theta]^2 + \\ [\omega(\rho\cos\theta\cos\sigma - R\cos\sigma + R_P\cos\lambda\sin\sigma) + \Omega(\rho\cos\theta - R)]^2\end{matrix}} d\phi \tag{3.66}$$

3.10 Material removal with large angle changes

When $R \geq R_P \geq R \sin\frac{\theta_1}{2}$, not only the circular path has material removal for the vertical bisector of the corner. The linear path also produces 2 material removals for some of the vertical bisectors [34]. The vertical bisector is divided into 3 segments, 2 cases (Fig. 3.33).

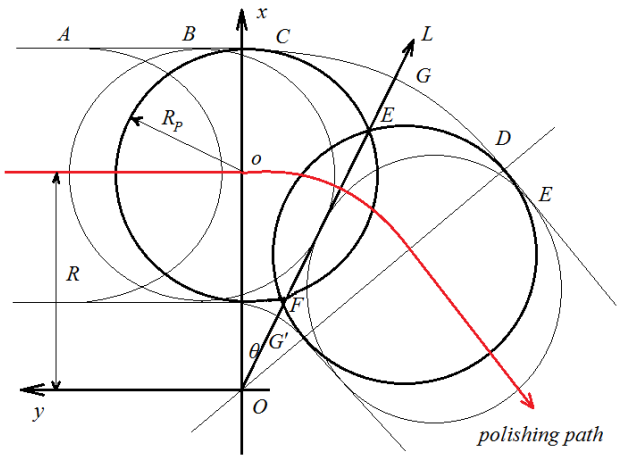

Fig. 3.33 The movement of the tool along the curve ($R \geq R_P \geq R \sin\frac{\theta_1}{2}$)

The vertical bisector L of the arc is already touched as the tool moves along the straight line, and material removal occurs on L as it is polished in a straight line. As shown in Fig. 3.34, material removal on L has three main effects: the AB segment, the BC segment, and the CD segment.

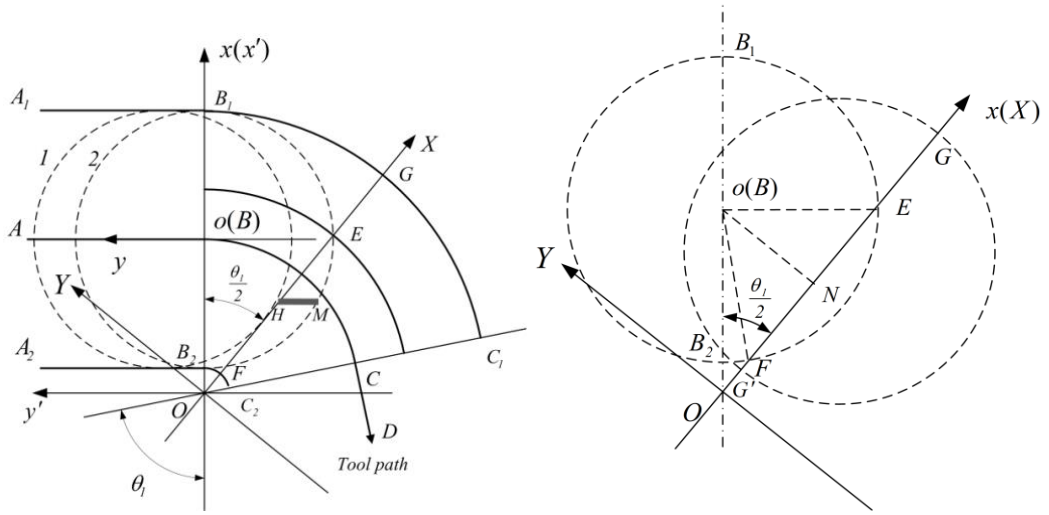

(a) General schematic and its coordinate system definition (b) Partial schematic

Fig. 3.34 Schematic diagram of line segment material removal ($R \geq R_P \geq R\sin\frac{\theta_1}{2}$)

3.10.1 Mathematical modeling of linear path

Since L is the vertical bisector of the arc segment, the material removal of the AB segment and the CD segment on L is equivalent. As shown in Fig. 3.34, the tool just touches the vertical bisector L when it is in position 1 and moves to position 2 to move along the circular path. Therefore, the effect of the straight-line segment AB on L is investigated by studying the material removal of the tool from the position 1 to the position 2.

The coordinate *o-xy* is established at point B, and the *O-x'y'* is established at O (Fig. 3.34(a)). Where the y and y' directions are parallel to the AB segment path, and the x and x' directions are perpendicular to the AB segment. The tool intersects the X axis at point E and point F at position 2. In Fig. 3.34(b), $OB = R,\ BB_2 = R_P,\ OB_2 = R - R_P,\ BN = R\sin\frac{\theta_1}{2},\ ON = R\cos\frac{\theta_1}{2},\ FN = \sqrt{R_P^2 - R^2\sin^2\frac{\theta_1}{2}}$. In XOY, the values of F and E can be expressed by the following equation.

$$F\left(R\cos\frac{\theta_1}{2} - \sqrt{R_P^2 - R^2\sin^2\frac{\theta_1}{2}}, 0\right) \tag{3.67}$$

$$E\left(R\cos\frac{\theta_1}{2}+\sqrt{R_P^2-R^2\sin^2\frac{\theta_1}{2}},0\right) \tag{3.68}$$

The tool moves from position 1 to position 2. In the *X* direction, only the *EF* segment has material removed and the rest has no effect. The point $H(\rho,0)$ is any point on the *EF*, and the *HM* can be regarded as the polishing band of the point *H* point material removal. At this point, the following equation can be obtained through the geometric relationship.

$$HM=\sqrt{R_P^2-\left(R-\rho\cos\frac{\theta_1}{2}\right)^2}-\rho\sin\frac{\theta_1}{2} \tag{3.69}$$

$$HM=q \tag{3.70}$$

Therefore, the coordinates of *M* could be expressed in *O-XY*.

$$M\left(\rho+q\sin\frac{\theta_1}{2},-q\cos\frac{\theta_1}{2}\right) \tag{3.71}$$

A straight line passing through *HM* can represent the following parameter form in the coordinate system *O-XY*.

$$\begin{cases} X(t)=t \\ Y(t)=-\cot\frac{\theta_1}{2}t+\rho\cot\frac{\theta_1}{2} \end{cases} \tag{3.72}$$

The point *O* is on the x-axis and the distance from the point *O* is *R*, and the following coordinate transformation is performed between *o-xy* and *o-x'y'*.

$$\begin{cases} x=x'-R \\ y=y' \end{cases} \tag{3.73}$$

Further, there is a coordinate transformation between *O-XY* and *o-x'y'* as follows.

$$\binom{X}{Y} = \begin{pmatrix} \cos\frac{\theta_1}{2} & -\sin\frac{\theta_1}{2} \\ \sin\frac{\theta_1}{2} & \cos\frac{\theta_1}{2} \end{pmatrix} \binom{x'}{y'} \tag{3.74}$$

After transformation

$$\begin{cases} x = \cos\frac{\theta_1}{2} X + \sin\frac{\theta_1}{2} Y - R \\ y = \cos\frac{\theta_1}{2} Y - \sin\frac{\theta_1}{2} X \end{cases} \tag{3.75}$$

Discuss the velocity distribution in the contact circle in *O-XY*.

$$\begin{aligned} v_s(X,Y) &\approx \sqrt{(v_{\omega x}^P + v_{\Omega x}^P)^2 + \left(v_{\omega y}^P + v_{\Omega y}^P\right)^2} \\ &= \sqrt{[\omega(-R_P \sin\lambda \sin\sigma - y\cos\sigma) - \Omega \mathrm{y}]^2 + [\omega(x\cos\sigma + R_P \cos\lambda \sin\sigma) + \Omega x]^2} \\ &= \sqrt{\begin{matrix} \left[\omega\left(-R_P \sin\lambda \sin\sigma - \left(\cos\frac{\theta_1}{2} Y - \sin\frac{\theta_1}{2} X\right)\cos\sigma\right) - \Omega\left(\cos\frac{\theta_1}{2} Y - \sin\frac{\theta_1}{2} X\right)\right]^2 \\ + \left[\omega\left(\left(\cos\frac{\theta_1}{2} X + \sin\frac{\theta_1}{2} Y - R\right)\cos\sigma + R_P \cos\lambda \sin\sigma\right) + \Omega\left(\cos\frac{\theta_1}{2} X + \sin\frac{\theta_1}{2} Y - R\right)\right]^2 \end{matrix}} \end{aligned} \tag{3.76}$$

Calculating polished removal on vertical bisector L (x direction), calculate polished removal depth in coordinate system *O-XY* when the tool passes a straight line through any point H between EF. That is, the material removal rate w_p of the unit path length is integrated from the point M to the point H, and polished depth on the point H could be obtained.

$$h_{AB}(\rho) = \int_{L_{HM}}^{1} w_P dl \tag{3.77}$$

$$\rho \in \left[R\cos\frac{\theta_1}{2} - \sqrt{R_P^2 - R^2\sin^2\frac{\theta_1}{2}}, R\cos\frac{\theta_1}{2} + \sqrt{R_P^2 - R^2\sin^2\frac{\theta_1}{2}}\right]$$

Substituting the previous formula.

$$h(\rho) = -\frac{3k_P F_n R}{\pi v_a a^3} \int_t^{t+q\sin\frac{\theta_1}{2}} v_s\big(X(t), Y(t)\big) \cdot \sqrt{X'^2(t) + Y'^2(t)}\, dt \tag{3.78}$$

Since the material removal on the vertical bisector of the arc is considered, the effect of the *CD* segment on its material removal is the same as that of the *AB* segment. Therefore, the overall linear path is twice as deep as the *AB* segment on the vertical bisector of the corner.

3.10.2 Mathematical modeling of curve trajectories

Material removal occurs as the tool head is polished along the arc BC through the centerline *L*. As shown in Fig. 3.35, the definitions of the coordinate systems *o-xy* and *O-XY* are the same as before. *H* is a point on the x-axis. When *H* is between *E* and *G* or between *F* and *G'*, L_1L_2 forms a polishing tape with point *H* material removal. When *H* is between *E* and *F*, $L_1'L_2'$ forms a material removal point of point *H*.

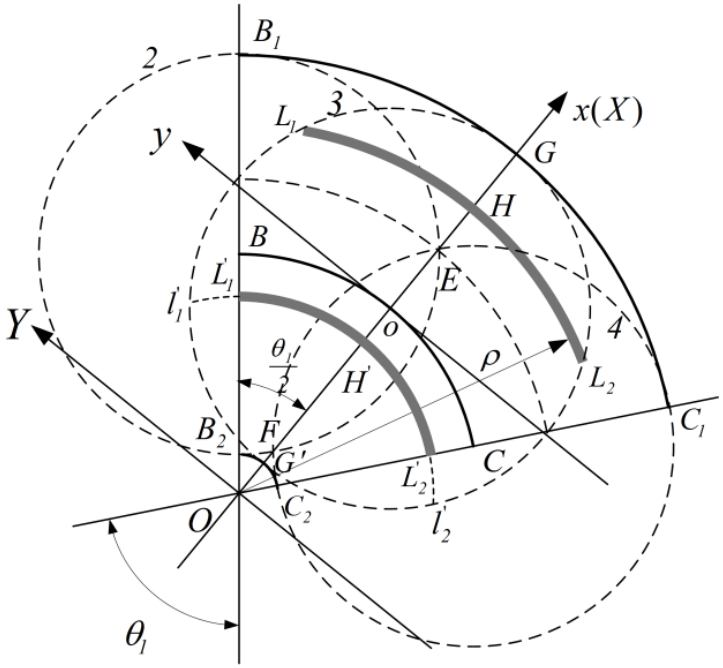

Fig. 3.35 Schematic diagram of material removal of circular segments

$$\rho \in \left[R\cos\frac{\theta_1}{2} + \sqrt{R_P^2 - R^2\sin^2\frac{\theta_1}{2}}, R + R_P\right] \text{ or}$$

$\rho \in \left[R - R_P, R\cos\frac{\theta_1}{2} - \sqrt{R_P^2 - R^2\sin^2\frac{\theta_1}{2}}\right]$, corresponds to the *EG* segment and the *FG′* segment. The material removal depth at any point on *EG* and *FG′* is cumulatively formed by a polishing band of radius ρ. The circle of radius ρ has two intersections with the contact circle of the tool, and both intersections are in the sector formed by B_1B_2 and C_1C_2. Polished depth at H at this time could be expressed.

$$h(\rho) = -\frac{3k_P F_n R}{\pi v_a a^3}\int_0^{\phi_1(\rho)} f(\rho,\phi)\,d\phi \tag{3.79}$$
$$R - R_P \le \rho \le R + R_\rho$$

$\rho \in \left[R - R_P, R\cos\frac{\theta_1}{2} + \sqrt{R_P^2 - R^2\sin^2\frac{\theta_1}{2}}\right]$, not all points on the tool will pass the midline *L*. Considering any point *H′* between the *EF*s, when the tool finally moves from position 2 through position 3 to position 4, only the $L_1'L_2'$ passes through point *H′* on the arc $l_1'l_2'$ where *H′* is located. Material removal at point *H′* is formed. In this case, polished depth on the point *H′* is obtained coefficient *wp* from $-\theta_1/2$ to $\theta_1/2$.

$$h'_{BC}(\rho) = -\frac{3k_P F_n R}{2\pi v_a a^3}\int_{-\frac{\theta_1}{2}}^{\frac{\theta_1}{2}} f(\rho,\phi)\,d\phi = -\frac{3k_P F_n R}{\pi v_a a^3}\int_0^{\frac{\theta_1}{2}} f(\rho,\phi)\,d\phi \tag{3.80}$$

3.10.3 Establishment of a mathematical model for overall material removal

Overall polished profile on *L* in this case could be expressed.

$$h(\rho) = \begin{cases} h_{AB}(\rho) & \rho \in (R\cos\frac{\theta_1}{2} + \sqrt{R_P^2 - R^2\sin^2\frac{\theta_1}{2}}, R + R_P) \cup \left(R - R_P, R\cos\frac{\theta_1}{2} - \sqrt{R_P^2 - R^2\sin^2\frac{\theta_1}{2}}\right) \\ h'_{BC}(\rho) + 2h_{AB(\rho)} & \rho \in \left(R\cos\frac{\theta_1}{2} - \sqrt{R_P^2 - R^2\sin^2\frac{\theta_1}{2}}, R\cos\frac{\theta_1}{2} + \sqrt{R_P^2 - R^2\sin^2\frac{\theta_1}{2}}\right) \end{cases} \tag{3.81}$$

3.11 Material removal with sharp changes in angle

When R_P>R, the radius of the rotation and revolution polishing tool is very small, and the smaller the radius of rotation is less common, and the generality of the study is also discussed as a case. Similar to the previous case, the vertical bisector is divided into two parts [35, 36]. In fact, there is a very small special area that is more complicated, but because the area is small, it can be ignored (Fig. 3.36).

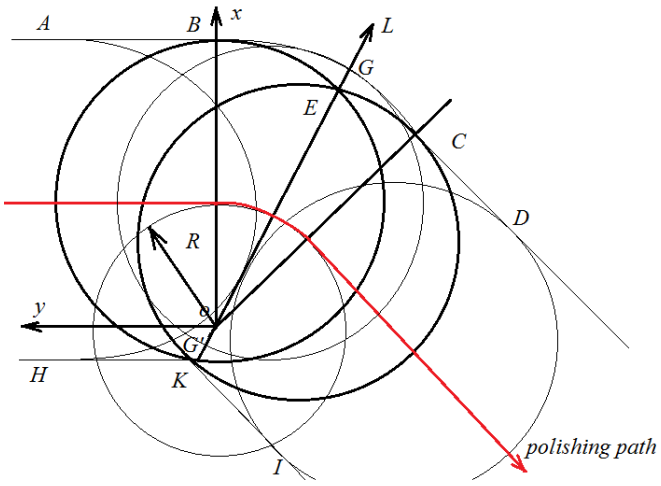

Fig. 3.36 The movement of the tool along the curve (R_P>R)

As shown in the Fig. 3.37, when R_p >R, the curvature center point O. At this time, the upper and lower boundaries by tool moving along path to the workpiece are $A_1B_1C_1D_1$ and A_2KD_2. The point G' is the intersection of the contact circle of position 3 and the x-axis, and G' in O-XY is (R-R_p, 0). K is the intersection, and the coordinate value in the coordinate system O-XY can be expressed as $K\left(\frac{R_P-R}{\cos\theta_1}, 0\right)$.

Through analysis, the material removal profile in the x direction is discussed separately. The EG segment is only affected by the circular polishing motion. EO and OD are affected by both circular motion and linear motion. $G'K$ is only affected by linear motion. However, since the $G'K$ length is very short, it can be ignored. Only the material removal of the GG' section is discussed.

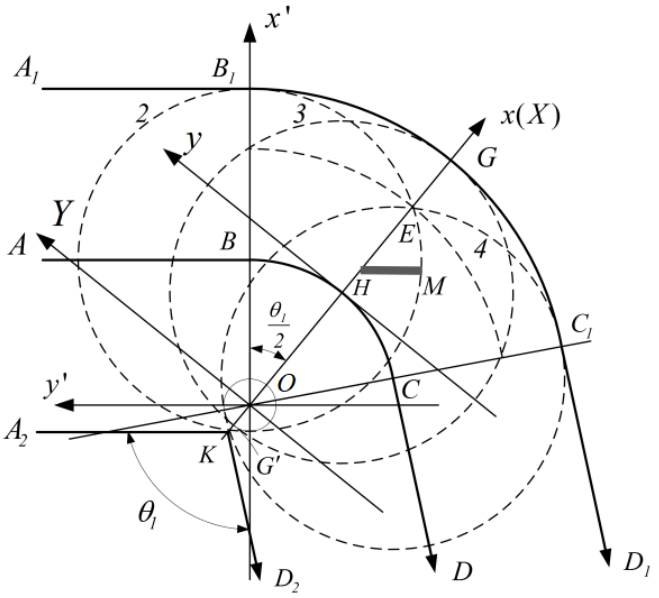

Fig. 3.37 Schematic diagram of material removal of circular segments ($R_p > R$)

3.11.1 Mathematical model material removal only for curved traces

The material removal on the *EG* segment is the same as in large angle changes, it is only affected by the arc segment. Therefore, material removal on the *EG* segment can be expressed.

$$h = h_{BC}(\rho) = -\frac{3k_P F_n R}{\pi v_a a^3}\int_0^{\phi_1(\rho)} f(\rho,\phi)\,d\phi \tag{3.82}$$

$$\rho \in \left[R\cos\frac{\theta_1}{2} + \sqrt{R_P^2 - R^2\sin^2\frac{\theta_1}{2}}, R + R_P\right]$$

3.11.2 Mathematical model material removal for straight and curved paths

The *OE* segment and the *OG'* segment are simultaneously affected by linear and circular trajectories. It is worth mentioning that the *OE* segment is swept at a forward speed along the circular path, while the *OG'* segment is swept at a speed opposite to the feed rate.

However, the material removal calculation method is the same, that is, the material

removal coefficient *wp* is integrated from $-\theta_1/2$ to $\theta_1/2$, so it can be discussed together. Material removal from straight segments and arcs is considered. In addition to the effect, the material removal profile of the *EG'* segment could be expressed.

$$h(\rho) = h_{BC}(\rho) + 2h_{AB}(\rho) \tag{3.83}$$

$$\rho \in \left[R - R_P, R\cos\frac{\theta_1}{2} + \sqrt{R_P^2 - R^2\sin^2\frac{\theta_1}{2}} \right]$$

This section investigates the effect of path on material removal during moving polishing. The material removal of the corner of the large curvature of the path is considered separately to meet the requirements of precise polishing of the curved parts. The material removal model was established by using the method of removal speed per unit path length. Influence of polishing path on material removal was path revealed.

3.12 Summary

In this chapter, mathematical removal models for fixed-point and single path polishing are established. The model combines processing conditions, material mechanics, physical properties, geometric relationships and more polishing influence factors. By comparing with the actual polished surface, the proposed mathematical models can basically predict the polishing depth and plan the polishing process.

At the same time, the entire plane was polished, and the results were analyzed. The shape of the bottom of the actual removal area after the entire plane polishing is undulating. The experimental results did not reach a smooth plane, and it is thought to be caused by the connection between the tool and the tool holder. There is a clearance fit between the tool and the tool holder. In scanning type polishing, the tool slightly oscillates inside the tool holder due to frequent changes in the polishing direction.

A polishing mathematical model of the curve trajectory is established. The material removal of linear trajectories and circular trajectories on the vertical bisector of

transitional corners is classified and the material removal of the polished path corners is modeled. Other complex polishing paths can be modeled and analyzed using similar methods in this chapter to optimize the polishing process. This work is expected to open the door to path planning.

The rotation and revolution polishing method is designed to polish freeform optical elements. After the polishing of the fixed point, line and plane, it proves that the rotation and revolution polishing method is stable and effective. Research in this chapter is the basis for polishing freeform optical elements. Other complex freeform surfaces can be studied and analyzed using similar methods in this chapter.

References

[1] C. Fan, J. Zhao, L. Zhang, W.S. Zhou and L.N. Sun: Local material removal model considering the tool posture in deterministic polishing, Proceedings of the Institution of Mechanical Engineers, Part C: Journal of Mechanical Engineering Science, **230** (2016) 2660-2675.

[2] W.B. Zhang, M.W. Shu, B. Lin and X.F. Zhang: Study on the removal function of annular polishing pad based on the computer controlled polishing technology, Applied Mechanics and Materials, **457-458** (2013) 552-555.

[3] J. Greenwood: Formulas for moderately elliptical Hertzian contacts, Journal of tribology, **107** (1985) 501-504.

[4] F. Klocke, O, Dambon and R. Zunke: Modeling of contact behavior between polishing pad and workpiece surface, Production Engineering, **2** (2008) 9-14.

[5] L. Zhang, H.Y. Tam and C. Yuan: An investigation of material removal in polishing with fixed abrasives, Journal of Engineering Manufacture, **216** (2002) 103–112.

[6] G. Savio, R, Meneghello and G. Concheri: A surface roughness predictive model in deterministic polishing of ground glass moulds, International Journal of Machine Tools and Manufacture, **49** (2009) 1-7.

[7] J. Greenwood: Analysis of elliptical Hertzian contacts, Tribology international, **30** (1997) 235-237.

[8] J. Greenwood, J. Williamson: Contact of nominally flat surfaces, Proceedings of the Royal Society of London Series A Mathematical and Physical Sciences, **295** (1966) 300-319.

[9] H. Wang and W.M. Lin: Removal model of rotation & revolution type polishing method, Precision Engineering, **50** (2017) 515-521.

[10] W.M. Lin, S. K. Chee, H. Suzuki and T. Higuchi: Polishing characteristics of a low frequency vibration assisted polishing method, Advanced Materials Research, **797** (2013) 450-454.

[11] W.M. Lin, T. Kasai, K. Horio and T. Doi: Surface characteristics of the polyurethane polisher in mirror-polishing process, Japan Society of Precision Engineering, **65** (1999) 1147-1152.

[12] W.M. Lin, H, Ohmori, Y. Yamagata, S. Moriyasu, A. Makinouchi and C. Liu, Ultraprecision polishing method of large X-Ray mirrors, The Japan Society of Mechanical Engineers, **2** (2000) 121-122 (in Japanese).

[13] W.M. Lin, M. Ohmura, M. Fujimoto, Y. Wu and Y. Yamagata: Proposal of a rotation & revolution type polishing (RRP) method and fundamental study on the precision profile polishing, Journal of the Japan Society for Abrasive Technology, **56** (2012) 256-261.

[14] W.M. Lin, H. Wang and F.M. Ji: Research on effect of parameters in Rotation & Revolution Type Polishing Method, Procedia CIRP, **71** (2018) 358-363.

[15] R.A. Jones: Computer controlled optical surfacing with orbital tool motion, Optical Engineering, **25** (1986) 785–790.

[16] W.M. Lin, Y. Watanabe, H. Ohmori and T. Kasai: Nano Precision Mirror Surface Finishing Method of Optical Elements with Combined Fabrication Process, Journal of the Japan Society of Polymer Processing, **18** (2006) 842-847.

[17] W.M. Lin, S. Yin, H. Ohmori, Y. Uehara and T. Suzuki, Fabrication of silicon mirror with ultraprecision synergistic finishing process of ELID-grinding and MRF, Journal of the Japan Society for Abrasive Technology, **49** (2005) 701-702(in Japanese).

[18] H. Suzuki, T. Moriwaki, T. Okino and Y. Ando: Development of ultrasonic vibration assisted polishing machine, Annals of the CIRP, **55** (2006) 385-388.

[19] D.W. Kim, S.W. Kim and J.H. Burge: Non-sequential optimization technique for a computer controlled optical surfacing process using multiple tool influence functions, Opt Express, **17** (2009) 21850-21866.

[20] C. Cheung, L. Kong and L. Ho: Modelling and simulation of structure surface generation using computer controlled ultra-precision polishing, Precision Engineering, **35** (2011) 574-590.

[21] X. Pessoles and C. Tournier: Automatic polishing process of plastic injection molds on a 5-axis milling center, Journal of Materials Processing Technology, **209** (2009) 3665-3673.

[22] G.L. Wang, X.Q. Zhou, X. Yang, H.B. Zhou and G.J. Chen: Material removal profile for large mould polishing with coated abrasives, The International Journal of

Advanced Manufacturing Technology, **80** (2015) 625–635.

[23] X. Chen, P. Guo and J. Ren: Optimization of removal function in computer controlled optical surfacing, 5th International Symposium on Advanced Optical Manufacturing and Testing Technologies, International Society for Optics and Photonics, (2010) 76551Y-7.

[24] T.C. Hung, S.H. Chang and C.H. Ding: Improvement of residual error in hydrodynamic polishing by recursive error compensation strategy, Microelectronic Engineering, **93** (2012) 27-34.

[25] H.Y. Tam, C.H. Lui and A.CK. Mok: Robotic polishing of free-form surfaces using scanning paths, Journal of Materials Processing Technology, **95** (1999) 191-200.

[26] F. Klocke, C. Brecher and R. Zunke: Corrective polishing of complex ceramics geometries, Precision Engineering, **35** (2011) 258-261.

[27] X. Jin and L. Zhang: A statistical model for material removal prediction in polishing, Wear, **274** (2012) 203-211.

[28] J. Chaves-Jacob, J.M. Linares and J.M. Sprauel: Improving tool wear and surface covering in polishing via toolpath optimization, Journal of Materials Processing Technology, **213** (2013) 1661-1668.

[29] T.S. Yaw, C.H. Tu and C.H. Chuen: An experimental study on tool wear of hydrodynamic polishing process, Wear, **246** (2000) 117-129.

[30] Y. Mizugaki, M. Sakamoto and T. Sata: Fractal path generation for a metal-mold polishing robot system and its evaluation by the operability, CIRP Annals Manufacturing Technology, **41** (1992) 531-534.

[31] C.A. Chen, Y.S. Juang and W.Z. Lin: Generation of fractal toolpaths for irregular shapes of surface finishing areas, Journal of materials processing technology, **127** (2002) 146-150.

[32] C. Fan, J. Zhao, L. Zhang, W.S. Zhou and J.C. Wu: Modelling of the Polished Profile in Computer-Controlled Polishing by a Sub-Aperture Pad, Machining Science and Technology, **19** (2015) 536-558.

[33] M. Yang and H. Lee: Local material removal mechanism considering curvature effect in the polishing process of the small aspherical lens die, Journal of Materials

processing technology, **116** (2001) 298-304.

[34] C. Fan, J. Zhao, L. Zhang, Y. S. Wong, G. S. Hong and W.S. Zhou: Modeling and analysis of the material removal profile for free abrasive polishing with subaperture pad, Journal of Materials Processing Technology, **214** (2014) 285-294.

[35] C. Fan: Predictive models of the local and the global polished profiles in deterministic polishing of free-from surfaces, Journal of Engineering Manufacture, **228** (2014) 868-879.

[36] H.C. Wang: Research on geometric model for axial symmetry aspheric optical parts machining by normal equidistance method, Advanced Materials Research, **154-155** (2010) 913-916.

Chapter 4 Polishing of electroless plated Ni-P as neutron mirror

Optical control of neutron beams is currently a hot research area. Due to the difficulty in controlling the direction of the neutron beam, the complexity of operation and the limitation of high cost, the application field of the neutron beam is limited. One of the best materials for the manufacture of neutron mirrors today is the polished Ni-P, which has good processability. In this chapter, a model based on the Preston equation is built and the model is validated. The polishing characteristics of the Ni-P surface were discussed, and an ultra-smooth surface was finally obtained by scanning polishing.

4.1 Introduction of neutron beam

X-rays are often mentioned in everyday life and are well known. This chapter introduces a wider range of neutron beams than X-ray applications. Unlike X-rays, which are widely used for surface analysis of materials, neutron beams are more widely used in the determination of organic structures and medical treatments. The neutron beam exhibits a stronger ability to identify the atomic and molecular structures of the material [1, 2]. Optical control of neutron beams is currently a hot research area. Due to the difficulty in controlling the direction of the neutron beam, the complexity of operation and the limitation of high cost, the application field of the neutron beam is limited. One of the best materials for the manufacture of neutron mirrors today is the polished Ni-P, which has good processability [3, 4]. In this chapter, a model based on the Preston equation is built and the model is validated. The polishing characteristics of the Ni-P surface were discussed, and an ultra-smooth surface was finally obtained by scanning polishing.

In the processing of electroless Ni-P mirrors, the right size of the processing tool is selected to maintain a stable polishing speed to achieve high precision and high-quality surface.

4.2 Mathematical modeling of single path polishing of small diameter tools

The market demand for high-quality Ni-P mirrors has increased, and the experiments in this chapter are still carried out on RRP equipment. However, after adjusting the two axes, it is equivalent to a single axis polishing machine with only a revolution axis. The polishing tool uses a small diameter polishing tool (Fig. 4.1). The small-diameter tool polishing method provides a stable polishing speed for stable polishing of the entire workpiece surface [5-17]. At the end of this chapter, the basic polishing characteristics of Ni-P mirror scanning polishing are discussed.

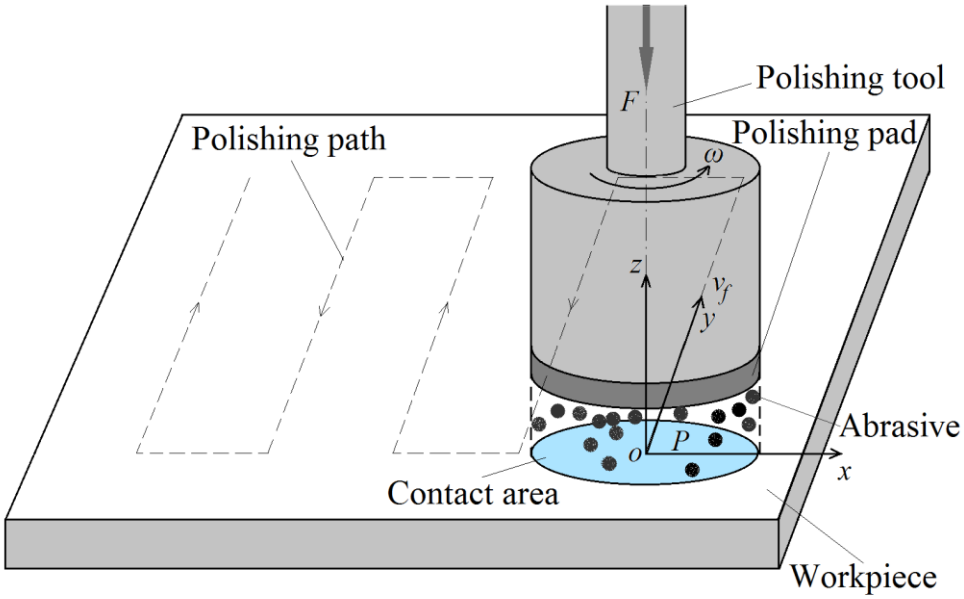

Fig. 4.1 Structure charts of polishing machine

Based on the Preston equation, the function of removal is represented by Eq. (4.1), where k is the Preston coefficient [18].

$$\delta = k \cdot P \cdot V \cdot t \tag{4.1}$$

P and V are pressure functions and relative speed distribution functions in the polished region, and t is the polishing time.

Establish a Cartesian coordinate system to describe the RRP special machining posture. The x axes are defined as measurement direction, the y axis is vertical direction of the measurement direction, and the z-axis is defined as the direction opposite to polished depth (Fig. 4.2). The origin of o-xy is at the center point o. o-xy is in the tangent plane of the point P.

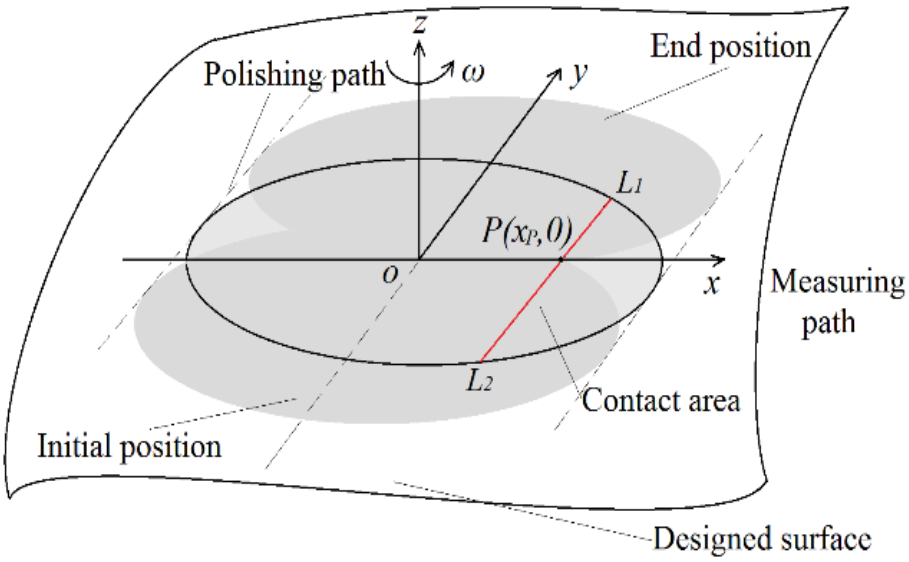

Fig. 4.2 Definition of polishing area coordinate system

In the Preston removal theory (Eq. (4.1)), we choose any point P in contact area. v_s is the relative speed, and p_c represents the positive pressure of the point P. Based on the Preston principle, Eq. (4.2) can be used to understand the depth of removal during dwell time dT.

$$dh = k_p p_c v_s dT \tag{4.2}$$

The path length of the polishing tool during that dwell time,

$$dl = dT v_f \tag{4.3}$$

Using Eq. (4.2) and Eq. (4.3), the material removal per unit path length E could be obtained by Equation (4.4).

$$E = \frac{dh}{dl} = k_p \frac{p_c v_s}{v_f} \tag{4.4}$$

Material removal of the *P* point on the x-axis in the polishing zone is considered. When the tool head passes the point *P* along the path, it corresponds to polished area passing through the point *H*. Assuming that the shape and size of the contact area are not abrupt near the point *O*, *L1* and *L2* can be regarded as the starting point and the ending point of the contact area in contact with *P* [19-22].

L1L2 could be a polishing strip, and the amount of material removed by each micro-element on the polishing strip depends on the contact pressure, line speed and feed rate of the micro-element through *P*. The material removal depth at the point *P* can represent the integral of *E* along *L1L2*.

$$h = \int_{L_2}^{L_1} E\, dl \tag{4.5}$$

The small diameter flat polishing tool was chosen in the experiment, and the pressure was uniform. The equation shows the pressure distribution function of the polished area. Where F_n is the polishing force of the tool.

$$p_c = \frac{F_n}{\pi R_p^2} \tag{4.6}$$

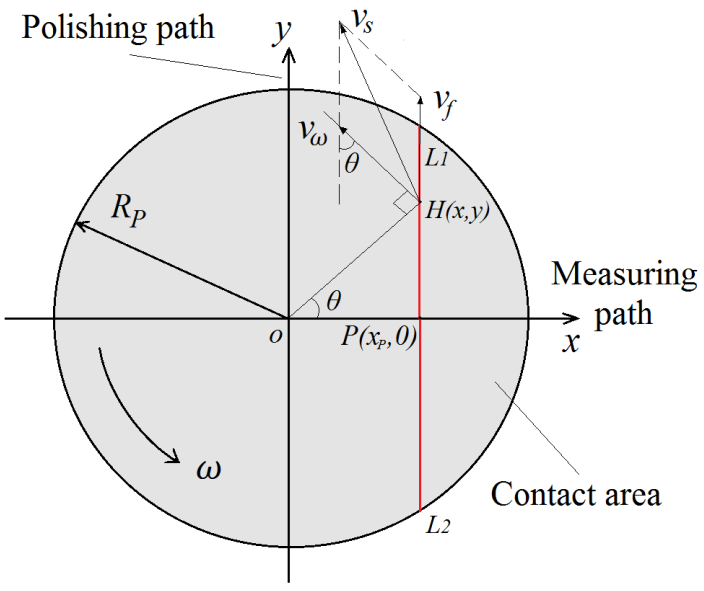

Fig. 4.3 Polishing area velocity distribution

Since the end face of the polishing tool is flat, the relative speeds of the points of different radius in the polishing zone are not uniform. The velocity function of the contact area is distributed as shown below, and ω is tool angular velocity. v_ω is the linear velocity of any point H, and v_f is the tool feed speed. And θ is the angle between the two linear velocities (Fig. 4.3). According to the geometric relationship and the motion synthesis method, the linear velocity of the point H can be expressed by Eq. (4.7).

$$v_\omega = \omega\sqrt{x^2 + y^2} \tag{4.7}$$

$$\cos\theta = \frac{x}{\sqrt{x^2+y^2}} \tag{4.8}$$

Therefore, in the contact area, the relative velocity v_s of each point can be obtained by Eq. (4.9).

$$v_s = \sqrt{v_f^2 + v_\omega^2 + 2v_f v_\omega \cos\theta} \tag{4.9}$$

Finally, the contact area, pressure distribution function, relative speed function is substituted and sorted.

$$h(x) = \frac{2k_P F_n}{v_f \pi R_P^2} \int_0^{\sqrt{R_P^2 - x^2}} v_s \, dy \tag{4.10}$$

After the above formula is used for y integration, it is an expression with x as the variable. When x is taken from $-R_P$ to R_P, the material removal profile (function shape) and the removal depth (value of z) can be obtained.

4.3 Experimental verification of the model

4.3.1 Experimental system and conditions

The RRP polishing machine consists of a polishing body and a control section. The movements of the XYZ axis are controlled by the PC, and the direction and speed of rotation are controlled by the motor controller [23]. The polishing experiment was performed on an RRP system with a machine resolution of 0.001 mm. Fig. 4.4 shows the experimental setup. The polishing liquid is dropped on the polishing zone through the abrasive nozzle, and the new polishing liquid is continuously applied during the polishing process [24-30]. The polishing tool (ϕ5 mm) was used in scan-type polishing in Fig. 4.5. The material of the polishing pad is suede and the thickness is 1.3 mm.

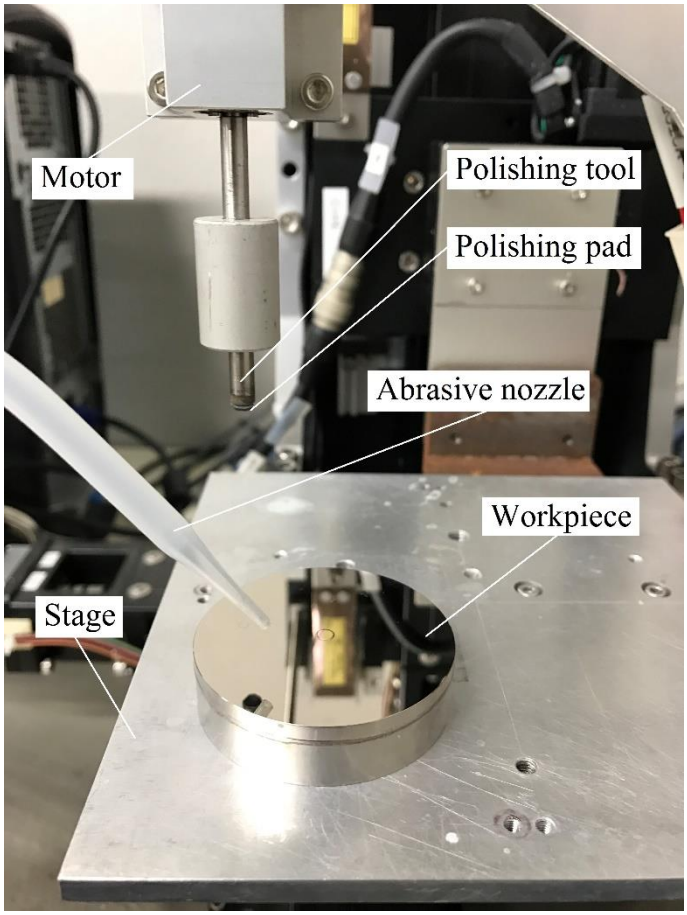

Fig. 4.4 Photograph of experimental setup

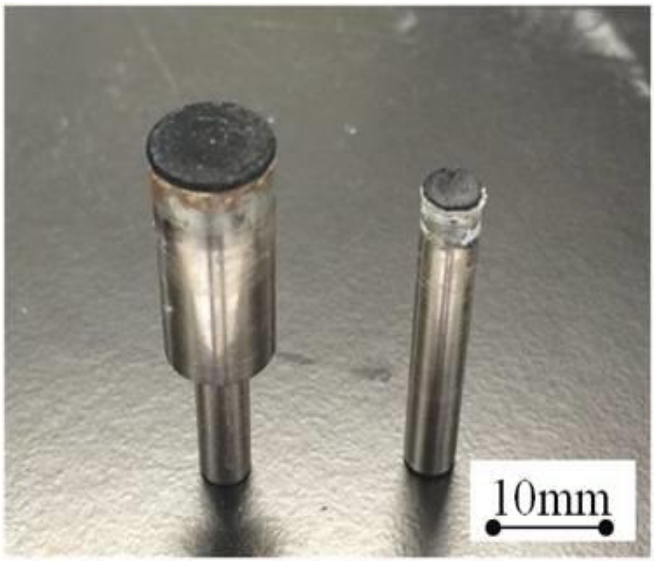

Fig. 4.5 Photograph of scan polishing tools (left: ϕ10 mm, right: ϕ 5 mm)

Fig. 4.6 shows the XY and YX scan paths used in the second stage planar polishing experiments. In the actual plane polishing process, the XY scan path is first applied and then the YX scan is performed.

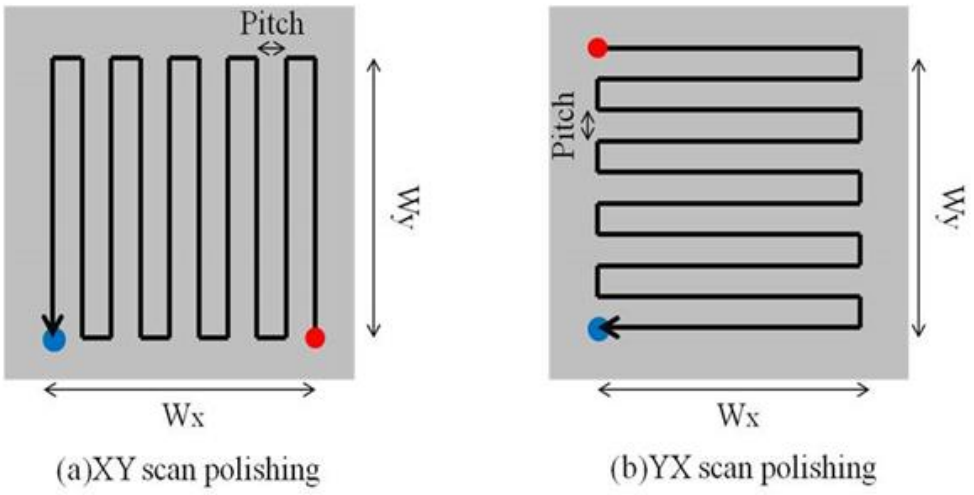

Fig. 4.6 Polishing scan path

After measuring 9 white points (Fig. 4.7) in the figure, the average value obtained is the surface roughness of the measuring workpiece (50 mm × 50 mm).

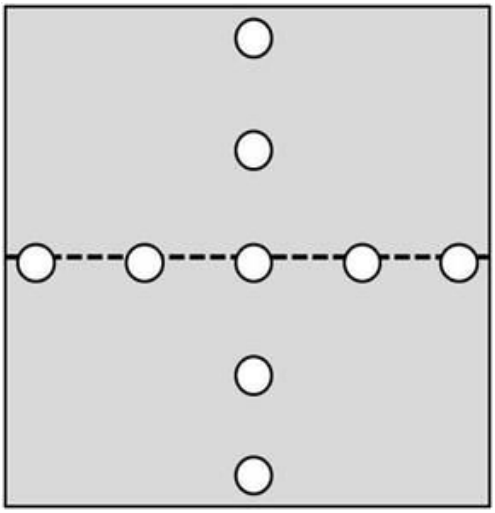

Fig. 4.7 Measurement point of scan polishing

4.3.2 Determination of Preston coefficient

The Preston wear coefficient k_P needs to be measured in the experiment. In polishing using the scan polishing method, the relative speed can be considered to be constant. The simplified relative speed is shown in the equation below

$$v_s = \frac{\omega R_P}{2} \tag{4.11}$$

Based on the Preston equation, x and y are selected as the variation of the double integral, and x and y are integrated to obtain the obtained Eq. 4.12.

$$\iint_s^S h(x,y)dxdy = k_P T \iint_S^S p_c(x,y)v_s(x,y)dxdy \tag{4.12}$$

The left side of the equation can be considered as the product of the bottom area and the height, and the result of the multiplication is the material removal volume. The right side can be regarded as the product of area and pressure, and the result of multiplication is positive pressure [31-33].

$$V = k_P T v_s \iint_S^S p_c(x,y)dxdy = k_P T v_s F_n \tag{4.13}$$

Finally, the Preston coefficient could be determined by Eq. (4.14), where ρ_d is the density of the workpiece. Δm is the weight difference before and after polishing.

$$k_P = \frac{V}{v_s F_n T} = \frac{\Delta m}{v_s F_n T \rho_d} = \frac{\Delta m}{\frac{\omega R_P}{2} F_n T \rho_d} \tag{4.14}$$

Looking at Eq. 4.14, if the Preston coefficient k_p is calculated, the following physical quantities are necessary. The mass change before and after the workpiece is polished, relative velocity v_s, pressure and workpiece density. k_P value could be achieved.

After a large number of experiments, we have found efficient and stable data for the rotation speed and the polishing pressure. The electroless plated Ni-P was polished using free abrasive particles under these highly efficient and stable conditions (Table 4.1).

Table 4.1 Experimental conditions.

Experimental conditions	Values
Workpiece material	Electroless plated Ni-P surface (50mm×50mm)
Tool diameter	5 mm
Tool rotational speed	300 rpm
Tool moving speed	240 mm/min
Abrasive material	Colloidal silica abrasive 10 wt % (23nm)
Polishing pressure	25 kPa
Abrasive supply	0.05 g
Scan method	XY scan, XY-YX scan
Scan pitch	0.05 mm, 0.5 mm, 2.5 mm

The phosphorus content of the Ni-P coating is 12 wt%. The hardness is 521 HV and

the density is 7.9 g/cm^3. The experiment was carried out at room temperature. Although the tool and the surface of the workpiece will produce polishing heat. However, the heat of polishing is not high, and the continuous replenishment of the polishing liquid will take away the heat. Therefore, it can be considered that the polishing heat does not affect the properties of the Ni-P plating layer.

The experiment in this chapter consists of two parts. The first part is a single path polishing experiment, which discusses the comparison between the theoretical removal function and the actual polishing profile. The second part is the whole surface polishing experiment of the workpiece. Small-diameter tools were used in both experiments. The entire surface polishing experiment used XY and YX scan paths for polishing experiments. Material removal, surface roughness, etc., polishing characteristics are discussed in this chapter.

4.4 Results and discussion

4.4.1 Experimental verification of single path material removal model

The blue curve represents the profile after polishing a single path. It was measured using a non-contact measuring instrument. The red curve represents the theoretical removal curve for a single path simulated using MATLAB software (Fig. 4.8). The actual and theoretical contours of a single path show approximate consistency, which confirms the mathematical model presented in this chapter. The experiment uses a thin disc-shaped polishing pad, and since the size of the polishing tool is very small, the shape of the end face remains substantially unchanged. The wear of the polishing tool is negligible. A pitch of 0.5 mm was used.

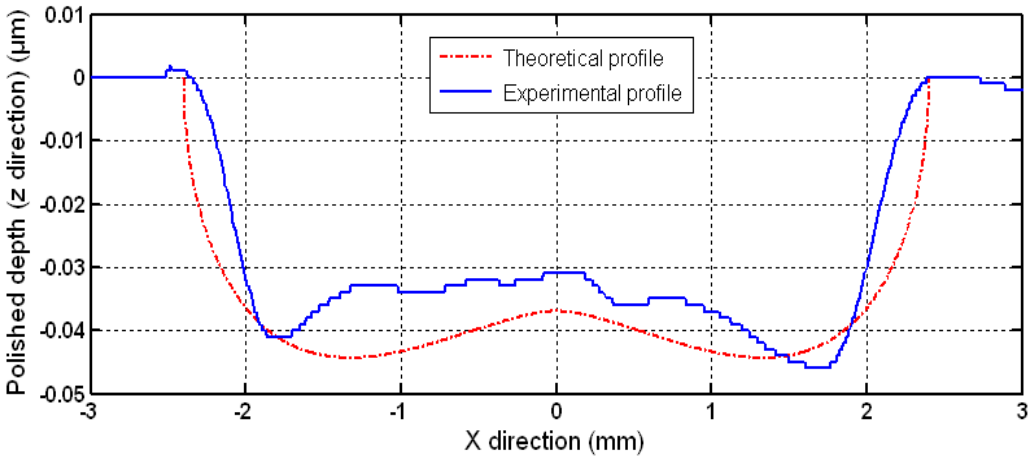

Fig. 4.8 Difference between theoretical and experimental profiles of single path

The following figure shows the actual removal area after XY-YX scanning polishing. Cross section of the polishing area and polishing depth are obtained (Fig. 4.9).

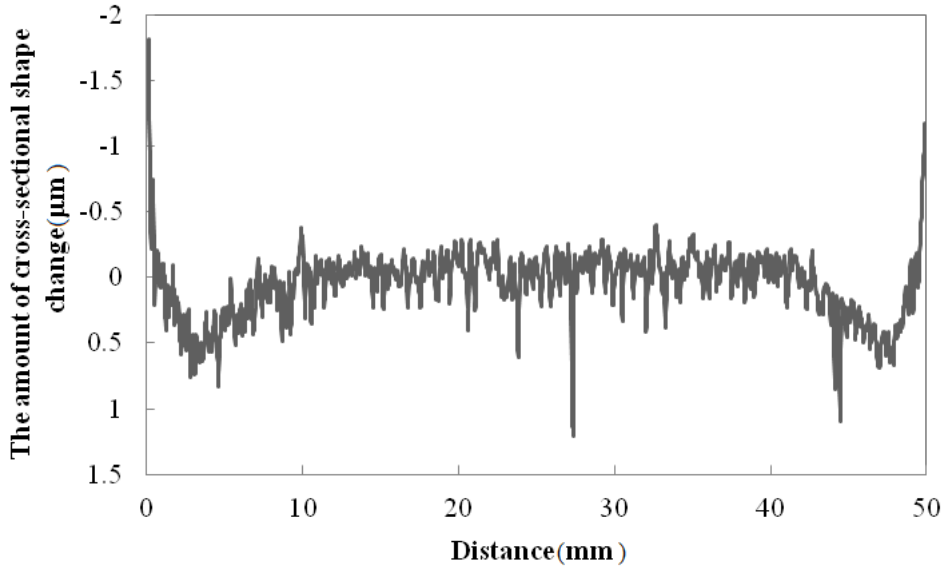

Fig. 4.9 Cross-sectional shape change after finish polishing

4.4.2 Discussion of surface quality

First, discuss the effect of the spacing between the polishing trajectories. After determining the appropriate spacing, this spacing will always be applied to complete

all the experiments in this chapter. In XY scanning, the relationship between different scanning pitches and surface roughness is given in the Fig. 4.10. After 13 minutes of polishing, a pitch of 0.5 mm produced a smooth surface (Ra 5 nm). The Fig. 4.11 shows photographs of the actual surface conditions after polishing for about 5 minutes in the XY scan with a scan pitch of 0.5 mm and 2.5 mm.

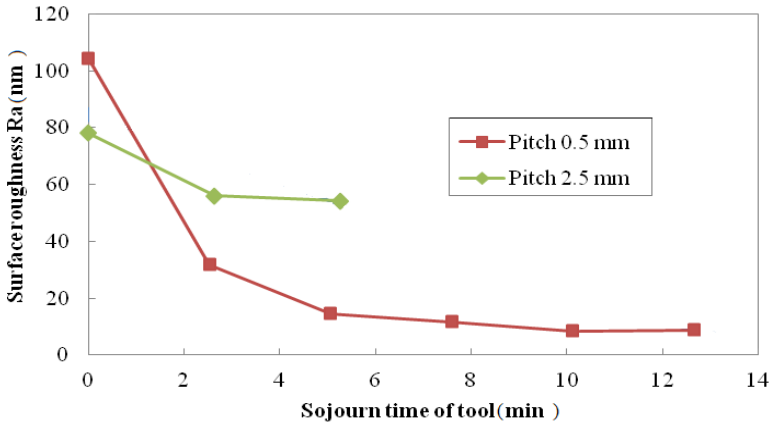

Fig. 4.10 Relationship between sojourn time and surface roughness with different scan pitch

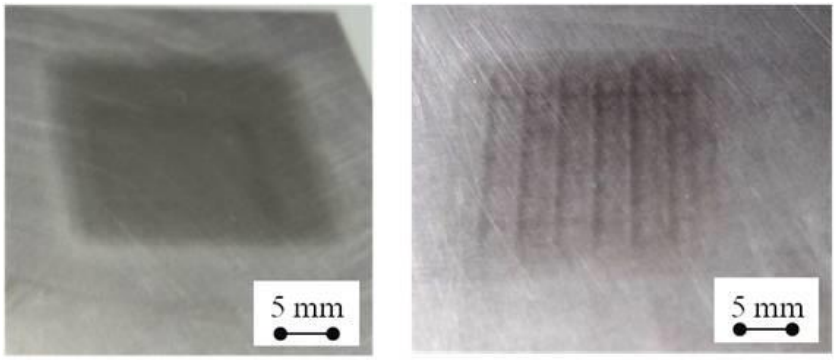

(a)Pitch 0.5 mm (b)Pitch 2.5 mm

Fig. 4.11 Photographs of surface conditions with scan pitch 0.5 mm and 2.5 mm

Comparing the surface of the workpiece with a polishing pitch of 0.5 mm, the polishing marks can be clearly polished at a pitch of 2.5 mm. When the pitch becomes larger, the fluctuation of the surface also becomes larger. Traces on the polished surface occurred at a polishing pitch of 2.5 mm. Comparing the two pitches, it is considered that the material removal is relatively small and produces a smoother surface when a

pitch of 0.5 mm was used.

The cross-sectional shapes of the two scanning paths after polishing were measured and compared. The material removal profile and polishing depth of the polishing zone can be derived. A pitch of 0.5 mm was used. A smoother machined surface can be obtained using the XY-YX scanning polishing method (Fig. 4.12).

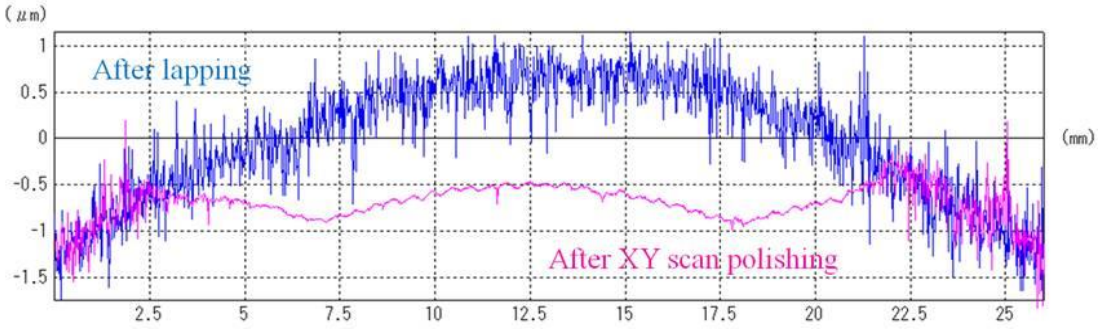

(a) XY scans polishing

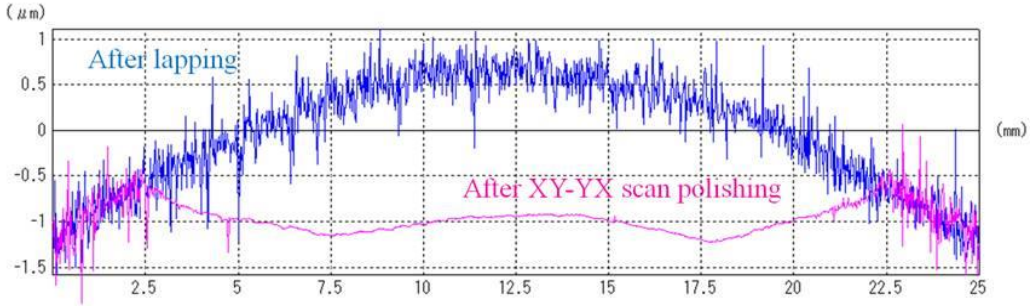

(b) XY-YX scans polishing

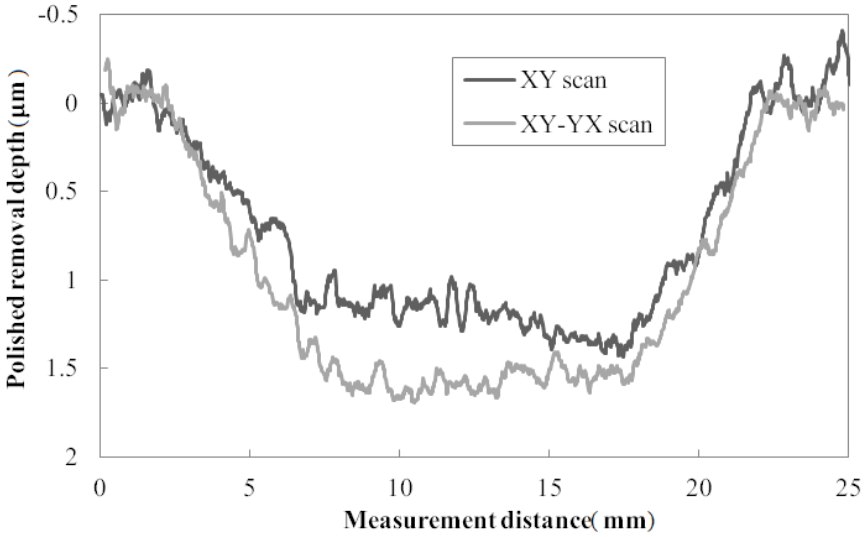

(c) Removal depth of XY scan and XY-YX scan polishing

Fig. 4.12 Comparison between cross-section shape of scan polishing

In a comparative experiment of two scan polishing paths, XY scan means polishing XY scan path twice. XY-YX scan means first performing XY scan polishing and then performing YX scan polishing once. The polishing feed speed is the same, so the total polishing time for both scan methods is the same. A pitch of 0.5 mm was used.

Within 10 minutes of polishing, the degree of surface quality improvement during XY scanning polishing and XY-YX scanning polishing showed the same tendency (Fig. 4.13 (a)). After 30 minutes, the surface roughness under both scanning polishing paths was decreased to Ra 1.7 nm. From the surface roughness data measurement, there is almost no difference.

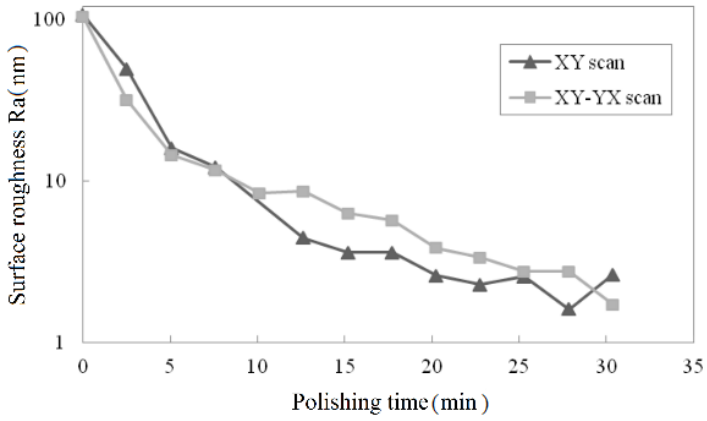

(a) Surface roughness

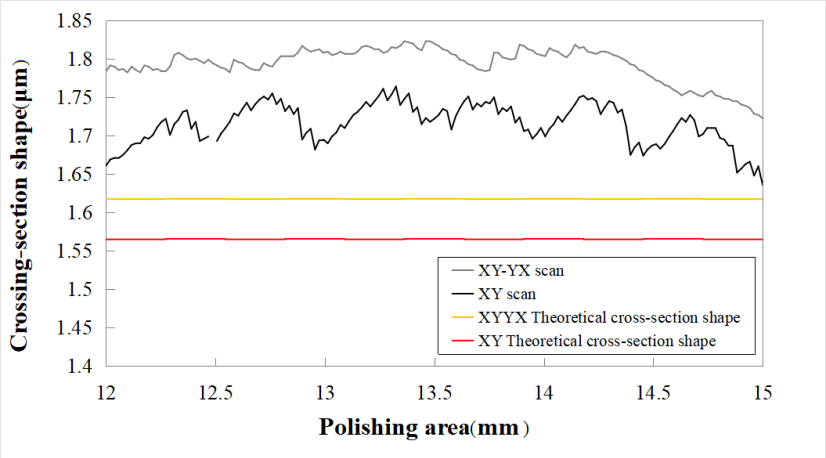

(b) Experimental and theoretical cross-section shape

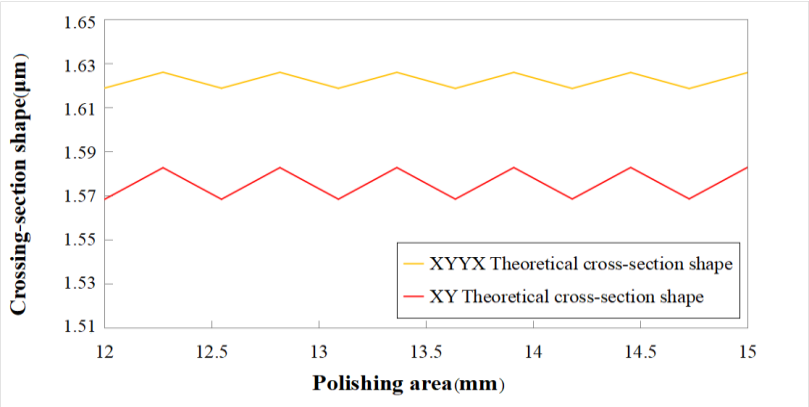

(c) Enlarged view of cross-section shape

Fig. 4.13 Relationship between polishing time and surface roughness with XY scan and XY-YX scan polishing

Figs. 4.13 (b) and (c) show the theoretical cross-sectional shape of the two trajectories after simulation using NarrowVPolish (version 1.1.14) software. NarrowVPolish is used to simulate material removal calculations and pressure distribution. This chapter uses this software to conduct theoretical studies of cross-sectional shapes. The simulation software was developed by Professor Une Atsunobu of the National Defense University of Japan. In the simulation results, there are some deviations between the theoretical and actual results. However, in the comparison of the two polishing trajectories, some laws can also be found.

In addition, in XY scanning polishing, the scanning pitch of the surface is not smooth. The polishing path is formed by XY-YX scanning to form an approximately ideal flat surface without a deformed cross-sectional shape. In future research, We hope to use NarrowVPolish software for more detailed and accurate simulation.

The Fig. 4.14 shows that after XY-YX scan of polishing, the roughness of the mirror surface reaches Ra 0.12 nm, which can visually see the reflection of the text. Regarding the polishing scan pitch in the previous experiments, high efficiency polishing was mainly considered. The purpose of this experiment is to obtain a high quality surface, so a pitch 0.05 mm was applied in this experiment.

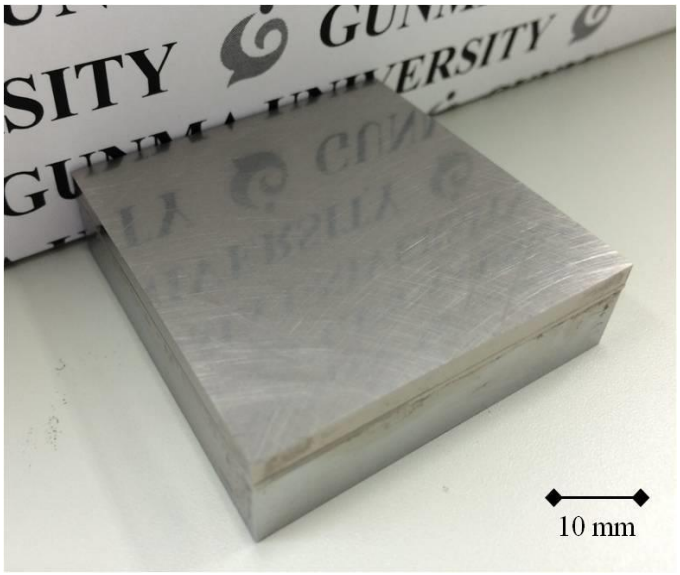

(a) Before polishing

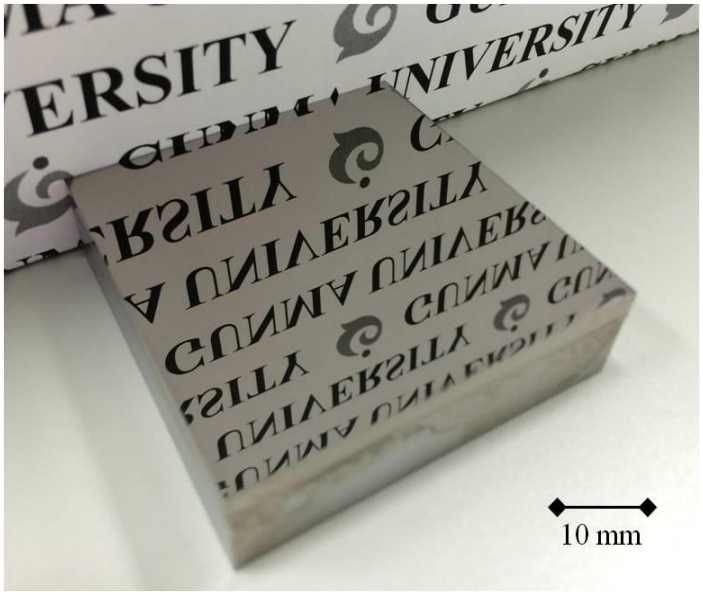

(b) Polished surface

Fig. 4.14 Photograph of electro-less plated Ni-P

4.5 Summary

This chapter describes the application prospects of neutron beams and the processing requirements of neutron mirrors. It is proposed to use the electroless Ni-P substrate as the mirror material to establish a mathematical removal model for single path polishing. The model combines processing conditions, material mechanics, physical properties, geometric relationships, etc., and is more general than previous models. By comparing with the actual processed surface, the proposed mathematical model can basically predict the polishing depth and plan the polishing process. Characteristics of roughness and other polishing characteristics are also briefly explained. The XY-YX polishing scan path achieves high surface quality. Roughness of Ra 0.12 nm could be achieved after XY-YX scan of polishing.

References

[1] M. Furusaka: First results from a mini-focusing small-angle neutron scattering instrument (mfSANS) with an ellipsoidal mirror, ICANS-XVIII, (2007) 25-29.

[2] K. Hirota: Development of a neutron detector based on a position-sensitive photomultiplier, The Journal of Physical Chemistry, **7** (2005) 1836-1838.

[3] W.M. Lin, H. Ohmori, Y. Yamagata, S. Moriyasu, T. Kasai, K. Horio and C Liu: A polishing method of large X-ray mirror surface, Advances in Abrasive Technology, **3** (2000) 175.

[4] H. Yasui: High removal rate ultra-smoothness polishing of Ni-P plated aluminum magnetic disk substrate by means high polishing speed with high polishing pressure, ASPE Annual Meetings, **27** (2002) 689-692.

[5] H. Wang and W.M. Lin: Removal model of rotation & revolution type polishing method, Precision Engineering, **50** (2017) 515-521.

[6] W.M. Lin, S. K. Chee, H. Suzuki and T. Higuchi: Polishing characteristics of a low frequency vibration assisted polishing method, Advanced Materials Research, **797** (2013) 450-454.

[7] C. Fan, J. Zhao, L. Zhang, Y. S. Wong, G. S. Hong and W.S. Zhou: Modeling and analysis of the material removal profile for free abrasive polishing with subaperture pad, Journal of Materials Processing Technology, **214** (2014) 285-294.

[8] H.C. Wang: Research on geometric model for axial symmetry aspheric optical parts machining by normal equidistance method, Advanced Materials Research, **154-155** (2010) 913-916.

[9] T.I. Suratwala, M.D. Feit and W.A. Steele: Toward deterministic material removal and surface figure during fused silica pad polishing, Journal of the American Ceramic Society, **93** (2010) 1326-1340.

[10] D.W. Kim, S.W. Kim and J.H. Burge: Non-sequential optimization technique for a computer controlled optical surfacing process using multiple tool influence functions, Opt Express, **17** (2009) 21850-21866.

[11] S. Hauth and L. Linsen: Cycloids for polishing along double-spiral toolpaths in configuration space, The International Journal of Advanced Manufacturing Technology,

60 (2012) 343-356.

[12] H. Suzuki, T. Moriwaki, T. Okino and Y. Ando: Development of ultrasonic vibration assisted polishing machine, Annals of the CIRP, **55** (2006) 385-388.

[13] M. Yang and H. Lee: Local material removal mechanism considering curvature effect in the polishing process of the small aspherical lens die, Journal of Materials Processing Technology, **116** (2001) 298-304.

[14] X. Chen, P. Guo and J. Ren: Optimization of removal function in computer controlled optical surfacing, 5th International Symposium on Advanced Optical Manufacturing and Testing Technologies, International Society for Optics and Photonics, (2010) 76551Y-7.

[15] M. Rososhansky and F.J. Xi: Coverage based tool-path planning for automated polishing using contact mechanics theory, Journal of Manufacturing Systems, **30** (2011) 144-153.

[16] L. Zhang, H.Y. Tam and C. Yuan: An investigation of material removal in polishing with fixed abrasives, Journal of Engineering Manufacture, **216** (2002) 103–112.

[17] G. Savio, R, Meneghello and G. Concheri: A surface roughness predictive model in deterministic polishing of ground glass moulds, International Journal of Machine Tools and Manufacture, **49** (2009) 1-7.

[18] F.W. Preston: The theory and design of glass plate polishing machines, Journal of the Society of Glass Technology, **11** (1927) 247–256.

[19] J.F. Song, X.Y. Yao and D.G. Xie: Effects of polishing parameters on material removal for curved optical glasses in bonnet polishing, The Chinese Journal of Mechanical Engineering, **5** (2008) 29–33.

[20] G.L. Wang, X.Q. Zhou, X. Yang, H.B. Zhou and G.J. Chen: Material removal profile for large mould polishing with coated abrasives, The International Journal of Advanced Manufacturing Technology, **80** (2015) 625–635.

[21] W.B. Zhang, M.W. Shu, B. Lin and X.F. Zhang: Study on the removal function of annular polishing pad based on the computer controlled polishing technology, Applied Mechanics and Materials, **457-458** (2013) 552-555.

[22] C. Fan, J. Zhao, L. Zhang, W.S. Zhou and J.C. Wu: Modelling of the polished

profile in computer-controlled polishing by a sub-aperture pad, Machining Science and Technology, **19** (2015) 536-558.

[23] W.M. Lin, H. Wang and F.M. Ji: Research on effect of parameters in rotation & revolution type polishing method, Procedia CIRP, **71** (2018) 358-363.

[24] C. Fan, J. Zhao, L. Zhang, W.S. Zhou and L.N. Sun: Local material removal model considering the tool posture in deterministic polishing, Proceedings of the Institution of Mechanical Engineers, Part C: Journal of Mechanical Engineering Science, **230** (2016) 2660-2675.

[25] F. Klocke, O, Dambon and R. Zunke: Modeling of contact behavior between polishing pad and workpiece surface, Production Engineering, **2** (2008) 9-14.

[26] W.M. Lin, T. Kasai, K. Horio and T. Doi: Surface Characteristics of the Polyurethane Polisher in Mirror-Polishing Process, Japan Society of Precision Engineering, **65** (1999) 1147-1152.

[27] W.M. Lin, H, Ohmori, Y. Yamagata, S. Moriyasu, A. Makinouchi and C. Liu, Ultraprecision polishing method of large X-ray mirrors, The Japan Society of Mechanical Engineers, **2** (2000) 121-122 (in Japanese).

[28] W.M. Lin, M. Ohmura, M. Fujimoto, Y. Wu and Y. Yamagata: Proposal of a rotation & revolution type polishing (RRP) method and fundamental study on the precision profile polishing, Journal of the Japan Society for Abrasive Technology, **56** (2012) 256-261.

[29] W.M. Lin, Y. Watanabe, H. Ohmori and T. Kasai: Nano precision mirror surface finishing method of optical elements with combined fabrication process, Journal of the Japan Society of Polymer Processing, **18** (2006) 842-847.

[30] W.M. Lin, S. Yin, H. Ohmori, Y. Uehara and T. Suzuki, Fabrication of silicon mirror with ultraprecision synergistic finishing process of ELID-grinding and MRF, Journal of the Japan Society for Abrasive Technology, **49** (2005) 701-702(in Japanese).

[31] C. Fan: Predictive models of the local and the global polished profiles in deterministic polishing of free-from surfaces, Journal of Engineering Manufacture, **228** (2014) 868-879.

[32] J.A. Greenwood: Formulas for moderately elliptical Hertzian contacts, Journal of

Tribology, **107** (1985) 501–504.

[33] R.A. Jones: Computer controlled optical surfacing with orbital tool motion, Optical Engineering, **25** (1986) 785–790.

Chapter 5 Conclusions

5.1 Summary of this thesis

This study focused on ultraprecision finishing method for freeform optical element. Its precision, surface roughness, processing size range and geometry have become an important level of manufacturing technology. As a key technology for ultraprecision finishing, aspherical processing technology has attracted more and more attention.

In chapter 1, the definitions of aspheric surfaces and aspherical curve equations were introduced. The measurement method of the aspherical surface was described. The current ultraprecision manufacturing method was also introduced. Finally, the ultraprecision machine tools with excellent performance were described in detail.

In chapter 2, the rotation and revolution polishing method was used as a polishing method for an aspherical lens mold. It improves the uniformity and density of the path and could process a variety of molds. The structure of rotation and revolution polishing device was detailed in this chapter. The experimental and measurement equipment of this paper has also been introduced. The selection of the polishing solution and the truing of the tool was also described in detail. This rotation and revolution polishing device needs to be simple in structure, low in cost and stable in processing. The basic parameters of 3D modeling were calculated and then 3D modeling was built using SolidWorks software.

In chapter 3, mathematical removal models for fixed-point and single path polishing were established. The removal profile was examined to be a Gaussian curve and the predictability of the profile was confirmed. The model combined processing conditions, material mechanics, physical properties, geometric relationships and more polishing influence factors. By comparing with the actual polished surface, the proposed mathematical models could basically predict the polishing depth and plan the polishing process.

At the same time, the entire plane was polished, and the results were analyzed. The shape of the bottom of the actual removal area after the entire plane polishing was

undulating. The experimental results did not reach a smooth plane, and it was thought to be caused by the connection between the tool and the tool holder. There was a clearance fit between the tool and the tool holder. In scanning type polishing, the tool slightly oscillates inside the tool holder due to frequent changes in the polishing direction.

A polishing mathematical model of the curve trajectory was established. The material removal of linear trajectories and circular trajectories on the vertical bisector of transitional corners was classified and the material removal of the polished path corners was modeled. Other complex polishing paths could be modeled and analyzed using similar methods in this chapter to optimize the polishing process.

In chapter 4, the application prospects of neutron beams and the processing requirements of neutron mirrors was described. It was proposed to use the electroless Ni-P as the mirror material to establish a mathematical removal model for single path polishing. By comparing with the actual processed surface, the proposed mathematical model could basically predict the polishing depth and plan the polishing process. The small-diameter polishing tool is used to mount the three-axis CNC machine tool for the entire plane polishing. The plane previously polished by the rotation and revolution polishing (RRP) method is not ideal. This chapter continues the previous mathematical theory and perfected the rotation and revolution polishing (RRP) method for point, line, and surface studies. Characteristics of roughness and other polishing characteristics were also briefly explained. The XY-YX polishing scan path achieved high surface quality. Roughness of Ra 0.12 nm could be achieved after XY-YX scan of polishing.

The rotation and revolution polishing method is designed to polish freeform optical elements. After the polishing of the fixed point, line and plane, it proves that the rotation and revolution polishing method is stable and effective. Research in this thesis is the basis for polishing freeform optical elements. Other complex freeform surfaces can be studied and analyzed using similar methods in this thesis.

5.2 Further prospect

Through the 3D modeling function of SolidWorks software, we build the 3D modeling of different parts. In the future, simulation analysis will be carried out to analyze the motion characteristics of the complex structure in space. The finite element analysis of the polishing force and heat between tool end face and workpiece should be done based on the established 3D modeling. The motion characteristics of complex structures with biaxial rotation should be analyzed. In particular, the stress of holder in connection with tool and axis of rotation motor need to be analyzed. The stress, strain and deformation of the structure should be determined, so that the designed polishing machine can reach the most stable state. Accurate realization of the polishing tool 3D model is necessary to provides a basic guarantee for the analysis of the polishing force in the processing area.

Related articles

【Original publication】

[1] H. Wang and W.M. Lin: Removal model of rotation & revolution type polishing method, Precision Engineering, **50** (2017) 515-521.
[2] W.M. Lin, H. Wang and F.M. Ji: Research on effect of parameters in Rotation & Revolution Type Polishing Method, Procedia CIRP, **71** (2018) 358-363.
[3] H. Wang and W.M. Lin: Research on scan polishing flat surfaces with a small diameter tool, International Journal of Abrasive Technology (投稿中).
[4] H. Wang and W.M. Lin: Material removal for plain optical glasses by Rotation & Revolution type polishing, Frontiers of Mechanical Engineering (投稿中).

【Conference presentation】

[1] H. Wang and W.M. Lin: Spot Polishing Models of Rotation & Revolution Type Polishing Method based on the Preston equation, Advanced Micro-Fabrication and Green Technology, **4** (2016) 66-69.
[2] H. Wang, F.M. Ji and W.M. Lin: Investigation on Deterministic Polishing of Electro-less Plated Ni-P Surface Based on Preston Equation, Proceedings of the 20th International Symposium on Advances in Abrasive Technology, **20** (2017) 635-640.
[3] F.M. Ji, H. Wang and W.M. Lin: Evaluation of CVD-SiC grinding properties using indentation experiment, Proceedings of the 20th International Symposium on Advances in Abrasive Technology, **20** (2017) 261-266.
[4] 林 偉民，王 賀：自転／公転型研磨スポットの理論検証，2017 年度精密工学会春季大会学術講演会講演論文集，(2017) 649-650.
[5] 林 偉民，王 賀： 小径研磨ツールの走査による大面積表面の研磨の検討，2017 年度砥粒加工学会学術講演会(ABTEC2017)講演論文集，(2017) 59-60.

【Award】

Excellent research award in the 9th MIRAI Conference on Microfabrication and Green Technology, Spot Polishing Models of Rotation & Revolution Type Polishing Method based on the Preston equation, Advanced Micro-Fabrication and Green Technology.

Acknowledgements

This research was done with the guidance and help of Prof. Weimin Lin. Here, I would like to express my most sincere gratitude. Prof. Weimin Lin profound professional knowledge, sincere and sincere attitude, rigorous academic attitude and professionalism have set me a model for outstanding researchers and a model for me to learn. I would like to especially thank Prof. Weimin Lin for carefully selecting the direction of the doctoral thesis for me, and patiently guiding my research process. Not only teaches me to study, but also teaches me how to do things for others, and also gives me a lot of care in life. Here, I would like to express my sincere respect and sincere gratitude to my beloved Prof. Weimin Lin.

Next, I would like to thank Prof. Ikuo Shohji, Prof. Masaaki Matsubara, Prof. Yoshihiko Hangai and Associate Prof. Atsushi Iwasaki for their guidance, encouragement and help to my thesis. The teacher's teacher-oriented approach and rigorous academic style are deeply in my mind. These are valuable spiritual treasures worthy of my lifelong learning. Here, I would like to express my heartfelt thanks to all the teachers who have helped me.

Finally, I would like to thank Ms. Haruko Mashimo of Gunma University for supporting the experiments.

In short, during the four-year Ph.D. program, I not only exercised my ability in academic research, but also enriched my life experience. I would like to express my sincere gratitude to the teachers, classmates and friends who have accompanied me for 4 years of graduate life.